REFERENCE ONLY

UNIVERSITY OF LONDON THESIS

Degree PhD Year 2006 Name of Author NORI, Massimiliano

Investigation on sound propagation for the measurement of diffusion in microporous solids

Student Massimiliano Nori

Supervisor Prof. Stefano Brandani

Subsidiary-Supervisor Prof. Haroun Mahgerefteh

A thesis submitted for the degree of Doctor of Philosophy

of the University of London

ProQuest LLC
789 East Eisenhower Parkway
P.O. Box 1346
Ann Arbor, MI 48106-1346

To my parents and my sister

Abstract

The basic definitions of micropore diffusivities and the experimental techniques applied for their measurement are reviewed. Through a historical perspective, the techniques are briefly described, with an emphasis on the measured property, the theoretical and practical limitations. As a result the need for a novel experimental technique has been identified. The extension of the frequency response (FR) method to frequencies in the audible sound range is proposed.

A detailed mathematical model is presented to describe the propagation of sound between two parallel adsorbing plates. The main body of the thesis is the description and derivation of a model that relates an acoustic quantity (i.e. propagation constant) to adsorption parameters (i.e. diffusivity and equilibrium constant) in microporous solids.

The theoretical analysis describes the ranges of physical parameters where the complete model reduces to simplified versions: classical absorption; isothermal limit; equilibrium control; temperature control.

Based on the theoretical study a prototype apparatus has been designed and constructed. The system allows for flexibility in the loading of adsorbent material, geometrical properties and gas used. Preliminary experimental results are reported and interpreted based upon the theory of acoustics described above.

Acknowledgements

I wish to express my gratitude to Professor Stefano Brandani for the scientific guidance and for the support during these years. I wish to acknowledge Professor Douglas Ruthven and Dr. George Manos for helping me to finalize the work.

My warmest thoughts to my parents Giuseppe and Anna, and my sister Grazia for their continuous encouragement.

I sincerely thank my office-mates Alfeno, Gianluca, Giovanna and Prim for their companionship.

I'm in debt to Xiu-Yan for helping me with the fitting of the experimental apparatus and hosting me in his house and to Professor Scott Fogler for giving me the possibility to work in his best-selling book.

Many thanks to the departmental friends especially Andrea, Carlos, Sarah and the friends at Lunch-Box: Wan, Ding and Joselo.

I would like to remember some of the friends with whom I spent my free time: Karin, Laetitia, Jeiran, Giulio, Chriss, Hai-Tao, Elise, Giovanna, Achint, Lapas (Bow), Andrei, Michele, Panos, Alessandra, Ivan, Dr Lee.

Contents

Chapter1. Measurement of Diffusivity in Zeolites: Fundamentals and Experimental techniques

Chapter2. Frequency Response Method to Study Diffusion in Microporous Solids

Chapter3. A Model for Sound Propagation in Presence of Microporous Solids

Chapter4. Parametric Study of the Model

Chapter5. A Prototype Experimental Apparatus and Preliminary Experimental Results

List of Figures

Chapter 1

Chapter 2

Chapter 3

Chapter 4

Fig.4.3 AC as function of s

Fig.4.4 PS as function of s

Fig.4.5 Reduced Frequency as function of the Shear wave number (s).

Fig.4.6 Module of Gq as function of k_d

Fig.4.7 ACads as function of k_d

Fig.4.8 Region of validity of Isothermal Adsorption, Classic and Ideal Sound Propagation (ISP).

Fig.4.9 Real Part of the Non Isothermal factor as function of the reduced diffusive frequency. Isothermal Adsorption.

Fig. 4.10 Real Part of the Non Isothermal factor as function of the Reduced Diffusive Frequency

Fig.4.11 Real Part of the Non Isothermal factor as function of the ΔH_{dim} for $k_d \rightarrow 0$.

Fig.4.12 Non Isothermal factor as function of the ΔH_{dim}

Fig.4.13 Real part ratio of the non-isothermal adsorption factor as function of the ΔH_{dim}.

Chapter 5

Fig. 5.12 Amplitudes as function of the frequency for CO_2

Fig. 5.13 Amplitudes as function of the frequency for air

Fig. 5.14 Amplitudes as function of the frequency for Helium

Fig. 5.15 Amplitudes as function of the frequency for N_2

Fig. 5.16 Normalised Amplitudes as function of the number of samples for CO_2

Fig 5.17 Normalised Amplitudes as function of the number of samples for Helium

Fig. 5.18 Improved Apparatus (Taken from ASTM E1050-98)

List of Tables

List of Symbols[1]

A*	marked molecule , mol
A	Langmuir equilibrium constant (3), - or component A (1), mol Relative amount adsorbed (2), -
a	adsorbent ratio surface-volume (3), m^{-1} or external-internal surface ratio (2), -
a_o	ideal sound velocity , m/s
a_T	Temperature Linearized Equilibrium constant,
a_p	Pressure Linearized Equilibrium constant,
B	amount of adsorbate molecules, mol
b	Langmuir equilibrium parameter , m^3/mol
c_A	concentration of the component A, mol/m^3
c_{A^*}	concentration of the tracer component A* , mol/m^3
c_B	concentration of the component B , mol/m^3
C_p	molar heat capacity of fluid (P=const) , J/(mol· K)
Cp_{hm}	homogeneous medium thermal capacity , J/(m^3· K)
C_s	average volumetric heat capacity of solid-adsorbate , J/(m^3· K)
C_V	molar heat capacity of fluid phase (V=const) J/(mol· K)
c	total molar concentration , mol/m^3
C	sound velocity , m/s
D	transport diffusivity, m^2/s
D_L	axial dispersion
D_A	diffusivity of a sorbate A in a microporous solid , m^2/s
D_{AB}	diffusivity in a mixture A-B , m^2/s
D_{self}	self diffusivity , m^2/s
D_{tracer}	tracer diffusivity , m^2/s
D_0	corrected diffusivity , m^2/s
D_∞	limiting diffusivity, m^2/s
D_p	macropore diffusion, m^2/s
D_{ij}'	Stephan Maxwell diffusivity, m^2/s
d_{cell}	characteristic size of the cell , m
dG_q	pressure-concentration transfer function
dG_T	Temperature transfer function
f	frequency, Hz
F	volumetric flow (3), m^3/s, Force (5), N
h	half slab distance , m

[1] Numbers in parentheses refer to the chapter in which the symbol is used. Where no chapter reference is given, symbols are common to several chapters.

h_s	slab width, m
J_A	diffusive molar flux of component A (1), mol/(m^2·s)
J_{A^*}	diffusive molar flux of the tracer component A*(1), mol/(m^2·s)
K	Henry's law adsorption equilibrium constant defined in terms of sorbate pressure, s^2/m^2 (3) and dimensionless equilibrium constant (1)
K_C	dimensionless equilibrium constant, solid volume basis
K_p	equilibrium constant based on the pressure,
K_T	equilibrium constant based on the temperature,
k	reduced frequency (3)
k_{-A}	surface resistance rate constant (2), s^{-1}
k_f	external mass transfer rate (1) , s^{-1}
L	straight Onsanger phenomenological coefficient (1), half slab width (2), m tube Length (5), m
L_x	cross Onsanger phenomenological coefficient
n	polytropic constant (3) and (4), - n, - integer (1)
n_{ads}	amount of adsorbed molecules , mol
N_A	molar flux of component A , mol/(m^2·s)
N_B	molar flux of component B , mol/(m^2·s)
P_p	macropore pressure , Pa
p_e	equilibrium pressure, Pa
p	pressure (1)-(5), pa or relative pressure perturbation (2)-(4), -
p_t	total pressure (1), pa
$\overline{p}$	pressure , Pa
p_s	equilibrium pressure , Pa
Q	dimensionless adsorbate concentration (3), -
q	adsorbate concentration (1), (2) and , Kg/m^3 or concentration relative perturbation (3), -
$\overline{q}$	adsorbate concentration (4), -
q_s	equilibrium adsorbate concentration (4), Kg/m^3 or saturation concentration (1), Kg/m^3
q_t	total concentration (1), Kg/m^3
R	process rate (2), mol/s
R	Gas Constant, J/(mol·K), or Characteristic Acoustic Impedance (5), kg/(m^{2}s)
R_c	Cylinder Radius (2), m
R_s	Sphere Radius (2), m
R_p	particle size (1) (m)
R_0	Specific Gas Constant, J/(Kg·K)
r	radius; radial coordinate (1), m resistance(5), N·s/m
r_c	crystal radius (1), (m)
S	sectional area (5), (m^2)
s	solid concentration (1), Kg/m^3
t	time, s

t_m	mean retention time, s
t_h	Characteristic time thermal surface resistance, s
T	temperature, K
T_e	equilibrium temperature , K
T_0	temperature of reference , K
T_f	temperature of fluid phase , K
T_{hm}	temperature homogeneous medium , K
T_{hms}	equilibrium temperature homogeneous medium , K
T_R	temperature solid surface , K
T_s	equilibrium temperature , K
u	percentage horizontal velocity , -
$\bar{u}$	horizontal velocity , m/s
v	volume relative perturbation (2), - or percentage vertical velocity (4), -
$\bar{v}$	vertical velocity, m/s
V	volume relative perturbation , m^3
$\bar{V}$	Volume , m^3
V_e	equilibrium Volume , m^3
V_f	Fluid-Phase Volume, m^3
V_s	Solid-Phase Volume, m^3
W	auxiliary variable (4), -
x_r	reactance (5), N·s/m
x	axial coordinate (4)-(5), m or molar fraction (1),
x_A	molar fraction of component A (1),
y	auxiliary variable (4),-
z	coordinate (1), vertical coordinate (4), m
Z	Mechanical impedance (5) (N·s/m)
$\langle z^2(t) \rangle$	mean square displacement (1), m

Greek Letters

Γ	propagation constant , -
ΔC	concentration perturbation , mol/ m^3
ΔP	pressure perturbation , Pa
ΔV	volume perturbation , m^3
$-\Delta H$	heat of adsorption , J/mol
δ	characteristic functions
ε	voidage fraction , -
ε_p	macropore porosity , -
Θ	transfer function
θ	total occupancy of the zeolite matrix (1), Laplace variable (3)
ϑ	surface resistance function (2)
ζ	Dimensionless vertical coordinate (4), - surface-intracrystalline resistances ratio (2)
λ	thermal conductibility (4), W/(m·K), wave-length (5), m
λ_w	wave length , m
λ_{hm}	thermal conductibility homogeneous medium , W/(m·K)
μ	chemical potential (1),(3) J/mol; viscosity (4) N·s/m
$\tilde{\mu}_a$	auxiliary variable, -
$\tilde{v}_a$	auxiliary variable, -
ξ	dimensionless horizontal coordinate (4), -
ρ	gas density relative perturbation , Kg/m^3
$\bar{\rho}$	gas density , Kg/m^3
ρ_s	equilibrium gas density , Kg/m^3
ρ_{hm}	average density solid-adsorbate phase , Kg/m^3
τ	dimensionless time , -
φ	pressure-volume phase lag
ψ	sorbate-pressure phase lag
ω	angular frequency, rad/s
Φ_v	viscous dissipation, $1/s^2$

Common Dimensionless Groups

$Ap = \frac{q_s K_p}{p_s} \frac{(1-\varepsilon)}{\varepsilon}$ is the ratio solid-gas phases hold-ups

$G_q(i) = \frac{\tanh\left(\sqrt{k_d i}\right)}{\sqrt{k_d i}}$ transfer function parameter

$\Delta T_{ad} = \frac{|\Delta H| q_s K_p}{(\rho Cp)_{hm} T_s}$ adiabatic temperature fluctuation

$\Delta H_{\text{dim}} = \frac{\Delta H}{RT_s}$ is dimensionless heat of adsorption.

$Cp_r = \frac{\rho Cp}{(\rho Cp)_{hm}} \frac{\varepsilon}{1-\varepsilon}$ gas and solid-adsorbate phases thermal capacities.

$Le = \frac{\lambda_{hm}}{D(\rho Cp)_{hm}}$ ratio between thermal and mass diffusivity.

η Reduced angular frequency

ζ Ratio diffusion – surface resistance

$k = \frac{\omega h}{a_o}$ Reduced frequency

$k_d' = \frac{\omega h^2}{D}$ Diffusive Reduced frequency

$k_\lambda' = \frac{\omega h^2 \rho_{hm} Cp_{hm}}{\lambda}$ Conductive Reduced frequency

$k_d = \frac{\omega h_s^2}{D}$ Diffusion Characteristic Frequency

$k_\lambda = \frac{\omega h_s^2 \rho_{hm} Cp_{hm}}{\lambda}$ Conduction Characteristic Frequency

$\gamma = \frac{Cp}{Cv}$ Ratio at pressure and at volume constant molar heat fluid phase

$s = h\sqrt{\frac{\rho_s \omega}{\mu}}$ Shear wave number

$\sigma = \sqrt{\frac{\mu C_p}{\lambda}}$ Square root of the Prandtl number

Subitamente questo suono uscìo
d'una dell'arche:però m'accostai,
temendo, un poco più al duca mio.
Dante, Canto X, Inferno
Divina Commedia

Chapter 1
Measurement of Diffusivity in Zeolites: Fundamentals and Experimental techniques

1.1 Introduction: Micropore Diffusion

Porous materials have a fundamental role in the chemical and petroleum process industries for reaction (i.e. catalysis) and separation (i.e. adsorption) purposes. The diffusion of sorbates in such catalyst or adsorbent can be the rate determining step of the overall reaction or adsorption process (Ruthven, 1984). The type of forces controlling the diffusion through the porous material depends strongly on the ratio pore diameter sorbate molecular diameter (Kärger and Ruthven, 1992).

The IUPAC classification that refers to small gaseous molecules as sorbates, establishes the following ranges for defining porous structures:

Micropores d<20 Å

Mesopores 20Å <d<500Å

Macropores d>500Å

Thereby micropore diffusion is the molecular mass transfer process in porous solids with pore sizes < 20 Å and the diffusing molecule never escapes from the force field of the pore wall, the effects of steric hindrance become important and often dominant and the diffusion is an activated process. The wide range [10^{-8} m^2/s: 10^{-20} m^2/s] of micropore diffusivities is due to the strong dependence of the micropore diffusivity on the sorbate-zeolite structures and interactions, so that no general theories are available as for the diffusion in isotropic media, or molecular and Knudsen diffusion.

Industrial applications based on micropore diffusional effects are zeolite catalysts (catalytic cracking, xylene isomerization, selective disproportionation of toluene, MTG reaction) and diffusion controlled separation processes (separation of linear/branched hydrocarbons, air separation by pressure swing adsorption). The micropore diffusion is the key datum for the appropriate design of reaction and separation units of these processes.

1.2 Micropore Diffusion Measurement

The experimental measurement of micropore diffusion is a standard approach for understanding the diffusional mechanism in a zeolite-sorbate system and for obtaining data for the design of industrial processes. The experimental techniques are usually classified as *macroscopic* and *microscopic* methods depending on whether the measured quantity is the mass flux at the surface of a crystal or the mean squared displacement of molecules inside the crystals. As a result macroscopic techniques typically yield Fickian diffusivities, while microscopic techniques yield self-diffusivities. An excellent review of both approaches and the results up to 1992 is available in the reference book by Kärger and Ruthven (1992), and additional reviews of macroscopic methods are also available (Rees, 1994; Ruthven and Brandani, 1997; Ruthven, 1997).

Fig.1.1 shows the historical development of these experimental techniques. From the first recorded experimental measurement (Tiselius, 1934) to the early 70s the *uptake rate measurement* (Barrer, 1978) has been the most widely applied technique. The introduction of the PFG-NMR (Kärger, 1971) has clearly introduced a dramatic change, since in many cases the new measurements resulted in diffusivities that were orders of

magnitude higher than those previously reported in the literature. This has led to an increased effort in the development of new techniques over the past thirty years and also to a careful reanalysis of the assumptions used in the previous measurements.

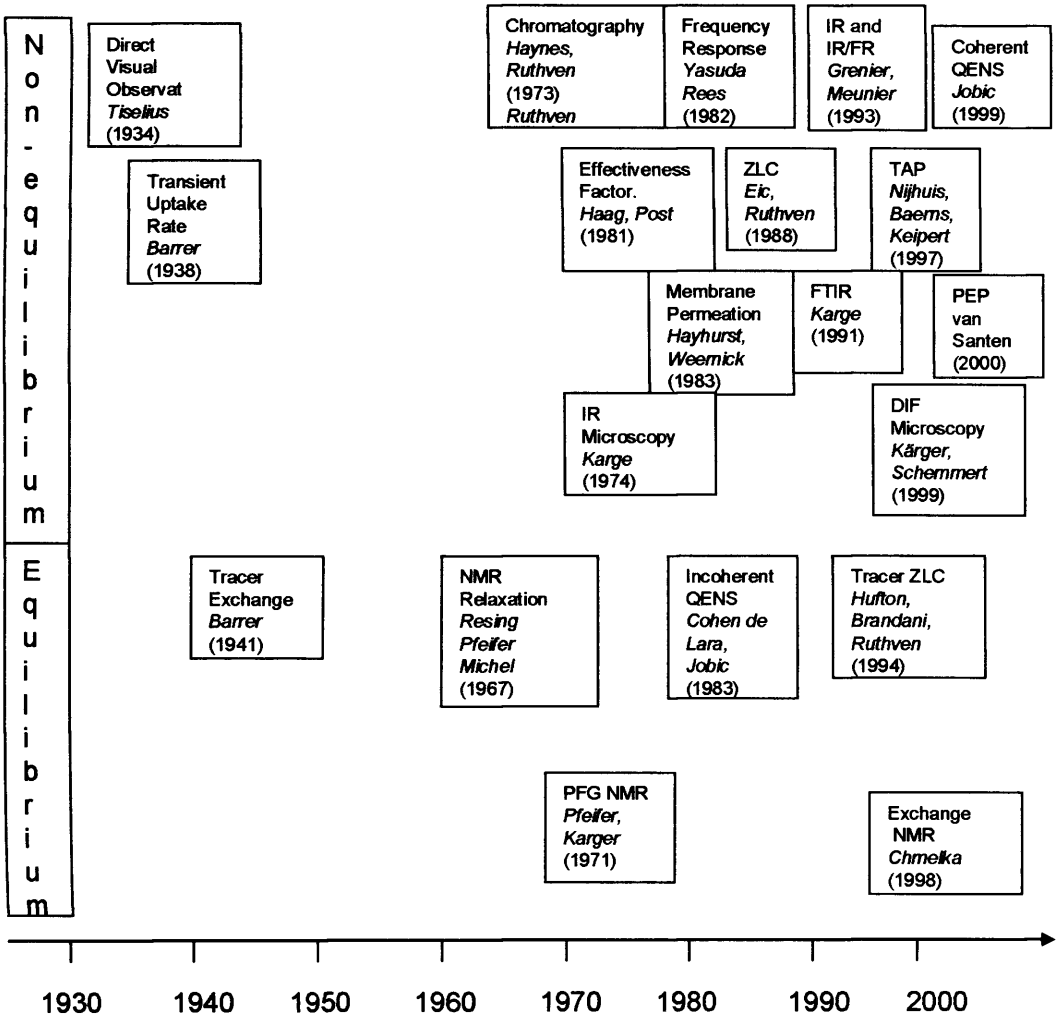

Fig.1.1 Historical development of diffusion in microporous solids (Kärger, 2003).

When comparing the different techniques it is useful to consider that different approaches lead to different diffusivities. Figure 1.2 shows a schematic representation of the conditions that lead to transport, tracer and self diffusion. In this contest it is important to underline also that time (i.e. ≥s) and length scales (i.e. ≥ μm) involved in

the macroscopic techniques are generally longer than the microscopic ones (i.e. ms; nm to μm).

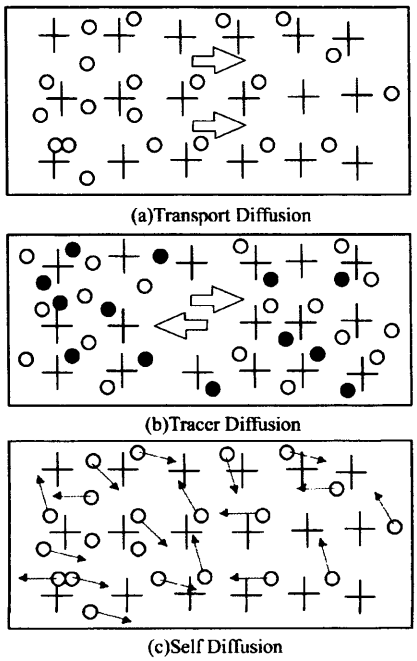

Fig.1.2 Transport Diffusion (a), Tracer Diffusion (b) and Self-Diffusion (c) (Kärger and Ruthven, 1992)

It is useful at this point to include a brief definition of the various diffusivities that can be measured in microporous solids (Ruthven, 2003), which will be followed by an overview of the most common experimental techniques.

1.2.1 Micropore Diffusivities

Irreversible thermodynamic considerations (Prigogine, 1971) and experimental proof (Haase and Siry, 1968) show that the driving force for the diffusive flux is the chemical potential.

For the diffusion of a single component in a porous adsorbent, under isothermal conditions:

$$J = -L\frac{\partial \mu}{\partial z} \tag{1}$$

where L is the Onsanger phenomenological coefficient in the presence of a concentration gradient and μ is the chemical potential of the adsorbate.

Analogously for the self-diffusion of a single component in a porous adsorbent

$$J = -L\frac{\partial \mu}{\partial z} - L_x\frac{\partial \mu^*}{\partial z} \tag{2}$$

Where L and L_x are the straight and cross Onsanger phenomenological coefficients in the absence of a gradient of concentration. μ and μ^* are the chemical potentials of the adsorbate and of the "marked" adsorbate .

1.2.2 Transport Diffusivity

Mass transfer due to a concentration gradient in a microporous solid (Fig.1.2.a) is governed by transport diffusion and the diffusive flux is traditionally expressed in terms of Fick's equation:

$$N = -D\frac{\partial q}{\partial z} \tag{3}$$

where D is the transport diffusivity and q is the concentration of the adsorbate. This diffusion and the diffusivity coefficient associated are conceptually similar to the more familiar situation of diffusion of two components in a fluid phase. Diffusion in a porous solid can be regarded as a special case of binary diffusion in which the diffusivity of one component (the solid) is zero. The possibility of a concentration gradient for a pure

component diffusing in a microporous solid under isothermal and isobaric conditions is determined by the framework of the solid.

Consequently the constitutive equation for the mass flux (Eq.3) has been derived from the constitutive equation for the mass flux of two components in a homogeneous phase (Kärger and Ruthven, 1992).

The molar flux relative to stationary coordinates of a component A in a mixture of A and B is given by:

$$N_A = x_A(N_A + N_B) + J_A \tag{4}$$

Where J_A represent the diffusive flux relative to the plane of no net molar flux:

$$J_A = -D_{AB} c \frac{\partial x_A}{\partial z} \tag{5}$$

It can be noted that D_{AB} is in principle a function of concentration and that Eq.(5) implies only that it is not a function of concentration gradient.

In extending Eq. (5) to the diffusion of a sorbates (q) in to a microporous solid (s), because of the rigid framework $N_s = 0$, and eqs (4) and (5) become respectively:

$$N = xN + J \tag{6}$$

$$J = -D(q+s)\frac{\partial x}{\partial z} \tag{6B}$$

Observing that $x = \frac{q}{q+s}$ and introducing Eq. (6B) in Eq. (6), after differentiation respect the spatial coordinate with s constant we obtain Eq. (3).

It is therefore clear that the diffusivity (D) defined according to Eq. (3) is consistent with D_{AB} defined according to Eq. (5).

Comparing Eq.(1) with Eq.(3) and assuming μ equal to the one of the ideal gas phase in equilibrium: $\mu = \mu(T) + RT\ln(P)$, we have

$$D = LRT\frac{\partial \ln(P)}{\partial q} \tag{7}$$

Eq. (7) relates the transport diffusivity D to the Onsanger phenomenological coefficient L.

1.2.3 Corrected Diffusivity

To clarify the physical meaning of the transport diffusivity, Eq. (7) is usually rewritten as

$$D = D_0\left(\frac{\partial \ln P}{\partial \ln q}\right)_T \tag{8}$$

$D_0 = LRT$ is referred to as corrected diffusivity and is a mobility coefficient. $\left(\frac{\partial \ln P}{\partial \ln q}\right)_T$ is a thermodynamic correction called the Darken correction factor (Darken, 1948) and is related to the driving force of diffusion. The Darken factor typically shows a strong concentration dependence, and as a result D_0 has a smaller variation with concentration than D. In many practical applications the transport diffusivity is determined using the assumption that the corrected diffusivity is constant and the knowledge of the equilibrium isotherm allows the calculation of the concentration dependence of D.

Considering for instance the Langmuir Isotherm:

$$D = D_0\left(\frac{\partial \ln P}{\partial \ln q}\right)_T = \frac{D_0}{1 - q/q_s} \tag{9}$$

shows that approaching the saturation limit ($q \to q_s$), the Darken factor and the resulting transport diffusivity go to infinity.

Eq. (9) also shows that in the dilute region where Henry's law is valid, $\left(\frac{\partial \ln P}{\partial \ln q}\right)_T \to 1$ and $D \to D_0$.

The temperature dependence of D is generally expressed in terms of the Eyring equation (1935),

$$D = D_\infty e^{-E/RT} \tag{10}$$

where E is the activation energy. However because of the concentration dependence of the diffusivity implicit in Eq. (8), it is appropriate (Ruthven and Loughlin, 1971) to correlate D_0 and the Darken factor independently with T, i.e.

$$D_0 = D_\infty e^{-E/RT} \tag{11}$$

1.2.4 Stefan Maxwell Diffusivity

The Stefan-Maxwell diffusion model is based on hydrodynamical phenomenological equations, the coefficient D_{ij} are evaluated in terms of a molecular model. The validity of Stefan assumption regarding the relations between the coefficients (D_{ij}=D_{ji}) hold to first approximation in the gas kinetic theory. (Hirschfelder et al., 1954; Truesdell, 1962). Krishna (1990) has extended this model to microporous diffusion considering the vacancies as an additional component and neglecting the transfer of momentum to the adsorbent. The resulting set of parameters (D_{ij}) has a microdynamic significance and is equivalent to the phenomenological coefficient (L) of irreversible thermodynamics:

D_{ij}' : reflects the rate of direct exchange between two sorbates i and j

D_{iv}': reflects the rate at which sorbate i exchanges positions with adjacent vacancies v.

For the diffusion of a sorbate (q) in a zeolite (s):

$$D_{qq}' = L\frac{RT}{q}\frac{\partial \ln p}{\partial \ln q} = D \tag{12}$$

$$D_{qv}' = L\frac{RT}{q} = D_0 \tag{13}$$

and the diffusive flux is given by:

$$J_1 = -D_{qq}'\frac{dq}{dz} = -D_{qv}'\frac{\partial \ln p}{\partial \ln q}\frac{\partial q}{\partial z} \tag{14}$$

The Stefan-Maxwell model allows the correlation of a wide range of patterns of concentration dependence of self and transport diffusivity.

1.2.5 Self-Diffusivity.

The random walk of molecules under equilibrium conditions (Brownian motion in the absence of a concentration gradient, Fig.1.2c) can be expressed terms of the self-diffusivity (Einstein, 1905). In one-dimensional form:

$$D_{self} = \frac{\left\langle z^2(t)\right\rangle}{2t} \tag{15}$$

Where $\left\langle z^2(t)\right\rangle$ is the mean square displacement and equivalently:

$$J^* = D_{self}\left.\frac{\partial q^*}{\partial z}\right|_{q_t = q+q^* = const} \tag{16}$$

Where the apex (*) indicates labelled molecules.

The significance of D_{self} can be clarified considering the situation in which there is a non-uniform distribution of marked molecules (*) (Kärger, 1973) within a uniform total concentration (See Fig.1.2.b, tracer experiment).

The fluxes of q and q^* (tracer) are given by Eq. (2) and:

$$J^* = -L^* \frac{\partial \mu^*}{\partial z} - L_x \frac{\partial \mu}{\partial z} \tag{17}$$

Introducing $\frac{\partial \mu}{\partial z} = \frac{RT}{q} \frac{\partial q}{\partial z}$ in eqs (2) and (17) and comparing these with Eq. (15) it possible to verify:

$$D_{self} = D_{tracer} = RT\left\{\frac{L}{q} - \frac{L_x}{q^*}\right\} \tag{18}$$

1.2.6 Self-Diffusivity and Transport Diffusivity

The relationship between D and D_{self} is obtained considering again the situation in which there is a non-uniform distribution of marked molecules (*) (Kärger, 1973) but in the presence of a concentration ($q_t = q+q^*$) gradient (See Fig.1.2.a, transport diffusion).

$$\frac{D_{self}}{D} = \frac{\partial \ln q_t}{\partial \ln p_t}\left[1 - \frac{q_t^2}{qq^*}\frac{L_x}{L}\right] \tag{19}$$

Comparing Eq. (19) with Eq. (8) (Darken equation) it follows that in the limit of low concentration:

$D \to D_0 \to D_{self}$;

While at finite loading the corrected and the self diffusivities coincide if the cross coefficient L_x can be neglected.

The analogue relation of Eq. (19) in terms of the Stefan-Maxwell model is given by:

$$\frac{D_{self}}{D} = \frac{\partial \ln q_t}{\partial \ln p_t}\left[1-\theta\left(1-\frac{D_v'}{D_{qq}.'}\right)\right]^{-1} \tag{20}$$

Where θ is the total occupancy of the zeolites matrix, $D_{qv}' = D_{q.v}' = D_v' = D_0$ the mobility and $D_{qq}.'$ the interchange coefficient.

On the basis of Stefan-Maxwell theory, Pasheck and Krishna (2001) have suggested at finite loadings the practical assumption $D_{qq}.' = D_0$ and obtained the following relation:

$$D_{self} = \frac{1}{\left(\frac{1}{D_0}+\frac{\vartheta}{D_0}\right)} \tag{21}$$

Eq. (21) has been validated using kinetic Monte Carlo simulations for the systems: methane, perfluoromethane and 2-methilhexane in silicalite.

This relation implies that at finite loading the corrected diffusivity is larger than the self diffusivity, which is a useful result when comparing results from macroscopic and microscopic techniques.

1.3 Experimental Techniques

In the measurement of Tiselius (1934) the variation of water profile in a sample of natural huelandite was monitored on the basis of the double refraction of light. The transport diffusivity was obtained indirectly using the appropriate mathematical model for the diffusion problem (Kärger and Ruthven, 1992).

In the *Uptake Measurement* (Barrer, 1938) the average concentration over a particle is monitored gravimetrically or volumetrically, after having subjected the sample under study to a pressure step in the surrounding atmosphere.

The transport diffusivity is extracted from the uptake curves (m_t/m_∞) comparing the experimental results with the mathematical model; the amplitude of the pressure step is generally small so that the diffusivity can be assumed constant (differential diffusivity). The main problem with this technique is that the measurement has to be performed in conditions so that the microporous diffusivity is the rate controlling step; for large crystals (long diffusional time) it is generally possible to achieve these conditions, but when sorption rates are rapid the uptake may be controlled by extracrystalline diffusion and/or heat transfer. Extracrystalline diffusion is due to the diffusion in the macropores of an adsorbent pellet and/or the diffusion trough the bed of particles. The heat transfer resistances are the conduction and radiation from the solid to the fluid, and the conduction in bed of particles and in the fluid. From the analysis of the shape of the uptake curve it is not always obvious how to detect the intrusion of such effects. Changing the sample quantity or the sample configuration is a common way to verify if intracrystalline diffusion is the controlling process (Kärger and Ruthven, 1992).

The indirect approach is generally simpler than measurements where the concentration gradient and the flux are directly measured and the diffusivity obtained from Eq. (3). *Membrane Permeation* (Hayhurst and Weernick, 1983) is a direct measurement of the transport diffusivity. Problems arise in the preparation of the zeolite membrane and in ensuring a perfect seal.

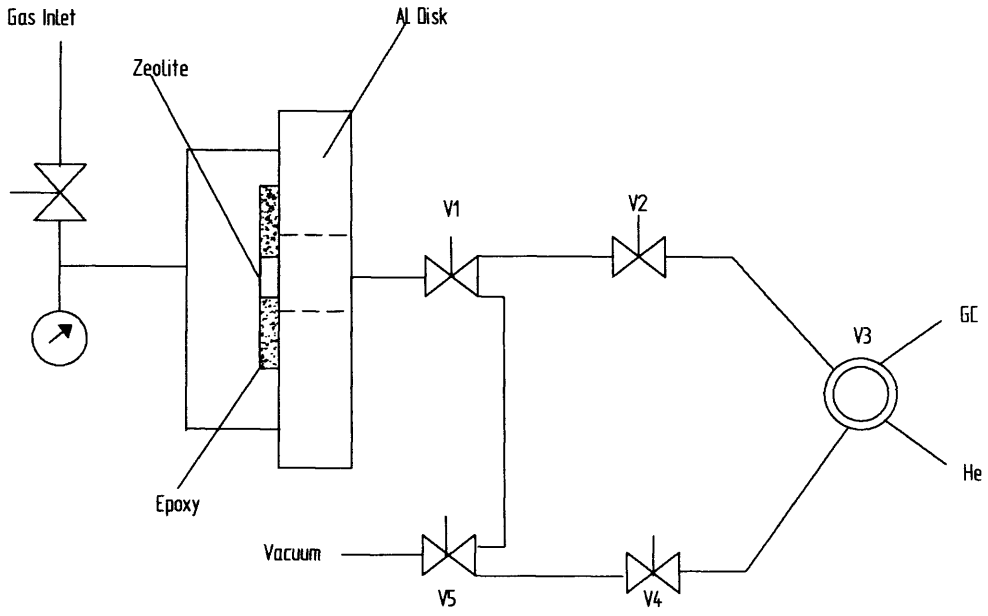

Fig. 1.3 Membrane Permeation (adapted from Kärger and Ruthven, 1992)

In 1971 the introduction of the pulsed field gradient technique of *NMR spectroscopy* (PFG NMR) (Kärger and Caro, 1974) allowed the measurement of the self-diffusivity in microporous solids.

In this technique, by recording the time dependence of the Larmor frequency of NMR-active nuclei, one is able to determine the propagator of the diffusants or, more accurately, of the nuclei under study. The propagator is the probability density function that represents the probability of finding at time t a random walker in the volume dr, at a distance r from the starting point. This technique has essentially no upper limit, but the smallest diffusivities still accessible are on the order of 10^{-14} m^2 s^{-1}.

The quasi-elastic neutron scattering (QENS) has been introduced more recently (Cohen de Lara et al., 1983). This technique is based on the analysis of the quasi-elastic broadening in the energy of the scattered neutron beam and variants of this technique allow the direct measurement of the transport diffusivity (Jobic et al., 1999).

Although a strict comparison between the uptake rate measurement and the microscopic techniques is possible only in the region of low concentration or between D_0 and D_{self} with the uncertainty associated with the estimation of the correction factor (See 1.2.5), the reanalysis of the uptake measurements obtained before the introduction of the PFG-NMR technique has shown that in many cases they were controlled by processes different from intracrystalline diffusion (Kärger, 2003).

For fast diffusing systems the limitations imposed by extracrystalline resistances to mass and heat transfer make it a challenge to derive reliable intracrystalline diffusivity values from direct sorption rate measurements, regardless of the technique used to follow the uptake. Based on the consideration that in flow systems both mass and heat

transfers are enhanced, in the early 70s the *chromatographic method* was introduced (Haynes and Sarma, 1973; Shah and Ruthven, 1977).

In the usual chromatographic experiment a steady flow of an inert (no adsorbing) carrier is passed through a small column packed with the adsorbent under study. At time zero a small pulse of sorbates is injected at the column inlet and the effluent concentration is monitored continuously.

However, the analysis of the chromatographic experiment has two additional problems compared to the uptake experiment: 1) the time domain solution is complex 2) The presence of the axial dispersion introduces an additional parameter.

To avoid the need to use the full time solution, the experimental curves are typically analysed based on the moments of the breakthrough or pulse response. The retention volume or mean retention time (first moment) is a measure of the adsorption equilibrium:

$$t_m = \frac{l}{v}\left[1+\left(\frac{1-\varepsilon}{\varepsilon}\right)K\right] \text{ (Biporous adsorbent)} \tag{22}$$

$$K = \varepsilon_p + (1+\varepsilon_p)K_c \tag{23}$$

K_c is the dimensionless equilibrium constant, expressed on a solid volume basis and K is the corresponding value on a particle volume basis.

The dispersion of the response peak (second moment about the mean) is determined by the combined effects of mass transfer resistance and axial mixing in the column and in dimensionless form is given by (Ruthven, 1984):

$$\frac{\sigma^2}{2t_m^{\,2}} = \frac{D_L}{vl} + \frac{\varepsilon v}{l(1-\varepsilon)}\left[\frac{R_p}{3k_f} + \frac{R_p^2}{15\varepsilon_p D_p} + \frac{r^2(K-\varepsilon_p)}{15K^2 D}\right]\left[1+\frac{\varepsilon}{(1-\varepsilon)K}\right]^{-2} \tag{24}$$

To separate the axial dispersion (D_L) and mass transfer contributions (k_f: external mass transfer rate D_p: macroporous diffusion) the experiments have to be carried out at different fluid velocity (v) and different particle size (R_p). This imposes an upper limit on the diffusional time constant r^2/D that can be measured since, if intraparticle diffusion is too rapid the contribution from axial dispersion becomes dominant and it is then impossible to extract reliable kinetic data.

The *Zero Length Column* (ZLC) (Eic and Ruthven, 1988) method is a chromatographic technique that eliminates the uncertainty due to axial dispersion, because the length of the column is short enough that the assumption of a uniform axial concentration is generally valid. A small sample of the adsorbent is equilibrated at a uniform sorbate concentration, preferably within the Henry's Law range, and then desorbed by purging with an inert gas at a flow rate high enough to maintain essentially zero sorbate concentration at the external surface of the particles or crystals. The desorption rate is measured by following the composition of the effluent gas.

A further advantage of the ZLC technique compare the traditional chromatographic method is that analysis is carried out directly in the time domain:

$$\frac{c}{c_0} = 2L\sum_{n=1}^{\infty}\frac{\exp\left(-\beta_n^{\,2}Dt/r^2\right)}{\left[\beta_n^{\,2}+L(L-1)\right]} \tag{25}$$

Where $L = \frac{1}{3}\frac{Purge Flow rate}{Crystal volume}\frac{r_c^2}{D}$ and β_n is given by the roots of the transcendental equation,

$$\beta_n \cot\beta_n + L - 1 = 0$$

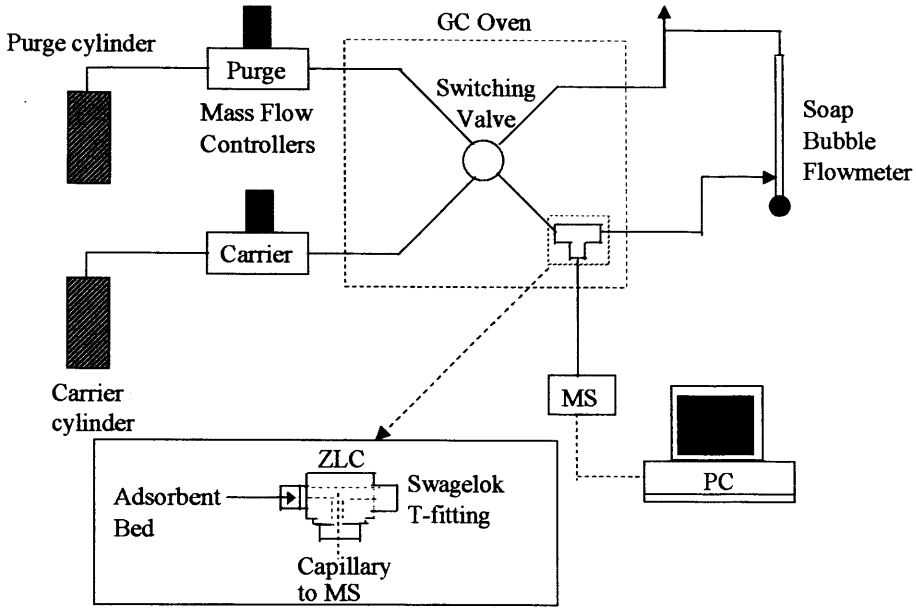

Fig. 1.4 ZLC experimental setup

The diffusional time constant can be extracted from the desorption curves in several different ways (Brandani and Ruthven, 1996; Brandani, 1998).

The versatility of the ZLC technique has been confirmed by various experimental studies (see for example Hufton et al., 1994; Brandani et al., 1996; Brandani et al., 1997; Brandani et al., 2000).

The *Frequency Response (FR)* (Yasuda, 1976) differs from the uptake rate and the chromatographic measurements because it is a pseudo-stationary method. It is one of the best macroscopic techniques and since the main aim of this study is the extension of this approach to higher frequencies a detailed review of this method is presented in Chapter 2.

1.4 Summary

The experimental results obtained with macroscopic and microscopic techniques are compared typically on the basis of Eq. (8) (Kärger and Ruthven, 1989). For several systems the results obtained by macroscopic and microscopic techniques are in agreement (e.g. Zeolite A) for a comparable number of systems there are discrepancies (e.g. NaX- benzene). For instance the NMR self-diffusivity for aromatics in NaX are two order of magnitude larger than the corrected diffusivity obtained with macroscopic techniques. These discrepancies have been attributed usually to different effects: Heat effects, External diffusional resistance, errors in analysis of macro rate data, Surface barrier resistance, Mobile-Immobile phase behaviour, Structural defects (Kärger and Ruthven, 1992), but no explanation seems completely convincing.

Obstacles in the comparison between macroscopic and microscopic techniques are also due to the fact that there is only a limited overlap where both approaches yield reliable results. The microscopic techniques have a limit on the slowest process that can be followed, while macroscopic methods have an upper limit of the diffusional time constant that can be determined, especially for strongly adsorbed components. This also implies that experimental investigations are limited to the use of large crystals and there is a clear need to extend macroscopic measurement to faster time constants in order to allow a better comparison with microscopic techniques and also to allow the detailed study of diffusion in small commercial crystals. The aim of this study is to extend the frequency response technique by considering the interaction between sound and an adsorbent material, which should allow the development of novel macroscopic

techniques which will result in an increase by several orders of magnitude of the range of diffusional time constants that can be investigated.

Chapter 2
Frequency Response Method to Study Diffusion in Microporous Solids

2.1 Introduction: Relaxation Techniques for Measuring Microporous Diffusivity

When a system at equilibrium is perturbed, self-adjustment to a new equilibrium state usually occurs (Bernasconi, 1976). The adjustment of the system to the new equilibrium conditions is a consequence of the dynamic nature of the equilibrium.

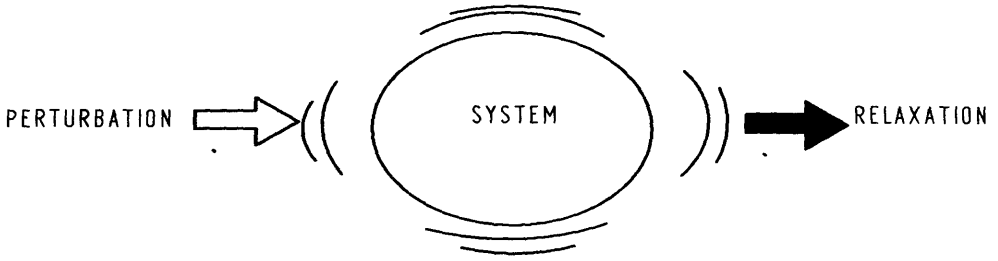

Figure 2.1 Principle of relaxation method (adapted from Yasuda, 1994).

The rate of this adjustment or the rate of "physicochemical relaxation" is the rate of the many processes that make up the equilibrium. Thus, by measuring the rate of physicochemical relaxation one can obtain the necessary information for an evaluation of the kinetic parameters.

Relaxation kineticists have used two different types of experimental approaches in studying physicochemical relaxation. The first involves a single perturbation of a physicochemical system at equilibrium, brought about by a sudden change of an external parameter such as temperature, pressure, or concentration (pulse or step-

method). The second class of techniques is known as stationary methods and the frequency response (FR) method falls in this class of techniques. Here the physicochemical system is subjected to an oscillating forcing function or oscillating perturbation interaction between the forcing function and the chemical system. This can lead to an oscillation in the position of the equilibrium, with a phase lag that depends on the relation between the physicochemical relaxation time and the frequency of the forcing function. At the same time energy is absorbed by the system. The relaxation time can be determined by an analysis of the absorbed energy or the phase lag.

The transient macroscopic techniques considered in Chapter 1 are in fact relaxation techniques (See Fig. 2.2.):

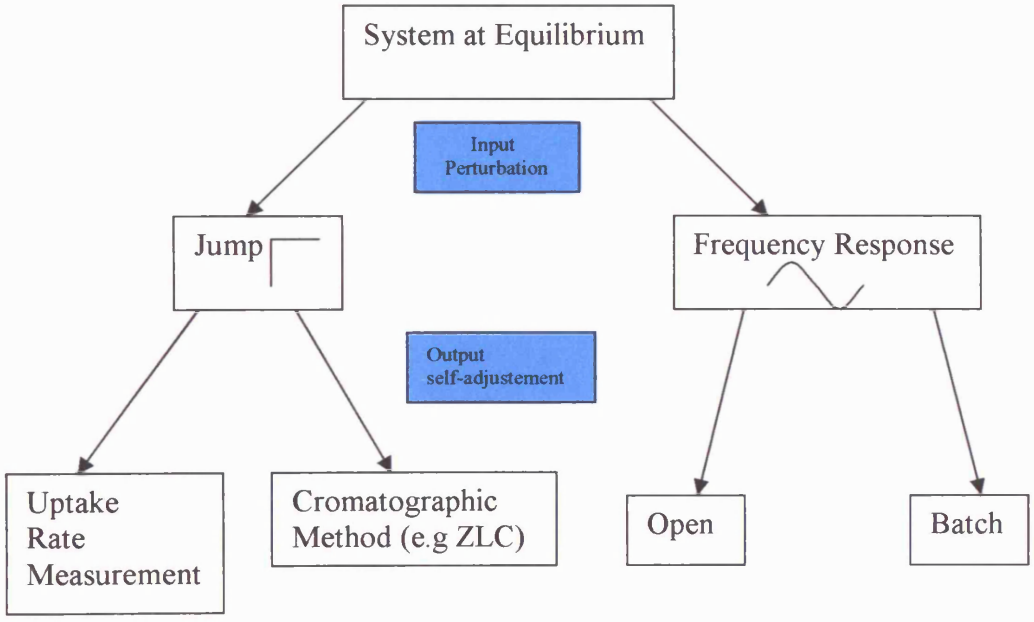

Figure 2.2 Relaxation Techniques applied to measure microporous diffusivity.

Although the choice of the appropriate technique depends on the specific characteristic of the sorbate-adsorbent system, Naphtali and Polinski (1963) and Yasuda (1994) have

underlined that increasing the complexity of the system the FR is more advantageous due to the higher sensitivity of the response compared to step or pulse methods.

2.2 Frequency Response: Open and Batch systems

The frequency response techniques (Yasuda, 1994), which have been applied to study mass transfer kinetics in a gas/surface system, may be divided into two groups. See Fig.2.3

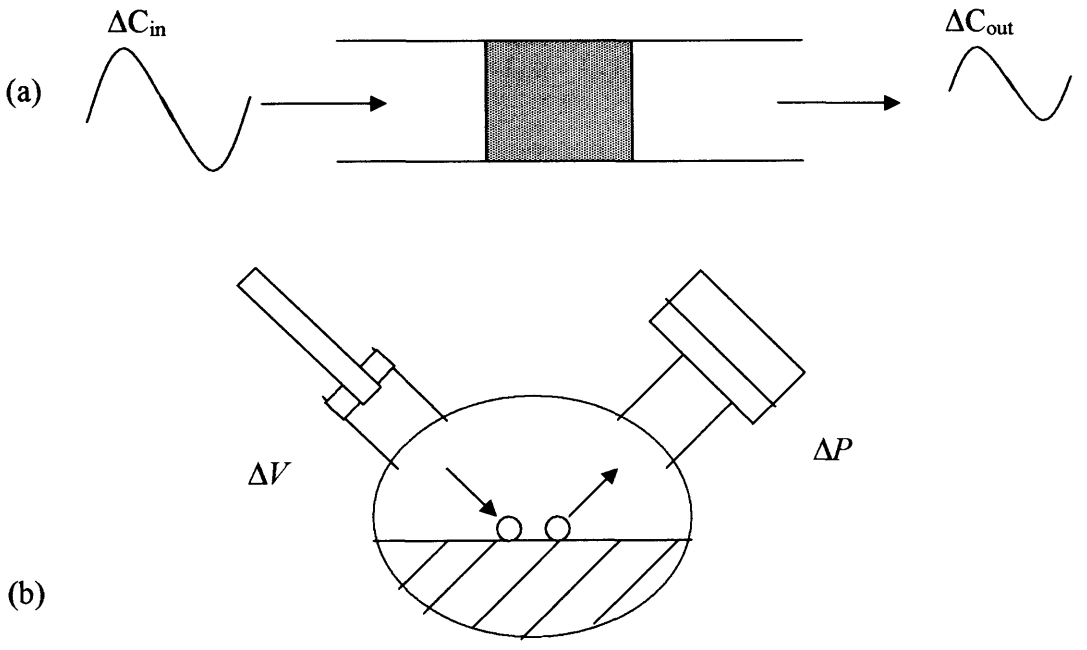

Figure 2.3 Frequency response techniques: (a) flow system (b) batch system. Adapted from Yasuda (1994).

In one group (a), the concentration at the inlet of a packed bed, $\Delta C_{in}(t)$ is varied sinusoidally in a flow system and the response is obtained from the data of $\Delta C_{out}(t)$ at

the exit. In the other group, (b), the gas space of a batch system is varied sinusoidally and the response is obtained from the pressure signal, $\Delta P(t)$, in the chamber.

The study of Boniface and Ruthven (1985) proposed an open system FR where the input sinusoidal concentration signal was obtained de-tuning an electronic flow control valve. Mass transfer kinetics and the adsorption equilibrium constant for bi-porous adsorbent systems were obtained. This study confirmed the capability of the FR to discriminate among different mass transfer resistances.

The theoretical analysis of Park et al. (1998), has considered different continuous and semi-batch configurations. Recently Sward and LeVan (2003a; 2003b) proposed an FR technique in which analogously with the batch techniques the controlled variable is the pressure instead of the concentration. However the difficulty in setting up an experimental system which will provide a sufficiently pure sinusoidal concentration or pressure at the adsorption column inlet has generally limited the interest in group (a) techniques. For instance the range of frequencies investigated by Boniface and Ruthven is (0.01-0.6 Hz) and in the system of Sward and LeVan (2003a), the upper frequency limit is 1.25 Hz.

The batch FR (group b) to study gas-solid dynamics was introduced by Naphtali and Polinski (1963). They presented a frequency spectrum for the nickel-hydrogen system where the pulse method failed to separate the complex adsorption phenomena occurring simultaneously but with different settling times on the catalyst surface.

Evnochides and Henley (1970) considered the FR to study diffusion of ethane in Polyethylene. In their system the adsorbed quantity was measured gravimetrically using a microbalance. Yasuda (1976) has reconsidered the theoretical analysis of Naphtali and Polinski (1963) introducing the **characteristic functions** for the determination of adsorption kinetic parameters for the Ethylene-Zinc Oxide system.

Applying the solution of Evnochides and Henley, Yasuda (1982) extended the method to the determination of vapour diffusion coefficients in Zeolites, monitoring the pressure in the system by a membrane gauge (See Fig. 2.4).

2.3 Basics of the batch FR

When a linear system is subjected to a harmonically varying input, the system output response, after a long time also exhibits harmonic behaviour with the same frequency. The response has, however, smaller amplitude and a phase lag due to finite internal transport/reaction rates. The FR method to study mass transfer kinetics measures the pressure response or the temperature (PFR or TFR (Bourdin et al. (1998)) of a closed sorption system to a periodic volume change.

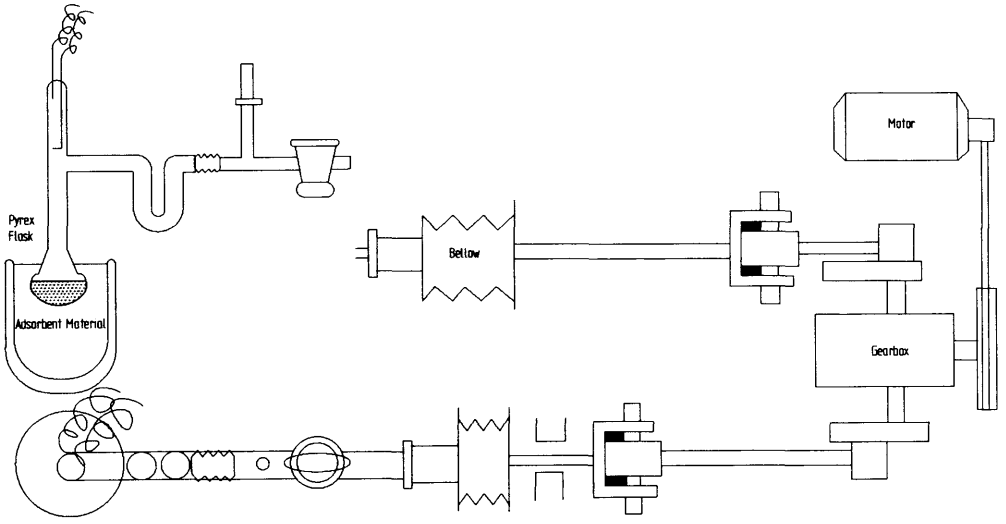

Figure 2.4 Schematic diagram of the original frequency response apparatus.

A comparison of the theoretical and the experimental amplitudes and phase lags allows the identification of the controlling transport mechanisms.

Fig.2.4 shows the apparatus of Yasuda (1976). The adsorbent is inserted in a Pyrex flask and equilibrated with the gas-phase. Pressure variation is followed using a Pirani gauge.

The pairs of pistons and cranks F1 and F2 generate a sinusoidal wave. Gearbox G reduces the speed of revolution. A variable-speed 40-W motor H drives this arrangement. The sinusoidal wave produced could be regarded as practically harmonic. Although this basic arrangement is common to all the FR apparatus (See table 2.1), the main effort of the investigators has been mainly to reduce the response time of the system in order to increase the frequency of the input signal.

Table 2.1 Characteristics of the FR Apparatus.

Apparatus	Volume[1] chamber dm^3	Modulation (% and shape)	Pressure gauge	Frequency Range (Hz)
Yasuda (1982)	~1.120	2.2 sinusoidal	membrane[2]	0.003-0.27
Van-Den-Begin and Rees (1989)	0.78	1 square-wave	differential[3](4 ms)	0.01-10
Bourdin et al. (1998)	0.6	1-2[4] square-wave sinusoidal	Fast Baratron gauge (1ms)	0.001-30
Conner et al. (2001)	0.584	1.5 sinusoidal	Capitance[5]-type	0.005-5

[1] The mean volume of sorption chamber (and the modulation) is not strictly the same at different temperatures
[2] MKS-Baratron, Type 210
[3] differential Baratron pressure transducer
[4] the chamber volume may vary up to 10% by compression of bellows
[5] MKS model 122A

2.4 Mathematical Modelling

An outline of the procedure for obtaining the characteristic functions for the diffusion in a plane sheet (Yasuda, 1982) will be presented.

Consider a sorption system initially at equilibrium:

$$q_e = f(T_e, p_e) \tag{1}$$

If this system is perturbed by a sinusoidal change in volume, Eq.(2), the pressure of the adsorbate diffusing into and out of the zeolite will reach a periodic steady state, Eq.(3):

$$\overline{V} = V_e[1 - V\cos(\omega t)] \tag{2}$$

$$\overline{p} = p_e[1 + p\cos(\omega t + \varphi)] \tag{3}$$

In eqs (1-3) the subscript e denotes the equilibrium value of the variable, the lower case variable preceding the transcendental function, either p or v, is the amplitude ratio, ω is the angular frequency of the perturbation, and φ is the phase lag of the pressure response to the variation in volume. Expressing the perturbations in complex notation: $\delta V = V_e V e^{i\omega t}$ and $\delta p = p_e p e^{i(\omega t+\varphi)}$, the in-phase ($\delta_{in}$) and out-of-phase ($\delta_{out}$) characteristic functions for a plane sheet are derived (Yasuda, (1982)) by combining the Fickian diffusion model, the mass balance, and the locally linear adsorption isotherm of the adsorbate/adsorbent system on the basis of the following assumptions :

1) The system is isothermal
2) The diffusional processes under consideration are Fickian

3) The diffusion coefficients are time and position invariant, and are constant over the induced concentration range.
4) The adsorption at the pore mouth of the micropore follows the Langmuir kinetics with constant adsorption and desorption rate constants.
5) Each sorbent particle is exposed to the same bulk-phase environment, (the pressure is homogeneous throughout the gas space).
6) The sorbent particles are identical to one another.

Yasuda (1994) underlined that assumption 5 is the fundamental assumption in this method, since this assumption allows writing the overall mass balance in the gas phase as:

$$\frac{d}{dt}\left(\frac{\bar{p}\bar{V}}{RT_0}\right)+\frac{dB}{dt}=0 \tag{4}$$

where B represents the adsorbed molecules,

$$B=\int_0^{V_s} q dV_s = B_e\left(1+Ae^{i(\omega t+\phi+\psi)}\right) \tag{5}$$

A and ψ are obtained from the solution of the diffusive problem of a slab whose surface concentrations are in equilibrium with a periodically varying pressure (Carslaw and Jaeger, 1959).

Substituting eqs (2), (3) and (5) and defining $\delta=\frac{\delta V}{\delta p}-1$, Eq. (4) becomes:

$$K\delta=\frac{\delta V}{\delta p}-1 \tag{6}$$

$$K\delta_{in}=\frac{V}{p}\cos\varphi-1 \tag{7}$$

$$K\delta_{out} = \frac{V}{p}\sin\varphi \tag{8}$$

The functional forms are derived in Appendix A and the resulting solution is given by:

$$\delta_{in} = \frac{1}{2\eta}\left\{\frac{\sinh 2\eta + \sin 2\eta}{\cosh 2\eta + \cos 2\eta}\right\} \tag{9}$$

$$\delta_{out} = \frac{1}{2\eta}\left\{\frac{\sinh 2\eta - \sin 2\eta}{\cosh 2\eta + \cos 2\eta}\right\} \tag{10}$$

where the reduced angular frequency η is a function of the angular frequency ω, the thickness of the plane sheet L, and the diffusion coefficient D:

$$\eta = \left(\frac{\omega L^2}{2D}\right)^{1/2} \tag{11}$$

and K is related to the local slope of the adsorption isotherm at p_e and T_e :

$$K = \frac{RT_e}{V_e}\left(\frac{dB}{dp}\right)_e \tag{12}$$

Assumption 4 is not critical, since the batch frequency response technique is a differential technique, the intensity of the frequency spectrum under set experimental conditions is dependent on the local gradient of the isotherm, and
not on the global nature of the isotherm. However the range of pressure that can be studied is limited by the isotherm behaviour.

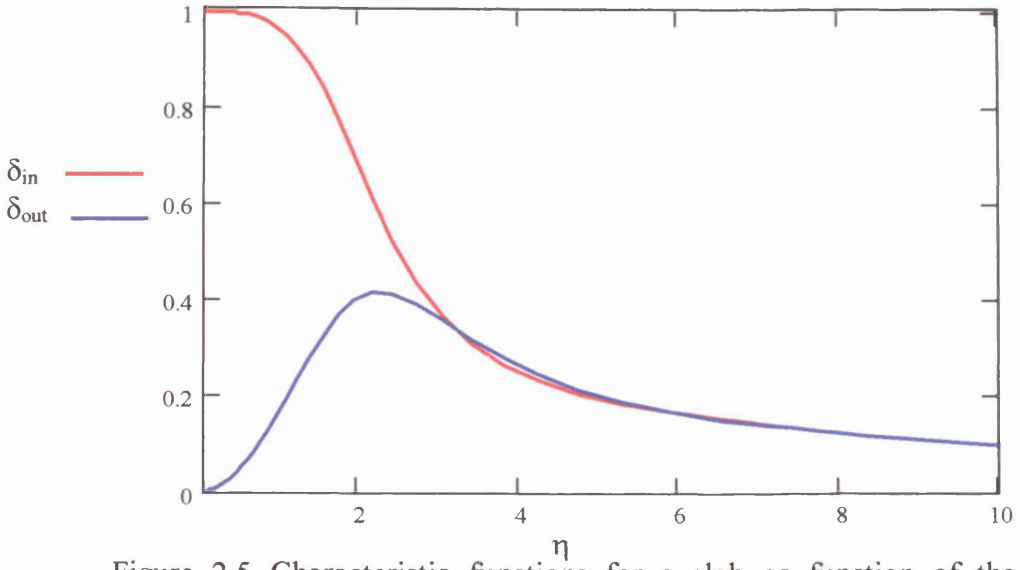

Figure 2.5 Characteristic functions for a slab as function of the reduced angular frequency.

The characteristic functions are an useful way of analysing FR data because from the out-phase, eq. (8), the characteristic time $\frac{L^2}{D}$ may be determined distinctly from the position where the maximum appears ($f_{corner} \approx \frac{0.4 * D}{L^2}$ for a slab of thickness 2L). From the in-phase, eq. (7), the equilibrium constant K can be determined for $\omega \to 0$. For high frequencies both functions converge asymptotically to zero.

2.5 Extension of the model

The extension to other geometries, mass and thermal resistances follows the same methodology. Jordi and Do (1993) and Sun et al. (1993) presented detailed models for

non-isothermal adsorption-diffusion process in presence of extra crystalline resistances. In Table 2.2 various characteristic functions are summarized.

Table 2.2 Characteristic Functions

	Model	Characteristic functions	Reference
Particle Shape	Microporous diffusion Sphere	$\delta_{in} = \frac{3}{\eta}\left\{\frac{\sinh\eta - \sin\eta}{\cosh\eta - \cos\eta}\right\}$ $\delta_{out} = \frac{6}{\eta}\left\{\frac{1}{2}\left[\frac{\sinh\eta + \sin\eta}{\cosh\eta - \cos\eta}\right] - \frac{1}{\eta}\right\}$ $\eta = \left(\frac{2\omega R_s^{\,2}}{D}\right)^{1/2} \quad f_{corner} \approx \frac{1.8 * D}{R_s^{\,2}}$	Yasuda (1982)
	Parallelepiped anisotropic	$\delta_{in} = \left(\frac{8}{\pi^2}\right)^3 \sum_{l,m,n=1,3,5} \frac{\alpha_{lmn}^2}{l^2 m^2 n^2 \left(\alpha_{lmn}^2 + \omega^2\right)}$ $\delta_{out} = \left(\frac{8}{\pi^2}\right)^3 \sum_{l,m,n=1,3,5} \frac{\alpha_{lmn}\omega}{l^2 m^2 n^2 \left(\alpha_{lmn}^2 + \omega^2\right)}$ $\alpha_{lmn} = \frac{\pi^2}{4}\left(\frac{l^2 D_1}{a^2} + \frac{m^2 D_2}{b^2} + \frac{n^2 D_3}{c^2}\right)$	Oprescu et al. (1992)
	Infinite cylinder	$\delta_{inc} - i\delta_{outc} = \frac{2}{(1+i)\lambda} \frac{I_1[(1+i)\lambda]}{I_0[(1+i)\lambda]}$ $\lambda = \left(\frac{\omega R_c^2}{2D}\right)^{1/2} \quad f_{corner} \approx \frac{1 * D}{R_c^{\,2}}$	Jordi and Do (1994), Sun et al. (1993)

Table 2.2 cont.

Multiple Mass Transfer Resistance	Surface Barrier	$\delta^{SR}{}_{in} = \frac{1}{1+\omega_0^2 t_s^2}$ $\delta^{SR}{}_{out} = \frac{\omega_0 t_s}{1+\omega_0^2 t_s^2}$ $t_s = \frac{R_p a_p}{(\sigma+1)k_s}$ $f_{corner} \approx \frac{k_s}{R_p a_p}$	Sun et al. (1993)
	Surface Barrier And Microporous Diffusion	$\delta^{SR}{}_{in} = \left(\frac{ak_{-A}}{\omega}\right)^2 \left\{\frac{a+c\delta_{in}}{\bar{\theta}}\right\}$ $\delta^{SR}{}_{out} = \left(\frac{ak_{-A}}{\omega}\right)\left[\left[1-\left(\frac{ak_{-A}}{\omega}\right)\left\{\frac{\frac{ak_{-A}}{\omega}+c\delta_{in}}{\bar{\theta}}\right\}\right]\right]$ $\bar{\theta} = [(ak_{-A}/\omega)+c\delta_{in}]^2 + (a+c\delta_{in})^2$ a (ratio external-internal area) $c = 1-a$	Yasuda et al. (1991)
	Multiple Microporous Diffusion	$\delta_{in} = \sum_j \tilde{K}_j \delta_{jin}$ $\tilde{K}_j = \frac{K_j}{\sum_j K_j}$ $\delta_{out} = \sum_j \tilde{K}_j \delta_{jout}$	Yasuda (1982)
Heat Effects	Microporous Diffusion, Mass and Thermal Surface Resistance	$\delta_{in} = \left\{\frac{\eta_c(1+\omega_0^2 t_h^2)+\alpha_s(\eta_c^2+\eta_s^2)\omega_0^2 t_h^2}{(1+\alpha_s\eta_s\omega_0 t_h)^2+(1+\alpha_s\eta_c)^2\omega_0^2 t_h^2}\right\}$ $\delta_{out} = \left\{\frac{\eta_s(1+\omega_0^2 t_h^2)+\alpha_s(\eta_c^2+\eta_s^2)\omega_0 t_h}{(1+\alpha_s\eta_s\omega_0 t_h)^2+(1+\alpha_s\eta_c)^2\omega_0^2 t_h^2}\right\}$ $\alpha_s = \frac{a_T \Delta T}{a_p \Delta p}$ $\eta_c - i\eta_s = \frac{\delta_{in}-i\delta_{out}}{1+\omega_0 t_s(\delta_{out}+i\delta_{in})}$ $t_h = \frac{R_p C_p}{(\sigma+1)h_p}$ $\sigma = 0,1,2$	Sun et al. (1993)
	Purely heat-controlled	$\delta_{in} = \left\{\frac{1+(1+\alpha_s)\omega_0^2 t_h^2}{1+(1+\alpha_s)^2\omega_0^2 t_h^2}\right\}$ $\delta_{out} = \left\{\frac{\alpha_s\omega_0 t_h}{1+(1+\alpha_s)\omega_0^2 t_h^2}\right\}$	Do and Ruthven (1989)

2.5.1 Effect of particle shape

The solution for the spherical geometry (Yasuda, 1982) is shown in Fig. 2.6.

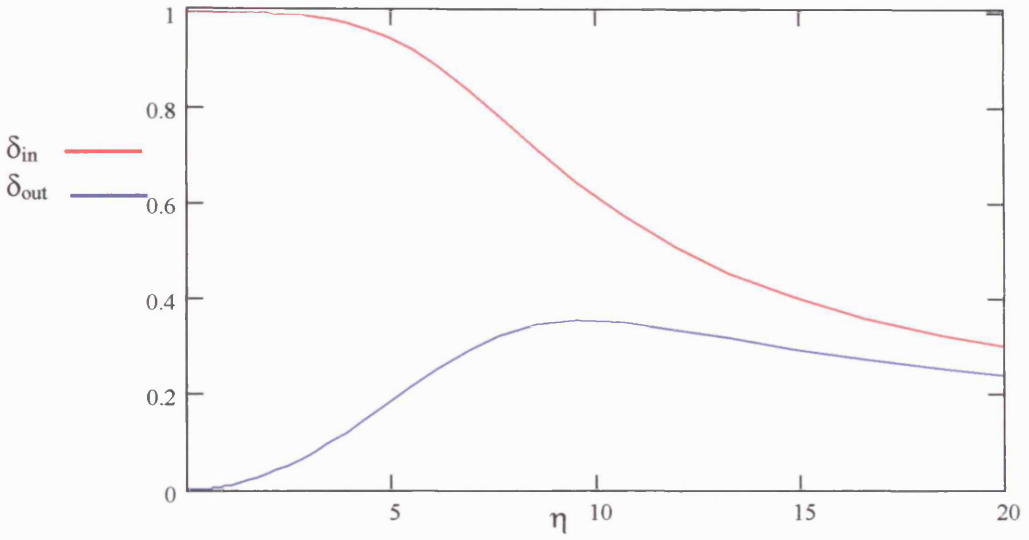

Fig. 2.6 Characteristic functions for a slab as function of the reduced angular frequency $\eta = \sqrt{2\omega R_s^{\ 2}/D}$

Here the in-phase function is well separated from the out-phase function compared to the slab geometry (see Fig.2.5).

The solution for a cylinder of infinite length has been given by Jordi and Do (1994) and Sun et al. (1993). Because the solution involves Bessel function of complex argument, it can be useful to note that

$$f_{corner} \approx \frac{1 * D}{R_c^{\ 2}} = 0.8 f_{sphere-equivalent}.$$

The solution (Oprescu et al., 1992) has been extended also to parallelepiped geometry with anisotropic diffusion (see table 2.2.) and applied to the study of the diffusion of Xenon in silicalite-1 (coffin shape) and of p-xylene in parallelepiped silicalite-2 (Shen and Rees, 1993).

In all the cases the characteristic functions trend is similar, while the presence of a crystals size distribution make the diffusion peak less pronounced (Sun et al., 1994).

2.5.2 Series and parallel mass transfer resistances

The presence of a surface resistance $(1/k_{-A})$ introduces an additional mass transfer resistance to the adsorption process, in series with respect to the microporous diffusion (D).

This modification, Yasuda et al. (1991), incorporates a rate constant for the surface resistance which is formally similar to the Langmuir kinetics (Yasuda, 1976) and the relative in-phase and out-of-phase components are given in Table 2.2 and shown in the following figure:

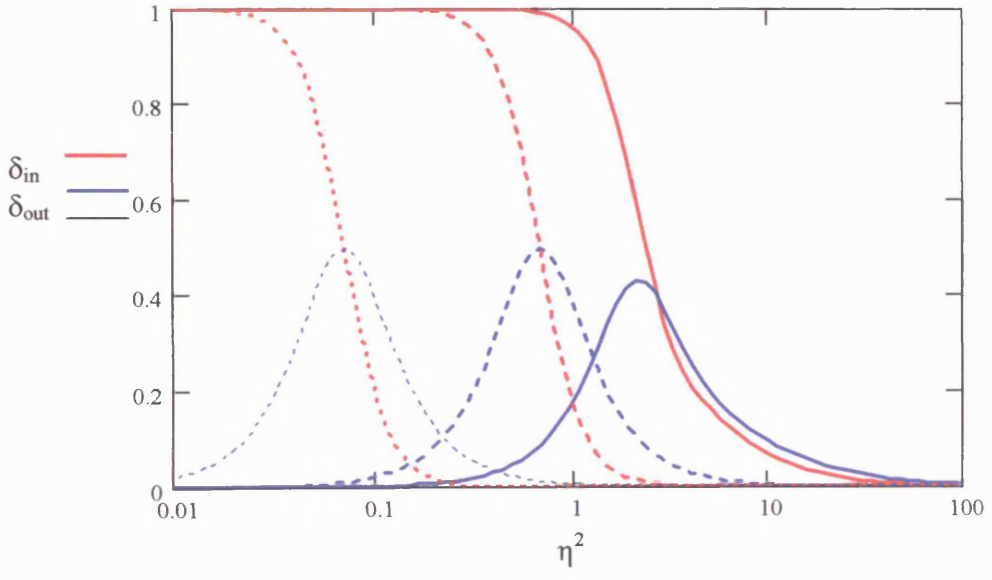

Fig.2.7 Theoretical in-phase and out-of-phase functions for surface resistance to diffusion. The parameter $\zeta = ak_{-A}L^2/D$ is 100(——), 1 (- -),0.01 (·····)

The parameter $\zeta = \frac{ak_{-A}L^2}{D}$ is the ratio of the diffusion and surface resistance time constants. The presence of a surface barrier can be easily detected because the characteristic functions intersect each other.

If the surface barrier completely controls the kinetics, the in-phase and out-of-phase functions intersect at the maximum point of the latter. The corresponding resonant angular frequency is the inverse of the characteristic time for the surface barrier. When both the diffusion and the surface barrier exist, the intersection occurs at higher frequency. Sun et al (1993) underlined that because the unusual behaviour pattern predicted by a surface barrier model, the LDF model is clearly not suitable for studying diffusion by the frequency response technique.

Sun et al. (1994) have extended the model to zeolite pellets (or loosely packed pile of zeolite crystals). Their analysis showed that when both macropore diffusion and micropore diffusion resistances are comparable, *macropore diffusion behaves like a surface barrier* and leads to an intersection of the in-phase and out-phase response functions. When either micropore diffusion or macropore diffusion is alone dominant, the frequency response is essentially the same.

The linearity of the system (Yasuda, 1994) implies that the ultimate response of the system will be the sum of the individual responses present in the system:

$$\delta_{in} = \sum_j \widetilde{K}_j \delta_{jin} \tag{13}$$

$$\delta_{out} = \sum_j \widetilde{K}_j \delta_{jout} \tag{14}$$

$$\widetilde{K}_j = \frac{K_j}{\sum_j K_j} \tag{15}$$

This is valid provided that the interactions among them are negligible.

For a process in which the local Henry's law constants are the same but the characteristics time constants differ by 2 orders of magnitude, an ultimate response is represented in Fig.2.8:

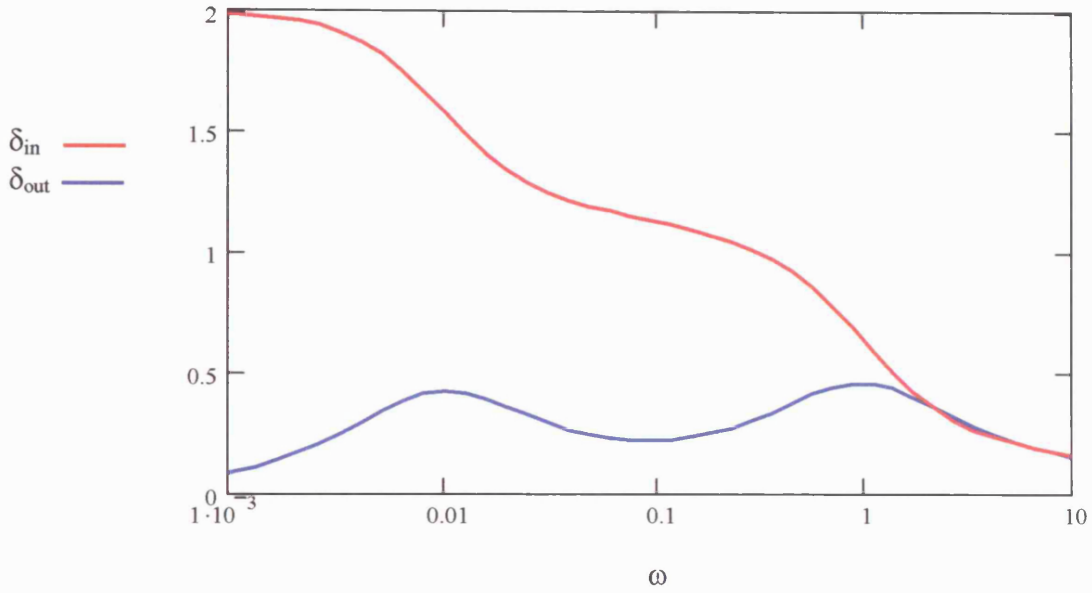

Fig. 2.8 Theoretical in-phase and out-of-phase functions for two indipendent diffusion processes.

The out-phase function shows a bimodal behaviour pattern. The first peak corresponds to the slower of the two independent diffusion processes. The zero frequency limit is the sum of the equilibrium constants defined according Eq. (11).

2.5.3 Heat effects

Because of the batch nature of the technique, the release of heat during the adsorption can cause strong deviations from the isothermal case. Sun et al. (1993), underlining that the use of a very small pressure changes cannot eliminate the heat effect since in a linear

closed system any effect is independent of the step size, developed a model including: heat transfer resistance, mass surface resistance and microporous diffusion;

The characteristic functions show two main differences with respect to the isothermal case:

1) the high frequency asymptote for the in-phase characteristic function does not go to zero but to a finite value depending on the magnitude of the non-isothermal effect;

2) the possibility of a bimodal behaviour for the out-phase characteristic function , one due to heat transfer, one to mass transfer;

Jordi and Do (1994) (monodisperse pore structure) and Sun et al. (1994) – (bidispersed pore structure) included in the non-isothermal models the solids-adsorbate conduction. Sun et al. (1994) defined the following parameter in the case of a non-isothermal system:

$$\delta = \frac{1-\varepsilon}{\varepsilon}\frac{|\Delta H| K_p}{C_S T_e}\left(\frac{|\Delta H|}{RT_e} - 1\right)$$

The possibility of a bimodal response due to thermal effects shows that even in the case of the FR, similar behaviour can be obtained from two very different physical mechanisms.

Shen and Rees (1991) observed that the out-of-phase curves for several systems were bimodal and this could not be explained by a single-diffusion model. The systems investigated were diffusion of n-butane and 2-butyne in "coffin-shaped" silicalite-1 and diffusion of p-xylene in nearly spherical silicalite-1. In order to describe this bimodal behaviour, Shen and Rees (1991) suggested that there are two independent diffusion processes occurring in the straight and sinusoidal channels of silicalite-1, respectively, each process having its own phase with its own equilibrium constant and diffusion rate.

Sun and Meunier (1993) do not agree with this interpretation and have argued that the bimodal behaviour of the frequency response curves for the molecule of n-butane that are more flexible than the p-xylene and 2-butyne and therefore have less difficulty in turning at the intersections, the relatively high coverage for the experiments make unlikely that the interaction between the two diffusion fluxes is negligible.

They explained the bimodal behaviour in terms of thermal effects. The bimodal behaviour can be obtained when the diffusion time constant is sufficiently smaller than the time constant for heat transfer, i.e. when diffusion is sufficiently faster than heat transfer. The good agreement and the consistency of the equilibrium data used in their model suggest that the heat effect is in fact a possible explanation of the bimodal behaviour. However to confirm the assumption of two independent processes Shen and Ress (1993) made a comparative study with the diffusion data of p-xylene in silicalite-2, which contains only one set of straight channels. The frequency response of this system was found to exhibit only a single peak, indicating that only one diffusion process was involved.

2.6 Advantages and Limits of the FR

The most theoretically promising feature of the FR technique is its ability to discriminate between different rate-limiting mechanisms, which is due to the high sensitivity of the frequency response to the nature of the governing equations (Naphtali and Polinski (1963)). On the other hand the high sensitivity means that it is imperative to take into account all the physically possible limiting effects in the theoretical analysis (e.g. thermal effects).

Following Bourdin et al. (1998) the advantages for the FR are:

1) The possibility to measure relatively fast kinetics.
2) The high accuracy. The FR is a pseudostationary method and thus the accuracy increases with the measurement duration. (The method transforms a transient system into a quasi-stationary one, allowing precise measurements that are insensitive to small changes in experimental conditions (e.g., drifts).)
3) The direct dependence between the phase lag (in fact a time at a given frequency) and the characteristic times involved in the process.
4) The sensitivity to the mass transfer mode: Fickian diffusion or surface barrier.

It is important to recognize also the limitations of the FR technique. Broadly, the main limitations relate to the limited range of angular frequencies obtainable experimentally, the accuracy with which measurements may be obtained, and the inaccuracies in correcting for apparatus effects. Also inherent in the technique is the requirement to perform measurements under periodic steady-state conditions over a range of angular frequencies, which may be very time consuming for systems with slow dynamic characteristics. Furthermore, only two parameters, namely, the phase angle and amplitude ratio, are extracted from a large body of measured data.

Clearly, in order to discern all of the dynamic processes active in a given system, one needs to perform measurements covering the complete range of dynamic time scales. The range of frequency covered in the reported literature ranges from 0.001 to 30 Hz, corresponding to a dynamic process timescale range of about 0.03-1000 s. (Shen and Rees (1994)).

Another important limitation of the FR technique is the limited pressure range that may be covered before the accuracy of the experimental data is significantly degraded. Since the intensity of the frequency spectrum is proportional to the gradient of the adsorption

isotherm at equilibrium (see Eq. 12), systems with isotherms exhibiting a plateau or asymptotic features may only be investigated over a limited range of pressure.

Following Park et al. (1998) the main limitations can be summarised as:

- Relatively low experimental frequencies resulting from mechanical limitations of volume modulators.
- A demand for small amplitudes of the volume perturbations in order to satisfy assumptions of linearity.
- Non-isothermality, influencing the FR results considerably (Sun et al., 1993)

In the present study the main aim is to determine the possibility of generalizing the Frequency Response method to sonic frequencies (10 Hz - 20 kHz, see Chapter 3), and the linearity of the signal and thermal effects are object of a parametric analysis in Chapter 4.

Chapter 3
A Model for Sound Propagation in presence of Microporous Solids

3.1 Introduction

The extension of the frequency response technique to higher frequencies (>20 Hz) implies the need to consider a pressure wave in the sonic range (sound propagation). While in an open medium classical dissipative effects on the pressure wave can be generally neglected (See 3.2), in a confined medium the variation of amplitude (absorption) and the change of phase (dispersion) of the wave affects significantly the sound wave.

The absorption of sound is due to (Hirschfelder et al., 1954):

1) viscosity
2) thermal conductivity
3) diffusion
4) chemical reactions and phase change
5) time lag in the transfer of energy among the various degrees of freedom of the molecules.

(1) and (2) are indicated as classical mechanisms in ultrasonic literature, in order to distinguish them from the "molecular" absorption and dispersion.

Assuming that the amplitudes of the sound waves are sufficiently small, their propagation with absorption can be described by a set of linear differential equations, in terms of small perturbations about an average (Markham et al., 1951).

3.2 Ideal Sound Propagation

The sound equation for an ideal fluid (Crandall, 1927) in terms of pressure is given by:

$$\frac{\partial^2 p}{\partial x^2} - \frac{1}{a_0{}^2}\frac{\partial^2 p}{\partial t^2} = 0 \tag{1}$$

where a_0 is the ideal sound velocity.

Eq. 1 is hyperbolic and represents the equation for the propagation of waves. The general solution must include waves travelling with positive and negative velocities and will be of the type:

$$\bar{p} = A \cdot f(a_0 t - x) + B \cdot F(a_0 t + x) \tag{2}$$

The values of A and B, and the particular forms of $f(ct-x)$ and $F(ct+x)$ must be determined from the boundary conditions assigned in a particular problem.

In the following treatment we concentrate on sinusoidal functions[1] and only on the progressive wave, i.e. we will consider solutions of the form $f(ct-x) = e^{i\omega t - x}$.

In agreement with the following analysis we introduce the dimensionless time $\tau = \omega t$ and the dimensionless space coordinate $\xi = \frac{\omega x}{a_o}$. Therefore the solution that we will seek will be of the form: $f(ct-x) = e^{i\tau - \Gamma\xi}$ (3)

It will be shown that a solution of this form verifies the equation for the propagation of a sound wave with absorption, but in this case the propagation constant Γ is a complex value:

[1] The reason the sine function occupies a key position in wave theory is fundamentally that linear mathematical operations applied to sinusoidal functions of a definite period generate other sinusoidal functions of the same period,differing at most in amplitude and phase. Nonsinusoidal waves are found to change their shape as they progress, it is only sinusoidal waves that preserve their functional form in passing through the medium.

$$\Gamma = PS + iAC \tag{4}$$

The real part of Γ is the Phase Shift (PS) or the reciprocal of the wavelength λ multiplied by 2π that is related to the propagation velocity and the imaginary part is the absorption coefficient AC.

3.3 Sound Propagation in Confined Spaces.

The problem of the propagation of sound waves in gas contained in confined spaces was considered by Kirchhoff (1868) for a cylindrical geometry. The analytical solutions given in the literature can be divided roughly into two groups (Tijdeman, 1975). The first group comprises solutions obtained by analytical approximations of the full Kirchhoff solution, which is given in the form of a very complicated transcendental equation. The solutions of the second group have been derived directly from the basic equations governing the problem, by the introduction of one or more simplifying assumptions.

Kirchoff 's solution is a function of the following parameters:

$s = h\sqrt{\frac{\rho_s \omega}{\mu}}$ shear wave number

$\sigma = \sqrt{Pr} = \sqrt{\frac{\mu C_p}{\lambda}}$ square root of the Prandtl number

$k = \frac{\omega h}{a_o}$ reduced frequency

Zwikker and Kosten (1949) have derived an analytical approximation (Low Reduced Frequency Approximation: LRFA). Because of its simplicity this approximation of the full solution has been applied recently to the description of sound propagation in presence of vapour-liquid equilibrium (Raspet et al., 1999).

In Tijdeman's analysis (1975) it is demonstrated that most of the analytical solutions are dependent only on the shear wave number, s, and that they are adequately represented by the LRFA. In the same analysis Tijdeman shows that the exact solution has a strong dependence on the reduced frequency, k, for relatively small values of the shear wave number ($s \leq 4$).

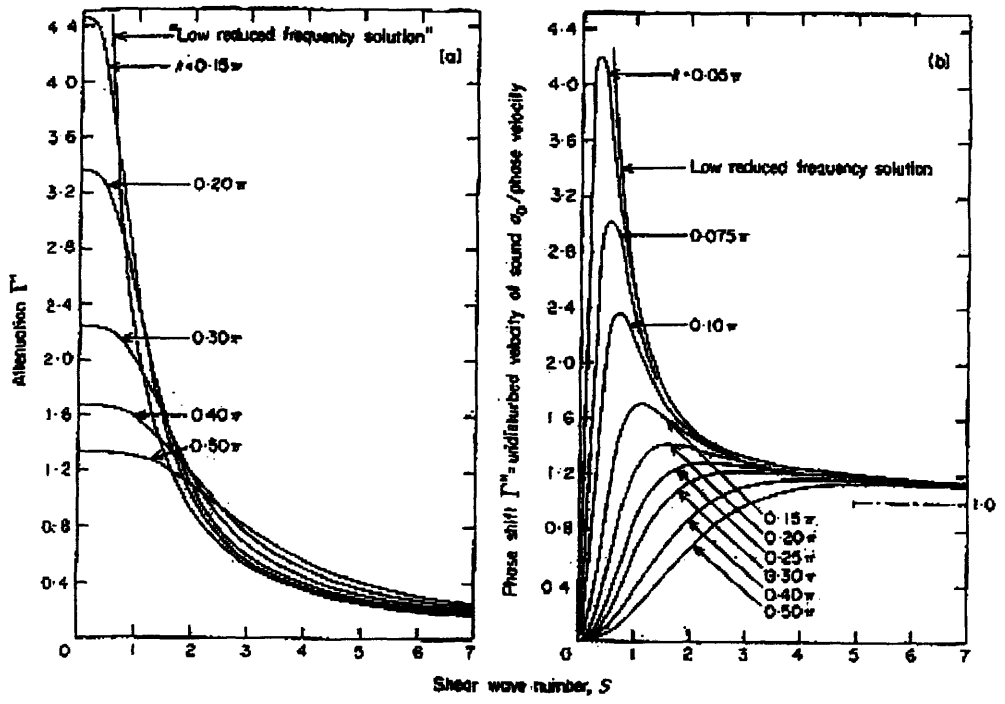

Fig.3.1 Exact solution of the Attenuation and Phase Shift as functions of shear wave number and reduced frequency. From [Tijdeman, 1975]

From Fig. 3.1 it is possible to see that the Phase Shift is more sensitive to the reduced frequency, but for $s > 2$ and $k > 0.1\ \pi$ the LRFA yields a sufficiently accurate approximation to the solution of sound propagation.

Given this general result and the analogy of phase change due to adsorption to that of vapour-liquid equilibrium we have applied the Low Reduced Frequency Approximation (LRFA) in order to obtain a theoretical solution for a sound wave propagating between two adsorbing walls.

3.3.1 General Model

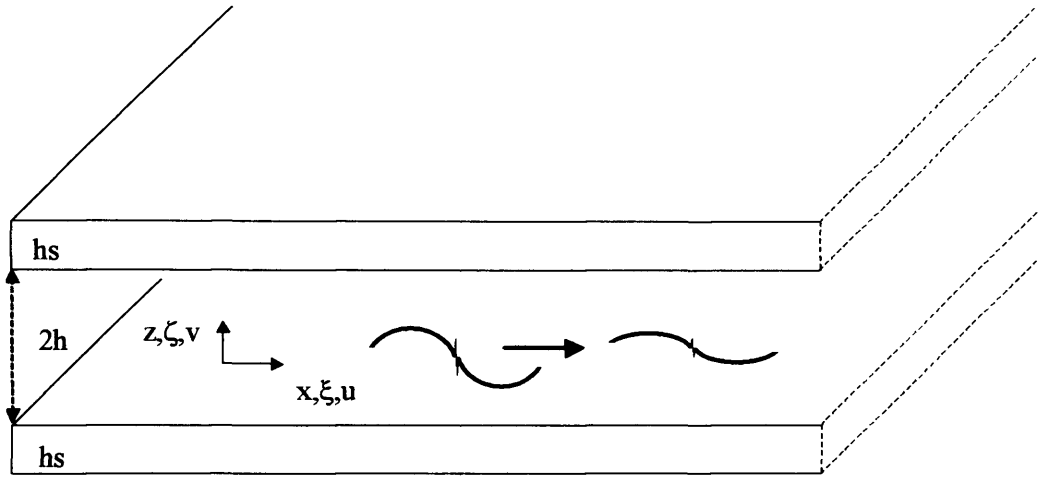

Fig.3.2 Model geometry: Two layers of a microporous solid of h_S depth.

We consider the simple geometry of two layers of an adsorbent microporous solid of infinite width separated by a gas that adsorbs on the solid's surface.

A planar sound wave propagates in the x direction (Fig. 3.2). The assumptions made allow us to consider the 2-D problem and sound propagation can be described (Landau and Liftshitz, 1997) using the Navier-Stokes equations in vertical and horizontal directions,

$$\bar{\rho}\left[\frac{\partial \bar{u}}{\partial t}+\bar{v}\frac{\partial \bar{u}}{\partial z}+\bar{u}\frac{\partial \bar{u}}{\partial x}\right]=-\frac{\partial \bar{p}}{\partial x}+\mu\left\{\frac{\partial^2 \bar{u}}{\partial x^2}+\frac{\partial^2 \bar{u}}{\partial z^2}+\frac{1}{3}\frac{\partial}{\partial x}\left[\frac{\partial \bar{u}}{\partial x}+\frac{\partial \bar{v}}{\partial z}\right]\right\}=0 \tag{5}$$

$$\bar{\rho}\left[\frac{\partial \bar{v}}{\partial t}+\bar{v}\frac{\partial \bar{v}}{\partial z}+\bar{u}\frac{\partial \bar{v}}{\partial x}\right]=-\frac{\partial \bar{p}}{\partial z}+\mu\left\{\frac{\partial^2 \bar{v}}{\partial x^2}+\frac{\partial^2 \bar{v}}{\partial z^2}+\frac{1}{3}\frac{\partial}{\partial z}\left[\frac{\partial \bar{u}}{\partial x}+\frac{\partial \bar{v}}{\partial z}\right]\right\}=0 \tag{6}$$

the continuity equation,

$$\frac{\partial \bar{\rho}}{\partial t}+\bar{u}\frac{\partial \bar{\rho}}{\partial x}+\bar{v}\frac{\partial \bar{\rho}}{\partial z}+\bar{\rho}\left[\frac{\partial \bar{u}}{\partial x}+\frac{\partial \bar{v}}{\partial z}\right]=0 \tag{7}$$

the equation of state.

$$\bar{p}=\bar{\rho}R_o T \tag{8}$$

and the energy balance

$$\bar{\rho} C_p \left[\frac{\partial \bar{T}}{\partial t} + \bar{u} \frac{\partial \bar{T}}{\partial x} + \bar{v} \frac{\partial \bar{T}}{\partial z} \right] = \lambda \left[\frac{\partial^2 \bar{T}}{\partial x^2} + \frac{\partial^2 \bar{T}}{\partial z^2} \right] + \frac{\partial \bar{p}}{\partial t} + \bar{u} \frac{\partial \bar{p}}{\partial x} + \bar{v} \frac{\partial \bar{p}}{\partial z} + \mu \Phi \tag{9}$$

where

$$\Phi_v = 2 \left[\left(\frac{\partial \bar{u}}{\partial x} \right)^2 + \left(\frac{\partial \bar{v}}{\partial z} \right)^2 \right] + \left(\frac{\partial \bar{v}}{\partial x} + \frac{\partial \bar{u}}{\partial z} \right)^2 - \frac{2}{3} \left(\frac{\partial \bar{u}}{\partial x} + \frac{\partial \bar{v}}{\partial z} \right)^2 \tag{10}$$

Because of the adsorption-desorption process at the interface, the concentration of the adsorbate phase and the temperature of the solid change. As a result the diffusion of the sorbate and thermal conduction in the solid have to be considered.

Eqs (5)-(10) have to be coupled to the solid phase mass and energy balances

$$\frac{\partial \bar{q}}{\partial t} = D \left(\frac{\partial^2 \bar{q}}{\partial z^2} + \frac{\partial^2 \bar{q}}{\partial x^2} \right) \tag{11}$$

$$\rho_{hm} Cp_{hm} \frac{\partial \overline{T_{hm}}}{\partial t} = \lambda_{hm} \left(\frac{\partial^2 \overline{T_{hm}}}{\partial z^2} + \frac{\partial \overline{T_{hm}}}{\partial x^2} \right) \tag{12}$$

Eqs (5)-(12) suffice to obtain the solution for the seven unknown quantities: namely, the velocities in the horizontal and vertical directions, the density, the temperature, the pressure, the concentration of the sorbate and the temperature of the solid.

Eqs (5)-(12) can be linearized according to the acoustic approximation (i.e. only first order terms are considered) and made dimensionless following Tijdeman's notation (1975). A general procedure is available to solve this set of equations if they are formulated in terms of gas pressure (Tijdeman, 1975). To achieve this one has to eliminate the solid phase variables. Consider the dimensionless mass and energy balances of the solid which can be written as

$$\frac{\partial q}{\partial \tau} = \frac{1}{k_d'} \frac{\partial^2 q}{\partial \zeta^2} \tag{13}$$

$$\frac{\partial T_{hm}}{\partial \tau} = \frac{1}{k_\lambda'} \frac{\partial^2 T_{hm}}{\partial \zeta^2} \tag{14}$$

where q and T_{hm} are the relative variations of the sorbate concentration with respect to the average value (i.e. $\bar{q} = q_s(1+q(x,z,t))$ and $\overline{T_{hm}} = T_{hms}(1+T_{hm}(x,z,t)))$, $\tau = \omega t$, $k_d' = \frac{\omega h^2}{D}$ diffusive reduced frequency, $k_\lambda' = \frac{\omega h^2 \rho_{hm} Cp_{hm}}{\lambda}$ conductive reduced frequency and the dimensionless vertical coordinate $\zeta = \frac{z}{h}$, and the corresponding set of boundary conditions:

(a) At the solid surfaces the vertical mass flux must be equal to the diffusive flux and the horizontal velocity must be zero:

$$\zeta = 1,-1 \quad u = 0 \ \ and \ \ v = -\frac{Dq_s}{e^{i\omega t}\rho_s a_0 h}\frac{\partial q}{\partial \zeta} \quad .$$

Before linearization the continuity of the vertical flux is written as $\bar{\rho}\cdot\bar{v} = -D\left.\frac{\partial \bar{q}}{\partial z}\right|_{z=-H}$

(b) At the solid surfaces the following condition on the heat flux must be verified:

$$\zeta = 1,-1 \quad \frac{-\Delta HDq_s}{h}\frac{\partial q}{\partial \zeta} - \frac{\lambda_{hm}T_{hms}}{h}\frac{\partial T_{hm}}{\partial \zeta} = -\frac{\lambda T_s}{h}\frac{\partial T}{\partial \zeta}e^{i\omega t}$$

Before linearization the heat flux condition is written

$$-\Delta HD\frac{\partial \bar{q}}{\partial z} - \lambda_{hm}\frac{\partial \overline{T}_{hm}}{\partial z} = -\lambda\frac{\partial \overline{T}}{\partial z}$$

(c) At the solid surface the sorbate concentration is at equilibrium (Sun et al., 1993) with the fluid phase:

$$\bar{q} = q_s(1+q(x,-1,t)) = q_s + \left(\frac{\partial \bar{q}}{\partial P}\right)(\bar{p}-p_s) + \left(\frac{\partial \bar{q}}{\partial T}\right)(\overline{T}-T_s)$$

$$\zeta = 1,-1 \quad q = K_p \cdot pe^{i\omega t} + K_T \cdot Te^{i\omega t}$$

(d) At the solid surface there is thermal equilibrium between the solid and fluid: i.e.,

$$\zeta = 1,-1 \quad T_{hm} = Te^{i\omega t}$$

(e) At the base of the solid layer the diffusive and conductive fluxes must be zero:

$$\zeta = \frac{h+h_s}{h}, -\frac{h+h_s}{h}, \quad \frac{\partial q}{\partial \zeta} = 0 \ \ and \ \ \frac{\partial T_{hm}}{\partial \zeta} = 0$$

To recast the model equations in a form that allows the application of the solution procedure of Tijdeman (1975) in the case of sound propagation in a tube it is therefore necessary to express the surface concentration $\frac{\partial q}{\partial \zeta}$ and temperature gradients $\frac{\partial T_{hm}}{\partial \zeta}$ as function of the external concentration and temperature respectively. This corresponds to finding the transfer function

$$\left.\frac{\partial \tilde{q}}{\partial \zeta}\right|_{\zeta=-1} = \left(K_p \tilde{p} + K_T \tilde{T}\right) dG_q(\vartheta) \tag{15}$$

$$\left.\frac{\partial \tilde{T}_{hm}}{\partial \zeta}\right|_{\zeta=-1} = dG_T(\vartheta)\tilde{T} \tag{16}$$

where θ is the Laplace domain variable.

From the solution of the diffusion and energy equations in the Laplace domain, one can find the transfer function to be

$$dG_q(\vartheta) = \sqrt{k_d'\vartheta}\tanh\left(\sqrt{k_d'\vartheta}\frac{h_s}{h}\right) \tag{17}$$

$$dG_T(\vartheta) = \sqrt{k_\lambda'\vartheta}\tanh\left(\sqrt{k_\lambda'\vartheta}\frac{h_s}{h}\right) \tag{18}$$

Finally the equations are inverted to the time domain following the inversion theorem for periodic input (Stephanopoulos, 1984). Following the procedure of Tijdeman (1975) (see Appendix B) the solution for the pressure is given by:

$$p = Ae^{\Gamma\xi} + Be^{-\Gamma\xi} \tag{19}$$

where A and B can be determined by the boundary conditions on the ξ coordinate.

Γ is the propagation constant given by

$$\Gamma = \mathrm{i}\sqrt{\frac{\gamma}{n}}\sqrt{\frac{1}{\left(1-\frac{\tanh\left(\sqrt{\mathrm{i}}\,s\right)}{\sqrt{\mathrm{i}}\,s}\right)}} \tag{20}$$

where s is shear wave number and n is the polytropic equivalent coefficient given by

$$n=\left\{1-\left[\frac{\gamma-1}{\gamma}-\Xi\frac{\tanh\left(\sqrt{i}\,\sigma s\right)}{\sqrt{i}\,\sigma s}\right]+Ap\left[1+\Delta H_{dim}\left(\frac{\gamma-1}{\gamma}-\Xi\right)\right]\cdot\left|G_q(i)\right|\cdot e^{\left(i\arg\left(G_q(i)\right)\right)}\right\}^{-1} \tag{21}$$

The real part of Γ is the Attenuation Coefficient (AC), a measure of the decrease of the sound amplitude while the imaginary part is the phase shift (PS).

$Ap=\frac{q_s K_p}{p_s}\frac{(1-\varepsilon)}{\varepsilon}$ is the ratio solid-gas phases hold-ups.

$G_q(i)=\frac{\tanh\left(\sqrt{k_d i}\right)}{\sqrt{k_d i}}$ is a complex function of the characteristic time of microporous diffusion trough the layer of the microporus material $k_d=\frac{\omega h_s^2}{D}$

Ξ is the non-isothermal adsorption factor.

$$\Xi=\frac{\frac{\Delta T_{ad}}{\sqrt{Le}}\left(1+\Delta H_{dim}\frac{\gamma-1}{\gamma}\right)\Psi(k_d,Le)+\frac{\gamma-1}{\gamma}}{\frac{\Delta T_{ad}}{\sqrt{Le}}\Delta H_{dim}\Psi(k_d,Le)+\sqrt{\frac{k_d}{Le}}\frac{\Phi(\sigma s,k_d,Le)}{\sigma s}Cp_r+1} \tag{22}$$

As it is possible to see from the expression for the polytropic constant (Eq.21) the heat of adsorption affects Γ in two ways:

1) the gas thermal conduction modifying the surface temperature

2) the adsorption equilibrium.

Here $\Delta T_{ad}=\frac{|\Delta H|q_s K_p}{(\rho Cp)_{hm}T_s}$ and represents the adiabatic temperature fluctuation.

$\Delta H_{dim}=\frac{\Delta H}{RT_s}$ is the dimensionless heat of adsorption.

Le is the Lewis number $Le = \dfrac{\lambda_{hm}}{D(\rho Cp)_{hm}}$ and represents the ratio between thermal and mass diffusivity.

$Cp_r = \dfrac{\rho Cp}{(\rho Cp)_{hm}} \dfrac{\varepsilon}{1-\varepsilon}$ represents the ratio between the gas and solid phase thermal capacities.

$\Psi(k_d, Le) = \Psi(k_d, k_\lambda) = \dfrac{\tanh\left(\sqrt{k_d i}\right)}{\tanh\left(\sqrt{k_\lambda i}\right)}$ and $\Phi(\sigma s, k_d, Le) = \Phi(\sigma s, k_\lambda) = \dfrac{\tanh\left(\sqrt{i}\sigma s\right)}{\tanh\left(\sqrt{k_\lambda i}\right)}$ are complex functions of the characteristic frequencies associated with molecular transport processes: microporous diffusion $k_d = \dfrac{\omega h_s^2}{D}$, thermal conduction through the solid layer $k_\lambda = \dfrac{\omega h_s^2 (\rho Cp)_{hm}}{\lambda_{hm}}$ and thermal conduction through the gas phase $(\sigma s)^2 = \dfrac{\omega h^2 (\rho Cp)}{\lambda}$.

The solution for the other acoustic variables becomes:

$$u = \frac{i\Gamma}{\gamma}\left[1 - \frac{\cosh\left(\sqrt{i}\,\zeta s\right)}{\cosh\left(\sqrt{i}\,s\right)}\right]\left[Ae^{\Gamma\xi} - Be^{-\Gamma\xi}\right] \tag{23}$$

$$v = -ik\left\{\left[Ae^{\Gamma\xi} + Be^{-\Gamma\xi}\right]\left[\zeta - \left[-\Xi\frac{\sinh\left(\sqrt{i}\,\sigma s\zeta\right)}{i^{5/2}\sigma s\cosh\left(\sqrt{i}\,\sigma s\right)} + \frac{\gamma-1}{\gamma}\zeta\right]\right]\right.$$
$$\left. + \frac{\Gamma^2\left[Ae^{\Gamma\xi} + Be^{-\Gamma\xi}\right]}{\gamma}\left[\zeta - \frac{\sinh\left(\sqrt{i}\,\zeta s\right)}{i^{1/2}s\cosh\left(\sqrt{i}\,s\right)}\right]\right\} \tag{24}$$

$$\rho = \left[Ae^{\Gamma\xi} + Be^{-\Gamma\xi}\right]\left[1 - \left[\Xi\frac{\cosh\left(\sqrt{i}\,\sigma s\zeta\right)}{\cosh\left(\sqrt{i}\,\sigma s\right)} + \frac{\gamma-1}{\gamma}\right]\right] \tag{25}$$

$$T = \left[Ae^{\Gamma\xi} + Be^{-\Gamma\xi}\right]\left[\Xi\frac{\cosh\left(\sqrt{i}\,\sigma s\zeta\right)}{\cosh\left(\sqrt{i}\,\sigma s\right)} + \frac{\gamma-1}{\gamma}\right] \tag{26}$$

Eqs (23)-(26) represent the set of solutions to the LRFA with solid adsorption.

3.3.2 Simplified Models

While it is useful to have derived this analytical solution, in order to understand the ranges in which adsorption kinetics may be investigated it is necessary to identify also the limiting solutions that can be obtained from this general one. Figure 3.3 shows the tree of the models that can be derived.

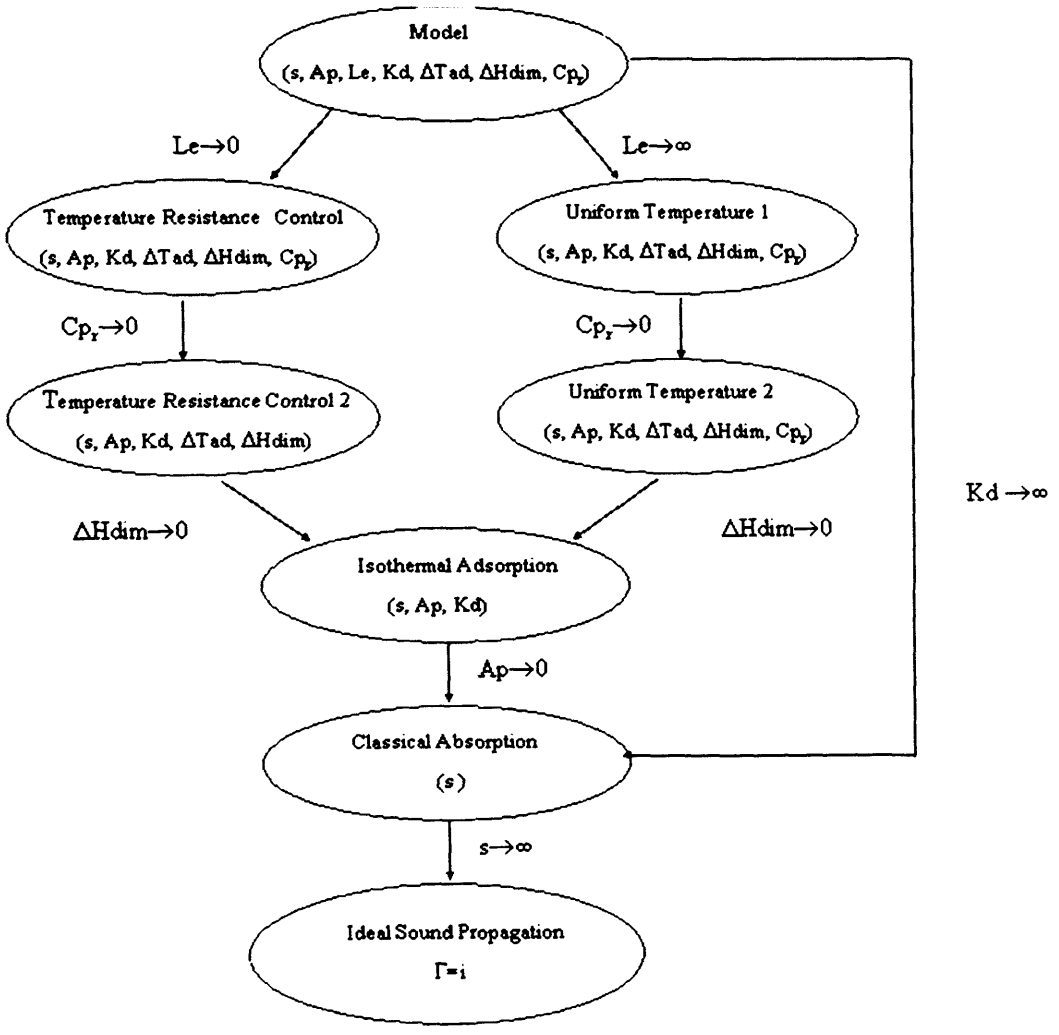

Fig.3.3 Models Tree.

This tree shows how, by setting specific values to the model parameters, it is possible to obtain a number of solutions. In particular one can see that by setting all the parameters

to their limiting values one recovers the solution n = γ, hence the name polytropic equivalent constant, and Γ = i corresponding to ideal sound propagation.

It is important to note is that by comparing the full solution to the simplified cases, it will be possible to carry out a parametric study which will be presented in Chapter 4.

Table 3.1 reports the solutions for all the models presented in Fig. 3.3.

Table 3.1 : Propagation Constants (and n, "polytropic equivalent")

Model	Γ Propagation Constant and n Polytropic Constant
General	$\Gamma = i\sqrt{\frac{\gamma}{n}}\sqrt{\frac{1}{\left(1-\frac{\tanh\left(i^{3/2}s\right)}{i^{3/2}s}\right)}}$ $n = \left\{1-\left[\frac{\gamma-1}{\gamma}-\Xi\frac{\tanh\left(i^{1/2}\sigma s\right)}{i^{1/2}\sigma s}\right]+Ap\left(1+\Delta H_{dim}\left[\frac{\gamma-1}{\gamma}-\Xi\right]\right)\cdot\left\|G_q(i)\right\|\cdot e^{\left(i\arg\left(G_q(i)\right)\right)}\right\}^{-1}$
Uniform Solid Temperature $Le\to\infty$	$\Gamma = i\sqrt{\frac{\gamma}{n}}\sqrt{\frac{1}{\left(1-\frac{\tanh\left(i^{5/2}s\right)}{i^{5/2}s}\right)}} = i\sqrt{\frac{\gamma}{n}}\sqrt{\frac{1}{\left(1-\frac{\tanh\left(i^{1/2}s\right)}{i^{1/2}s}\right)}}$ $n = \left\{1-\left[\frac{\gamma-1}{\gamma}-\Xi\frac{\tanh\left(i^{1/2}\sigma s\right)}{i^{1/2}\sigma s}\right]+Ap\left(1+\Delta H_{dim}\left[\frac{\gamma-1}{\gamma}-\Xi^{UT}\right]\right)\cdot\left\|G_q(i)\right\|\cdot e^{\left(i\arg\left(G_q(i)\right)\right)}\right\}^{-1}$
Isothermal Adsorption (Full model) $\Delta H_{dim}\to 0$	$\Gamma = i\sqrt{\frac{\gamma}{n}}\sqrt{\frac{1}{\left(1-\frac{\tanh\left(i^{5/2}s\right)}{i^{5/2}s}\right)}} = i\sqrt{\frac{\gamma}{n}}\sqrt{\frac{1}{\left(1-\frac{\tanh\left(i^{1/2}s\right)}{i^{1/2}s}\right)}}$ $n = \left\{1-\frac{\gamma-1}{\gamma}\left[1-\frac{\tanh\left(i^{1/2}\sigma s\right)}{i^{1/2}\sigma s}\right]+Ap\cdot\left\|G_q(i)\right\|\cdot e^{\left(i\arg\left(G_q(i)\right)\right)}\right\}^{-1}$
Ideal Fluid-Isothermal (Adsorption only) $s\to\infty$	$\Gamma = i\sqrt{\left(1-i\frac{DKa_o^2\left\|Q(i)\right\|\cdot e^{i\left(\arg Q(i)\right)}}{\omega\cdot h^2}\right)}$
Classical Absorption (Viscous Dissipation only) $Ap\to 0$	$\Gamma = i\sqrt{\frac{\gamma}{n}}\sqrt{\frac{1}{\left(1-\frac{\tanh\left(i^{1/2}s\right)}{i^{1/2}s}\right)}}$ $n = \left[1-\frac{\gamma-1}{\gamma}\left(1-\frac{\tanh\left(i^{5/2}\sigma s\right)}{i^{5/2}\sigma s}\right)\right]^{-1}$

Table 3.2 shows the corresponding values of the non-isothermal factor.

Table 3.2 Non-Isothermal Factor

Model	Ξ Non-Isothermal Factor
General	$\Xi = \dfrac{\dfrac{\Delta T_{ad}}{\sqrt{Le}}\left(1+\Delta H_{dim}\dfrac{\gamma-1}{\gamma}\right)\Psi(Kd,Le)+\dfrac{\gamma-1}{\gamma}}{\dfrac{\Delta T_{ad}}{\sqrt{Le}}\Delta H_{dim}\Psi(Kd,Le)+\sqrt{\dfrac{Kd}{Le}}\dfrac{\Phi(\sigma s,Kd,Le)}{\sigma s}Cp_r+1}$
Uniform Solid temperature(ut)	$\Xi^{UT'} = \dfrac{\Delta T_{ad}\left(1+\Delta H_{dim}\dfrac{\gamma-1}{\gamma}\right)G_q(i)+\dfrac{\gamma-1}{\gamma}}{\Delta T_{ad}\Delta H_{dim}G_q(i)+1}$
Isothermal Adsorption	$-\dfrac{\gamma-1}{\gamma}$
Ideal Fluid-Isothermal	$\gamma = 1$
Classical Absorption	$-\dfrac{\gamma-1}{\gamma}$

Finally it is useful to summarise briefly the results that are obtained in the case of classical absorption.

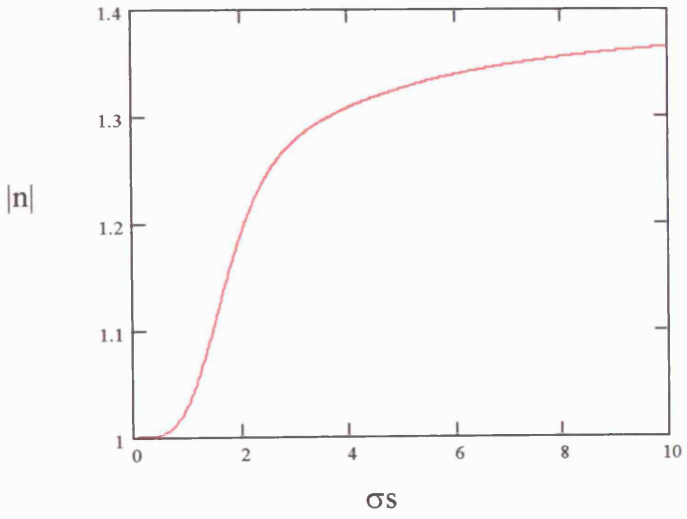

Fig.3.4 Polytropic constant as function of σs

In this case the polytropic constant is a function of the product σs, which means that the constant does not depend on the viscosity and only accounts for the effect of heat

conduction. The dependence of the polytropic constant with σs is shown in Fig. 3.4. The asymptotic values are $n = 1$ for $s = 0$, and $n = \gamma$ for $s \rightarrow \infty$, corresponding to isothermal and isentropic conditions, respectively.

3.4 Case study: CO2-Silicalite System

The attenuation coefficient for the system CO_2 – Silicalite is analysed in the pressure range [2 Torr-3 bar] at T = 304.55 K using the equilibrium parameters reported by Golden and Sircar (1994).

For this system we consider first the solution obtained in the case of an ideal gas phase with isothermal adsorption in the solid phase. This would correspond to the ideal conditions to investigate adsorption kinetics. Fig.3.5 shows the results as function of the natural frequency. This shows a maximum that, similarly to the FR in a slab geometry (Yasuda. and Sugasawa, 1982), corresponds to $f = \frac{0.42D}{h_S^2}$

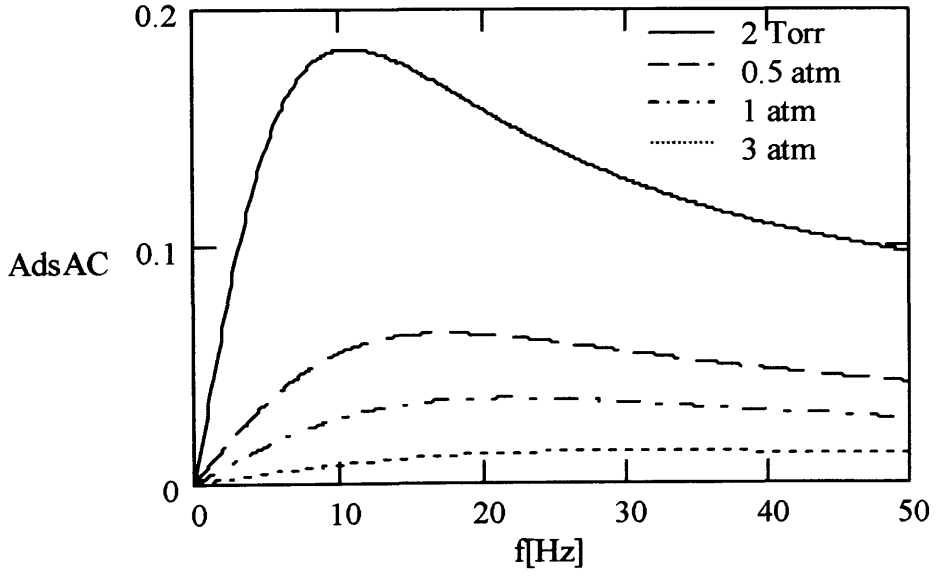

Figure 3.5 AdsAC as function of the natural frequency (h = 1mm, h_S = 10μm)

Figure 3.6 shows the effect of non-idealities in the gas phase, and the comparison between the AC for classical absorption and the effect of isothermal adsorption.

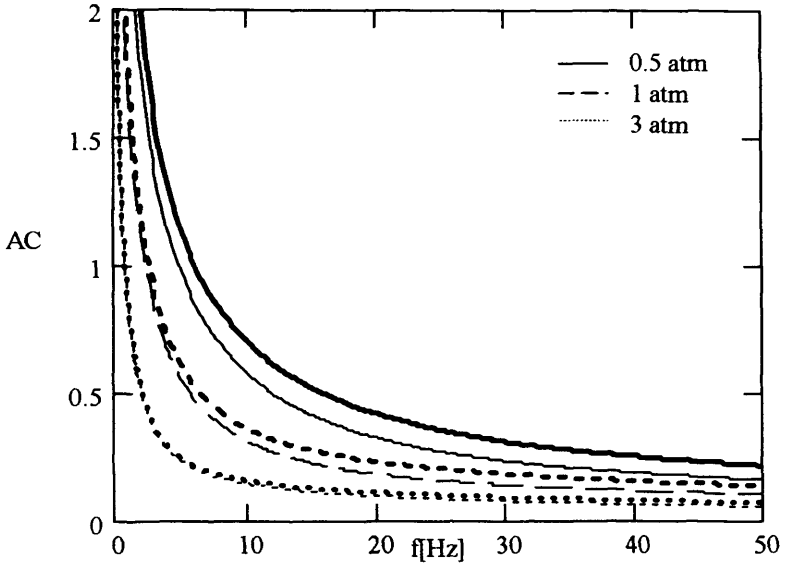

Figure 3.6 AC with adsorption (heavy line) and classic AC (thin line) as function of the natural frequency (h = 1mm, h_S = 10μm)

From this figure it is possible to see the effect of the adsorption isotherm. As the pressure increases, the slope of the isotherm decreases and the effect on sound propagation is reduced.

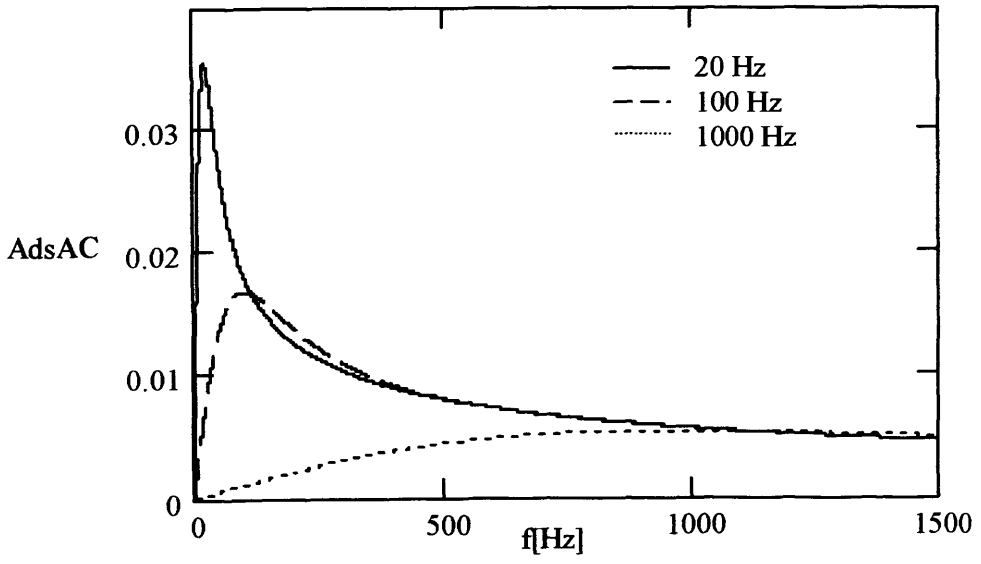

Figure 3.7 AdsAC as function of the natural frequency at P = 1atm.

Below atmospheric conditions, even for this relatively weakly adsorbed system, the effect of adsorption on sound propagation can be distinguished clearly.

Fig. 3.7 shows the AC for 3 different characteristic times corresponding to a solid fraction (h_s/h) of: 0.01, $4.5 \cdot 10^{-3}$, $1.5 \cdot 10^{-3}$. The reduction of the crystal size determines a reduction in spectrum amplitude due to the reduction of adsorbent mass for the same half slab distance (i.e. same classic absorption).

3.6 Summary

The solution to the modelling equations that has been derived suggests that adsorption affects the propagation of sound and this effect can be interpreted in a straightforward analogy with the FR technique, which corresponds to the limiting case of wavelength >> dimensions of the FR batch volume. The technique should be applicable to fast diffusing strongly adsorbed systems, which are difficult to measure using current macroscopic techniques. Classical effects and the effect of the temperature need to be carefully considered in order to specify the experimental conditions suitable for the determination of micropore diffusivities.

Chapter 4
Parametric study of the Model

4.1 Introduction

The model described accounts for the effect of adsorption and diffusion in porous solids on the propagation of a sound wave. The model is based on Kirchhoff's theory for sound propagation (1868) in a tube and an analytical solution has been obtained in the limit of the Low Reduced Frequency Approximation (LRFA) (Tijdeman,1975). While the parameters affecting the sound propagation in a non-adsorbent rigid porous solid are the porosity, the resistance constant (viscosity) and the structure factor (Zwikker and Kosten, 1949) in the presence of a porous adsorbent the effect of adsorption and mass transfer according to a diffusion model have been included.

The following parametric study aims to identify the key parameters of the model and to clarify the dependence of the solution on these parameters.

4.2 General Solution

As seen in Chapter 3 the solution to the general model is expressed in terms of the propagation constant Γ.

$$\Gamma = i\sqrt{\frac{\gamma}{n}}\sqrt{\frac{1}{\left(1-\frac{\tanh\left(\sqrt{i}\,s\right)}{\sqrt{i}\,s}\right)}} \tag{1}$$

$$n = \left\{1-\left[\frac{\gamma-1}{\gamma}-\Xi\frac{\tanh\left(\sqrt{i}\,\sigma s\right)}{\sqrt{i}\,\sigma s}\right]+Ap\left[1+\Delta H_{dim}\left(\frac{\gamma-1}{\gamma}-\Xi\right)\right]\cdot\left|G_q(i)\right|\cdot e^{\left(i\arg\left(G_q(i)\right)\right)}\right\}^{-1} \tag{2}$$

including σ (the square root of the Prandtl number) and γ (ratio of molar heats), Γ is a function of 7 dimensionless parameters: s the shear wave number, Ap and k_d related to adsorption and diffusion in the solid phase, ΔH_{dim} , ΔT_{ad} ,Cp_r and Le related to thermal effects.

$s = h\sqrt{\frac{\rho\omega}{\mu}}$ is the shear wave number, the equivalent of the Reynolds number for the acoustic problem.

$Ap = \frac{q_s K_p}{p_s}\frac{(1-\varepsilon)}{\varepsilon}$ is the ratio solid-gas phases hold-ups.

$k_d = \frac{\omega h_s^2}{D}$ is diffusion characteristic frequency.

$\Delta T_{ad} = \frac{|\Delta H| q_s K_p}{(\rho Cp)_{hm} T_s}$ represents the adiabatic temperature fluctuation.

$\Delta H_{\dim} = \frac{\Delta H}{RT_s}$ is dimensionless heat of adsorption.

Le is the Lewis number $Le = \frac{\lambda_{hm}}{D(\rho Cp)_{hm}} = \frac{k_d}{k_\lambda}$ and represents the ratio between mass and thermal diffusivities, i.e. $k_\lambda = \frac{\omega h_s^2 (\rho Cp)_{hm}}{\lambda_{hm}}$.

$Cp_r = \frac{\rho Cp}{(\rho Cp)_{hm}}\frac{\varepsilon}{1-\varepsilon}$ represents the ratio between the gas and solid phase thermal capacities.

4.3 Criteria for Limiting Solutions

To determine the numerical values for the parameters so that simplified versions of the general model should be applied, there is the need to define a quantitative criterion. This approach will identify the regions in which experiments should be carried out in order

to obtain meaningful information on mass transfer kinetics. In the sections that will follow the boundaries between models of increasing complexity will be defined using:

1) $\mathrm{Re}(\Gamma)$<1% and <10% to determine the range of the Classic Absorption and Ideal Sound Propagation models as functions of the shear wave number.

2) $\frac{\mathrm{Re}(\Gamma)-\mathrm{Re}(\Gamma^{i})}{\mathrm{Re}(\Gamma^{i})}$ <1% and <10% to determine range of validity of the Classic Absorption and Isothermal Adsorption models as functions of the Shear wave Number and Ap.

3) $\frac{\mathrm{Re}(\Xi^{UT})-\frac{\gamma-1}{\gamma}}{\frac{\gamma-1}{\gamma}}$<1% and <10% to determine the range of validity of the Uniform Temperature and Isothermal Adsorption models as functions of the ΔH_{dim}.

4) $\frac{\mathrm{Re}(\Xi)-\mathrm{Re}(\Xi^{UT})}{\mathrm{Re}(\Xi^{UT})}$<1% and <10% to determine the range of validity of the General Model and Uniform Temperature Models as function of the ΔH_{dim} and Le.

4.4 Classic Absorption -Ideal Sound Propagation

In the absence of adsorption (i.e. sound propagation between two slabs of non adsorbent material) the propagation of a sound wave is affected only by the shear stress and the thermal conduction of the gas phase. In Ultrasonic literature these effects are indicated as classical effects (Herzfeld, K. F, 1959). In this case the propagation constant Γ is given by:

$$\Gamma = i\sqrt{\frac{\gamma}{n_c}}\sqrt{\frac{1}{\left(1-\frac{\tanh\left(\sqrt{i}\,s\right)}{\sqrt{i}\,s}\right)}} \qquad (3)$$

where

$$n_c = \left\{1 - \frac{\gamma - 1}{\gamma}\left[1 - \frac{\tanh\left(\sqrt{i}\,\sigma s\right)}{\sqrt{i}\,\sigma s}\right]\right\}^{-1} \tag{4}$$

The solution differs from the LRFA solution (Tidjeman, 1975) only for different geometries. According the LRFA the propagation of a planar wave between two slabs, is then a function only of the shear wave number s, assuming σ and γ constants. In the limit of $s \to \infty$ (high frequency, low viscosity, large mean density or large tube radii) the propagation constant Γ reduces to the imaginary unit (i) (ideal **isentropic sound propagation**), no attenuation and Phase Shift = 1. In the limit of $s \to 0$ the propagation constant $\Gamma = i\sqrt{\gamma}$ **(ideal isothermal sound propagation)**. In Fig. 4.1 the value of the polytropic constant is shown as a function of the frequency.

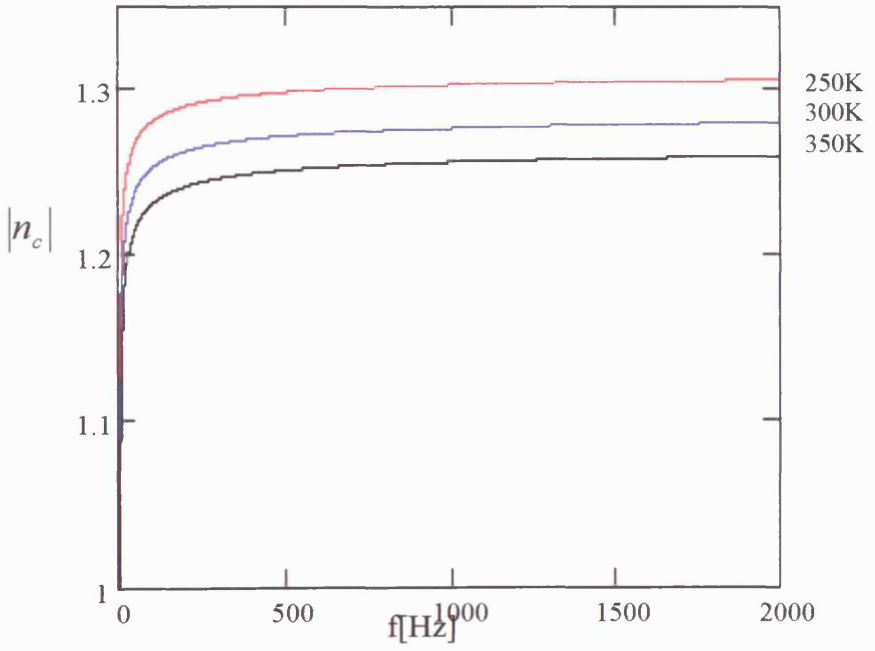

Fig.4.1 n for CO_2 as function of frequency in the temperature range [250K-350K]

At high frequency $|n_c|$ approaches the adiabatic limit γ, while at low frequency the isothermal limit $|n_c|$=1.

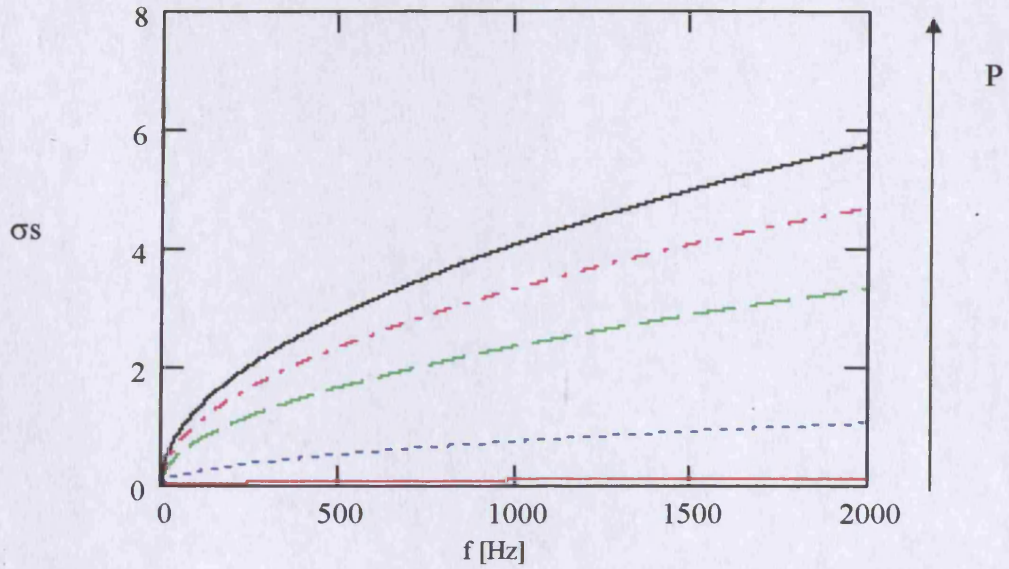

Fig.4.2 σs (CO_2 , T = 300K) as a function of the frequency in the range of pressure 1 Torr-3 bars, for a half slab distance h = 0.1mm.

The following diagrams show the Attenuation Coefficient and the Phase Shift as a function of the shear wave number.

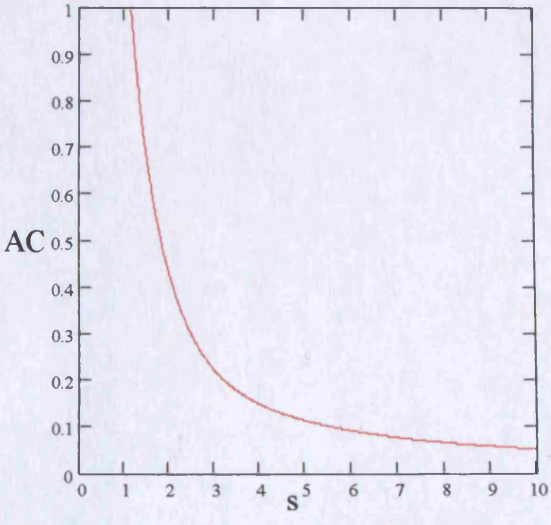

Fig.4.3 AC as function of s

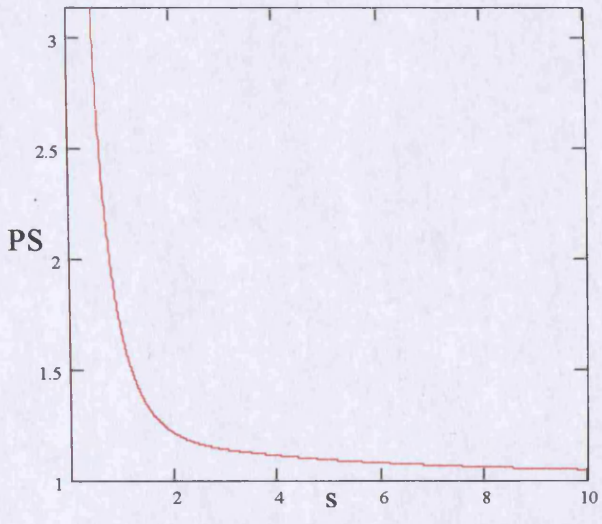

Fig.4.4 PS as function of s

From Figs 4.2-4.4 it is possible to verify that increasing the pressure, the dissipation due to classical effects decreases.

Figs 4.3 and 4.4 show that for s > 5.6 $\mathrm{Re}(\Gamma) - \mathrm{Re}(\Gamma^{i}) < 0.1$. This result is very close to the one found for the cylindrical geometry (Tidjeman, 1975). For simplicity it seems reasonable assume that for s >10, sound propagation can be considered ideal.

Fig.4.5 shows the reduced frequency k as a function of the shear wave number, for CO_2 at room temperature, showing that the LRFA assumption k << 1 is valid in the range of interest. (k<<1, and k/s<<1)

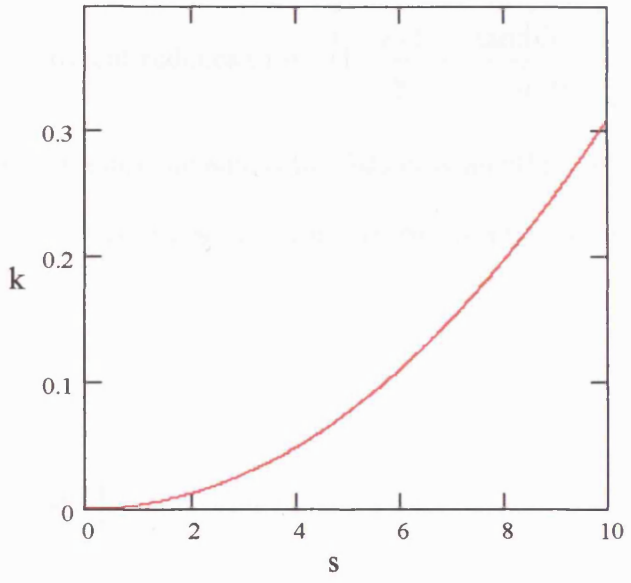

Fig.4.5 Reduced Frequency as function of the shear wave number (s).

4.5 Isothermal Adsorption - Classic

Because of the pressure dependence of the adsorption equilibrium, if a planar wave propagates between two slabs of adsorbent material, initially saturated with the gas, the fluctuations of the pressure determines fluctuations of the adsorbate concentration.

The fluctuations in the adsorbate concentration determine a spatial distribution of the concentration in the microporous solid and a relative diffusion problem.

In this case the polytropic coefficient is given by:

$$n=\left\{1-\frac{\gamma-1}{\gamma}\left[1-\frac{\tanh\left(\sqrt{i}\,\sigma s\right)}{\sqrt{i}\,\sigma s}\right]+Ap\cdot\left|G_q(i)\right|\cdot e^{\left(i\arg\left(G_q(i)\right)\right)}\right\}^{-1} \tag{5}$$

In the limit of high frequencies or long diffusion time ($k_d>>1$), $G_q(i)\to 0$ and the adsorption accordingly with the physical intuition has no effect on the sound wave and the Propagation Constant reduces to the classical one (Eq. 4).

In the limit of the low frequencies or short diffusion time (i.e. $k_d<<1$) $G_q(i)\to 1$,

and the polytropic coefficient reduces to $n=\left\{1-\frac{\gamma-1}{\gamma}\left[1-\frac{\tanh\left(\sqrt{i}\,\sigma s\right)}{\sqrt{i}\,\sigma s}\right]+Ap\right\}^{-1}$

implying that at low frequency the adsorption has only an effect on the phase shift.

To clarify the analysis it is useful to consider the limiting case of a fluid with no viscosity:

$$\Gamma=i\sqrt{\frac{\gamma}{n}} \tag{6}$$

$$n=\left\{1+Ap\cdot\left|G_q(i)\right|\cdot e^{\left(i\arg\left(G_q(i)\right)\right)}\right\}^{-1} \tag{7}$$

For $k_d<<1$, $n=\left\{1+Ap\cdot\right\}^{-1}$

We can observe that the modulus of the transfer function for the concentration gradient varies from 1 to 0 for k_d varying from 0 to ∞ and that AC shows a maximum related to a characteristic diffusional time k_d,

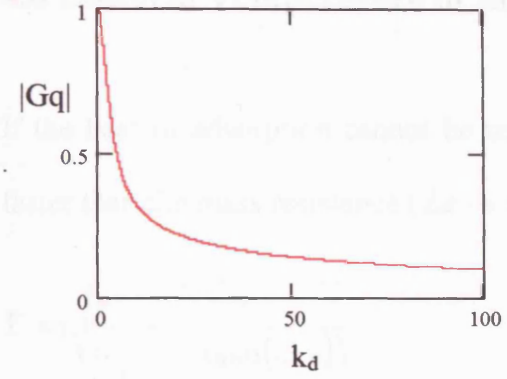

Fig.4.6 Module of Gq as function of k_d

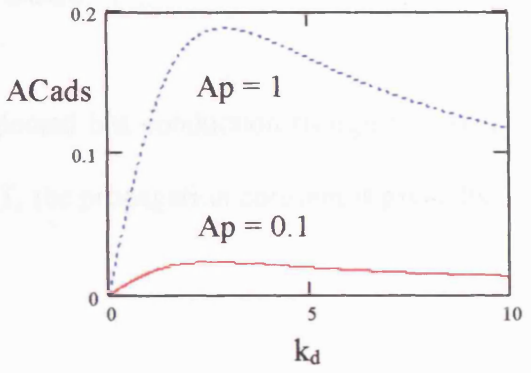

Fig.4.7 ACads as function of k_d

The maximum in ACads suggests the possibility of identifying the diffusional characteristic time by an attenuation measurement.

Consequently it is worth to consider the effect of Ap and s on the maximum attenuation.

The following diagram shows the regions of the validity of the criterion

$$\frac{\mathrm{Re}(\Gamma)-\mathrm{Re}(\Gamma^i)}{\mathrm{Re}(\Gamma^i)} < 1\% \text{ and } < 10\%$$

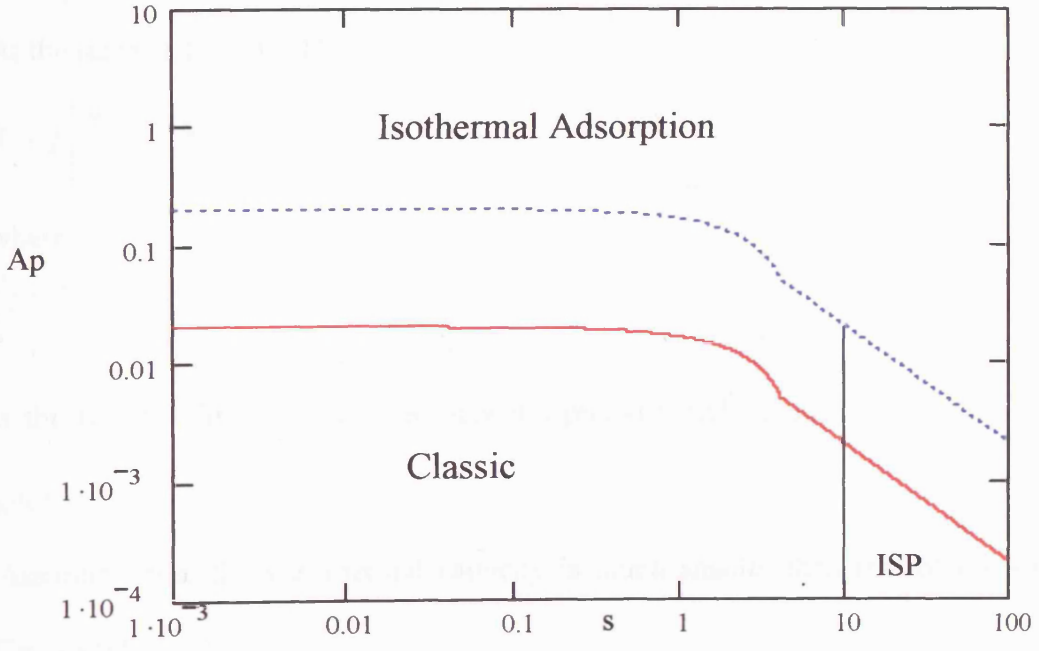

Fig.4.8 Region of validity of Isothermal Adsorption, Classic and Ideal Sound Propagation (ISP).

4.6 Uniform Temperature of the Solid

If the heat of adsorption cannot be neglected but conduction trough the solid is much faster than the mass resistance ($Le \to \infty$), the propagation constant is given by:

$$\Gamma = i\sqrt{\frac{\gamma}{n}}\sqrt{\frac{1}{\left(1-\frac{\tanh\left(\sqrt{i}\,s\right)}{\sqrt{i}\,s}\right)}} \tag{8}$$

$$n = \left\{1-\left[\frac{\gamma-1}{\gamma}-\Xi^{UT}\frac{\tanh\left(\sqrt{i}\,\sigma s\right)}{\sqrt{i}\,\sigma s}\right]+Ap\left(1+\Delta H_{dim}\left[\frac{\gamma-1}{\gamma}-\Xi^{UT}\right]\right)\cdot\left|G_q(i)\right|\cdot e^{\left(i\arg\left(G_q(i)\right)\right)}\right\}^{-1} \tag{9}$$

and Ξ^{UT} is the non-isothermal factor due to adsorption and it is given by:

$$\Xi^{UT} = \frac{\Delta T_{ad}\left(1+\Delta H_{dim}\frac{\gamma-1}{\gamma}\right)G_q(i)+\frac{\gamma-1}{\gamma}}{\Delta T_{ad}\Delta H_{dim}G_q(i)+\frac{Cp_r\tanh\left(\sqrt{i}\,\sigma s\right)}{\sqrt{i}\sigma s}+1} \tag{10}$$

and the corresponding gas temperature profile is:

$$T = p\left[\frac{\gamma-1}{\gamma}-\Xi^{UT}\frac{\cosh\left(\sqrt{i}\,\sigma s\zeta\right)}{\cosh\left(\sqrt{i}\,\sigma s\right)}\right] \tag{11}$$

At the surface $(\zeta = +,-1)$,

$$T = p\left[\frac{\gamma-1}{\gamma}-\Xi^{UT}\right] \tag{12}$$

where

$$\left[\frac{\gamma-1}{\gamma}-\Xi^{UT}\right] \tag{13}$$

is the transfer function between acoustic pressure and "acoustic" temperature of the solid.

Assuming that the gas thermal capacity is much smaller than that of the solid (i.e. $Cp_r \to 0$)

Parametric Study of the Model

$$\Xi^{UT'} = \frac{\Delta T_{ad}\left(1+\Delta H_{\dim}\frac{\gamma-1}{\gamma}\right)G_q(i)+\frac{\gamma-1}{\gamma}}{\Delta T_{ad}\Delta H_{\dim}G_q(i)+1} \tag{14}$$

$\Xi^{UT'}$ is a complex number, implying that there will be a phase shift between pressure and solid temperature.

In the limit of the low frequencies or short diffusion time (i.e. $k_d<<1$) $G_q(i)\to 1$, the non-isothermal factor reduces to

$$\Xi^{UT'} = \frac{\Delta T_{ad}\left(1+\Delta H_{\dim}\frac{\gamma-1}{\gamma}\right)+\frac{\gamma-1}{\gamma}}{\Delta T_{ad}\Delta H_{\dim}+1} \tag{15}$$

and because it is a real number there is no PS between acoustic pressure and temperature.

In the limit of high frequencies or long diffusion time ($k_d>>1$), $G_q(i)\to 0$ and the adsorption according to physical intuition has no effect on the sound wave.

In the limit of a very high heat of adsorption:

$$\lim_{\Delta H_{\dim}\to\infty}\Xi^{UT'} = \frac{\frac{|\Delta H_{\dim}|q_s K_p R}{(\rho Cp)_{hm}}\left(1+\Delta H_{\dim}\frac{\gamma-1}{\gamma}\right)G_q(i)+\frac{\gamma-1}{\gamma}}{\frac{|\Delta H_{\dim}|q_s K_p R}{(\rho Cp)_{hm}}\Delta H_{\dim}G_q(i)+1} = \frac{\gamma-1}{\gamma} \tag{16}$$

and the polytropic coefficient reduces to the classical one

$$n=\left\{1-\left[\frac{\gamma-1}{\gamma}-\Xi\frac{\tanh\left(\sqrt{i}\,\sigma s\right)}{\sqrt{i}\,\sigma s}\right]\right\}^{-1} \tag{17}$$

In the limit of very high heat of adsorption no adsorption occurs.

The following figures show non-isothermal factor as function of the reduced frequency, for different value of the dimensionless heat of adsorption:

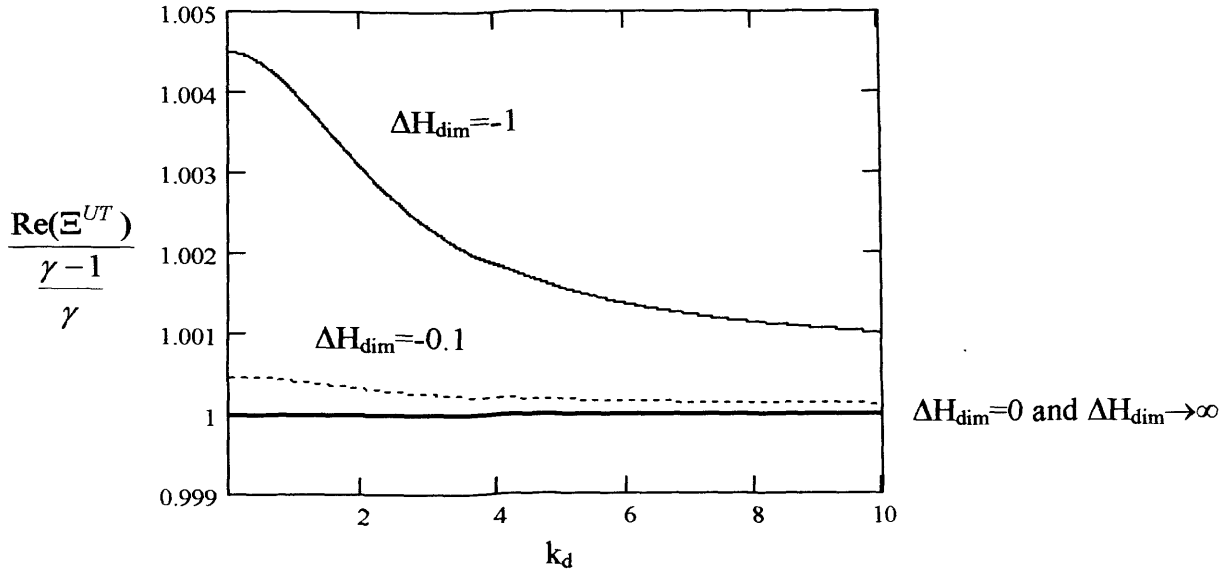

Fig.4.9 Real Part of the Non Isothermal factor as function of the reduced diffusive frequency. Isothermal Adsorption. ——

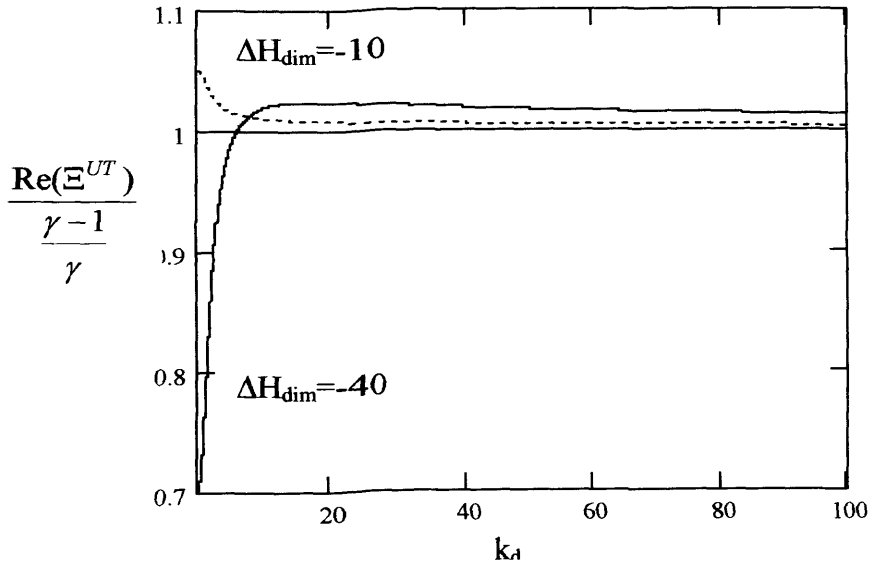

Fig.4.10 Real Part of the non isothermal factor as function of the reduced diffusive frequency .

In the limit of $\Delta T_{ad} = \frac{\Delta H q_s K_p}{(\rho Cp)_{hm} T_s} \to 0$ $\Xi^{UT'} = \frac{\gamma - 1}{\gamma}$, the isothermal adsorption model is obtained. Accordingly a criterion for neglecting thermal effects can be defined in terms of: $\left| \frac{\mathrm{Re}\left(\Xi^{UT'}\right) - \frac{\gamma - 1}{\gamma}}{\frac{\gamma - 1}{\gamma}} \right|$ <1% and <10% in the limit of $k_d \to 0$.

Because the main parameter is the heat of adsorption, for $\Delta H_{dim} < 2$ and $\Delta H_{dim} < 20$, the criteria are verified.

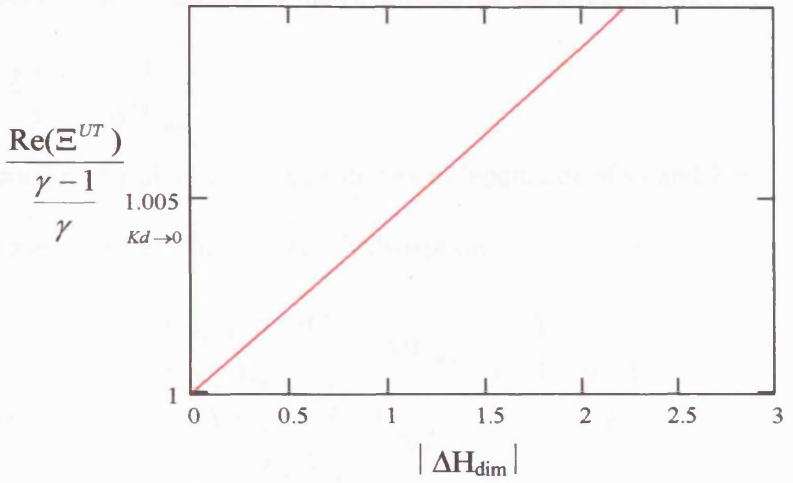

Fig.4.11 Real Part of the Non Isothermal factor as function of the ΔH_{dim} for $k_d \to 0$.

4.7 Temperature Resistance Control

If the mass diffusivity trough the solid is much faster than the thermal conduction (i.e. $Le \to 0$) the non-isothermal factor Ξ reduces to Ξ^{TC}

$$\Xi^{TC} = \frac{\Delta T_{ad}\left(1 + \Delta H_{dim}\frac{\gamma - 1}{\gamma}\right) G_q(i)}{\Delta T_{ad}\Delta H_{dim} G_q(i) + \frac{Cp_r \tanh\left(\sqrt{i\sigma s}\right)}{\sqrt{i\sigma s}}} \qquad (18)$$

and

$$n=\left\{1-\left[\frac{\gamma-1}{\gamma}-\Xi^{TC}\frac{\tanh\left(\sqrt{i}\,\sigma s\right)}{\sqrt{i}\,\sigma s}\right]+Ap\left(1+\Delta H_{dim}\left[\frac{\gamma-1}{\gamma}-\Xi^{TC}\right]\right)\cdot\left|G_q(i)\right|\cdot e^{\left(i\arg\left(G_q(i)\right)\right)}\right\}^{-1} \tag{19}$$

in the limit of $\Delta H_{dim}\to 0$, $\left(\Delta T_{ad}=\frac{\Delta H_{dim}Rq_sK_p}{(\rho Cp)_{hm}}\right)$,

$$n=\left\{1-\frac{\gamma-1}{\gamma}+Ap\cdot\left|G_q(i)\right|\cdot e^{\left(i\arg\left(G_q(i)\right)\right)}\right\}^{-1} \tag{20}$$

implying that also the gas temperature is uniform along ζ.

If the gas thermal capacity is much smaller of the solid one (i.e. $Cp_r\to 0$)

$$\Xi^{TC'}=\frac{\gamma-1}{\gamma}+\frac{1}{\Delta H_{dim}} \tag{21}$$

and according to physical intuition it is independent of k_d and Kp.

In the limit of a very high heat of adsorption:

$$\lim_{\Delta H_{dim}\to\infty}\Xi^{TC'}=\frac{\frac{\left|\Delta H_{dim}\right|q_sK_pR}{(\rho Cp)_{hm}}\left(1+\Delta H_{dim}\frac{\gamma-1}{\gamma}\right)}{\frac{\left|\Delta H_{dim}\right|q_sK_pR}{(\rho Cp)_{hm}}\Delta H_{dim}}=\frac{\gamma-1}{\gamma} \tag{22}$$

and the polytropic coefficient reduces to the classical one

$$n=\left\{1-\left[\frac{\gamma-1}{\gamma}-\Xi\frac{\tanh\left(\sqrt{i}\,\sigma s\right)}{\sqrt{i}\,\sigma s}\right]\right\}^{-1} \tag{23}$$

In the limit of very small heat of adsorption $\Xi^{TC'}$ diverges.

The following figure shows the non-isothermal factor as function of the dimensionless heat of adsorption.

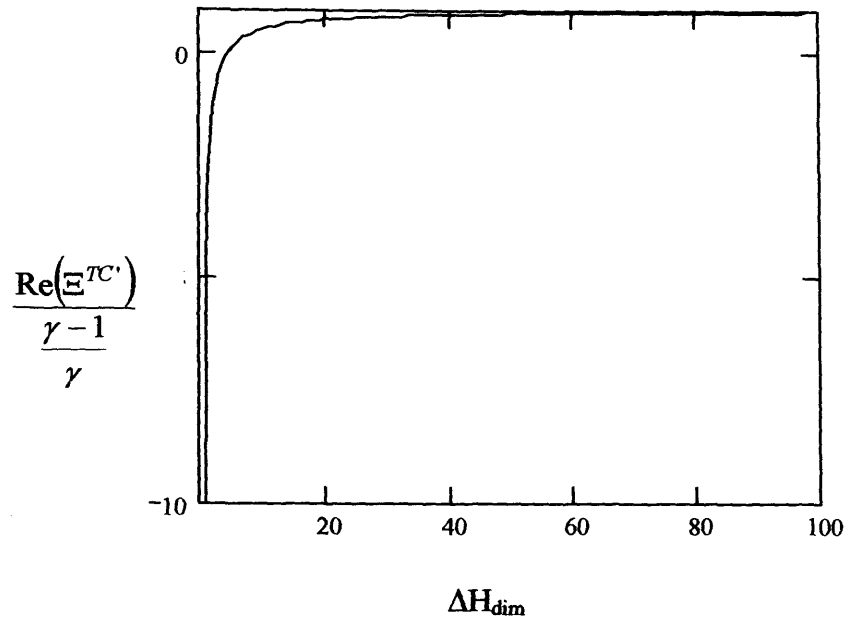

Fig.4.12 Non Isothermal factor as function of the ΔH_{dim}

4.8 General Model

$$\Gamma = i\sqrt{\frac{\gamma}{n}}\sqrt{\frac{1}{\left(1-\frac{\tanh\left(\sqrt{i}\,s\right)}{\sqrt{i}\,s}\right)}} \tag{24}$$

$$n=\left\{1-\left[\frac{\gamma-1}{\gamma}-\Xi\frac{\tanh\left(\sqrt{i}\,\sigma s\right)}{\sqrt{i}\,\sigma s}\right]+Ap\left(1+\Delta H_{dim}\left[\frac{\gamma-1}{\gamma}-\Xi\right]\right)\cdot\left|G_q(i)\right|\cdot e^{\left(i\arg\left(G_q(i)\right)\right)}\right\}^{-1} \tag{25}$$

and

$$\Xi=\frac{\frac{\Delta T_{ad}}{\sqrt{Le}}\left(1+\Delta H_{dim}\frac{\gamma-1}{\gamma}\right)\Psi(k_d,Le)+\frac{\gamma-1}{\gamma}}{\frac{\Delta T_{ad}}{\sqrt{Le}}\Delta H_{dim}\Psi(Kd,Le)+\sqrt{\frac{Kd}{Le}}\frac{\Phi(\sigma s,k_d,Le)}{\sigma s}Cp_r+1} \tag{26}$$

Assuming the gas thermal capacity is much smaller of the solid one (i.e. $Cp_r \to 0$)

$$\Xi = \frac{\frac{\Delta T_{ad}}{\sqrt{Le}}\left(1+\Delta H_{\dim}\frac{\gamma-1}{\gamma}\right)\Psi(k_d,Le)+\frac{\gamma-1}{\gamma}}{\frac{\Delta T_{ad}}{\sqrt{Le}}\Delta H_{\dim}\Psi(k_d,Le)+1} \tag{27}$$

in the limit of $\Delta H_{dim} \to 0$, we obtain the isothermal adsorption limit

$$\Xi = \frac{\gamma-1}{\gamma}$$

The criterion function $\frac{\mathrm{Re}(\Xi)-\mathrm{Re}(\Xi^{UT})}{\mathrm{Re}(\Xi^{UT})}$ has been evaluated for $k_d \ll 1$ where the deviation from the isothermal case shows a maximum (Figs 9 and 10). The following figures show the real part of the non-isothermal adsorption factor ratio as function of the dimensionless heat of adsorption for different values of Le.

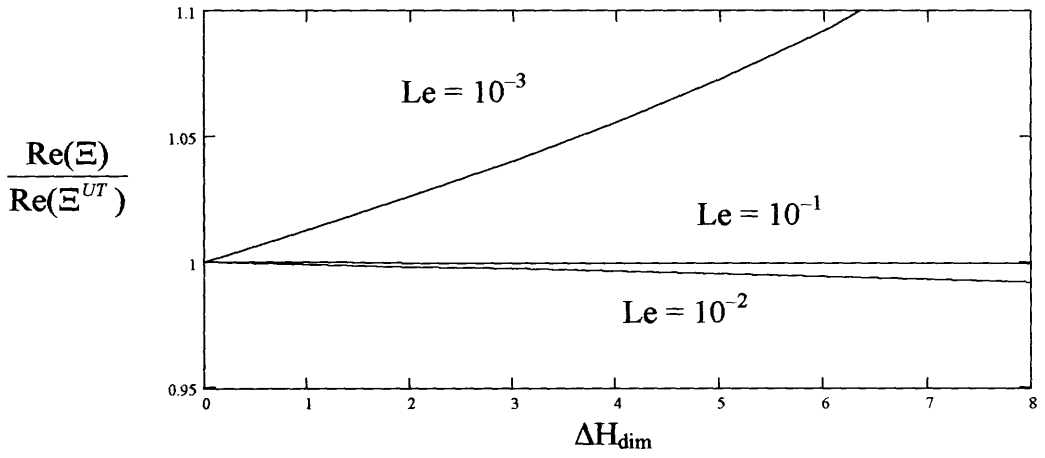

Fig.4.13 Real part ratio of the non-isothermal adsorption factor as function of the ΔH_{dim}.

Independently of the ΔH_{dim}, for Le>0.1 the Uniform Temperature model can be applied. The deviation can be positive or negative.

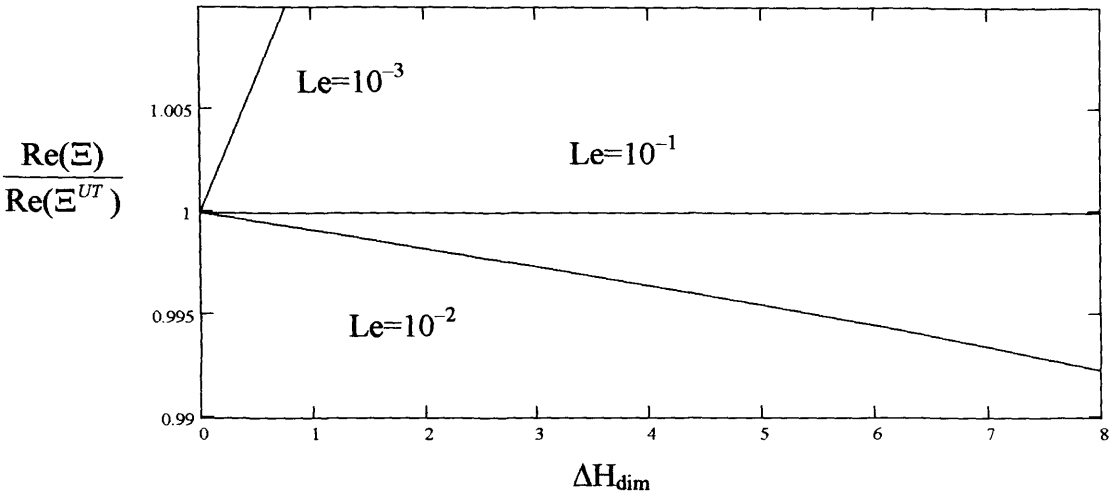

Fig.4.14 Real part ratio of the non-isothermal adsorption factor as function of the ΔH_{dim}.

4.9 Summary

The developed model predicts two fundamental aspects: 1) the presence of an adsorbent microporous material increases the effect of absorption and dispersion of the sound wave 2) AC presents a maximum related to the characteristic time of diffusion.

The parametric analysis of the model indicates that the important parameters are s, Ap, k_d , ΔH_{dim} and Le. On the basis of these dimensionless parameters the following numerical relations are proposed for the applicability of the different models:

1) Le>10 Uniform Temperature Model

2) Le<0.1 Temperature Resistance Control

3) $|\Delta H_{dim}|<2$ Isothermal Adsorption

4) Ap<0.01 Classic Absorption

For ordinary heat of adsorption the thermal effects have not significative effect. The analysis suggest that optimal experimental conditions for determining the microporous diffusivity from an AC measurement correspond to kd range [1-10] and for Ap>0.01, "independently" of the shear wave number.

Chapter 5

A Prototype Experimental Apparatus and Preliminary Experimental Results

5.1 Introduction

In order to obtain a proof of concept of the experimental technique a prototype apparatus was designed and constructed. The simplicity of the design and the flexibility of the apparatus are the basic criteria considered. The techniques applied for measuring acoustic impedance in porous materials are classified (Zwikker and Konsten, 1949):

a) constant length method, measuring maximum and minimum pressure in the tube
b) variable length method, measuring maximum and minimum pressure at the sound source
c) variable length method, measuring curve width of pressure at the source
d) variable length method, measuring the electrical impedance of the sound source
e) short length tube, measurement of pressure and velocity

In our apparatus the pressure is measured at the end of the tube, and the adsorbent material is located between the source of sound and the microphone (See Fig. 5.1).

5.2 Experimental Apparatus

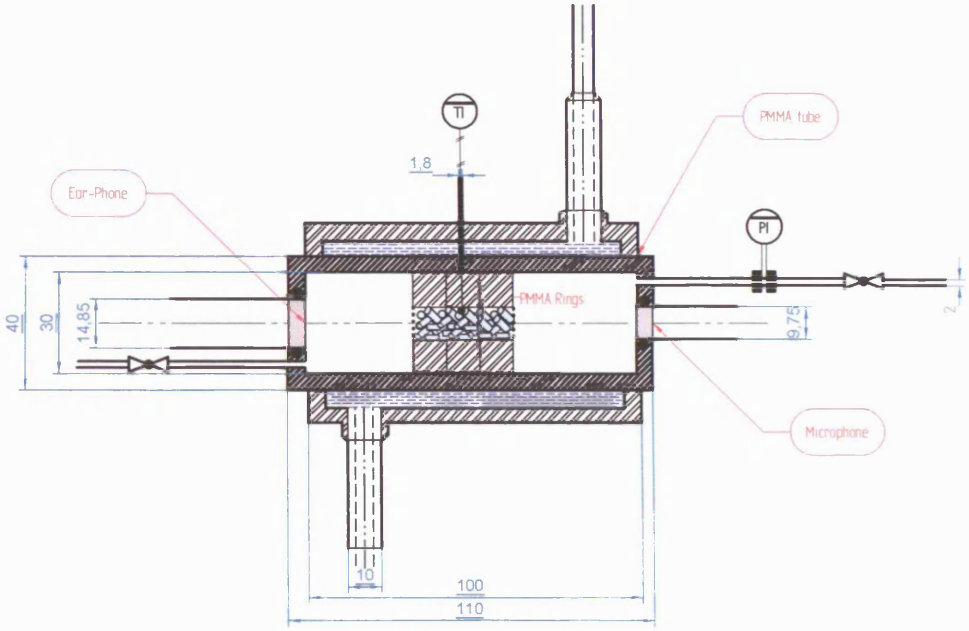

Fig. 5.1 Sketch of the experimental apparatus.

A sketch of the apparatus is shown in Fig. 5.1. It consists of a microphone and a loudspeaker (head-phone) connected through a tube (10 cm length, 3 cm internal diameter). The adsorbent material is introduced in a cylindrical chamber obtained using glass rings. The size of the chamber length and area can be modified changing the number of disks (1-3) and the internal diameter of the disks (0.5, 1, 2 cm: diameter) of the disks (See Fig. 5.2). The position of the microphone and the position of the loudspeaker can be varied. The sealing is made by using o-rings (See Fig. 5.2). The temperature of the chamber can be controlled using an external bath and a thermocouple (See Fig. 5.3), but all the current tests were run at room temperature.

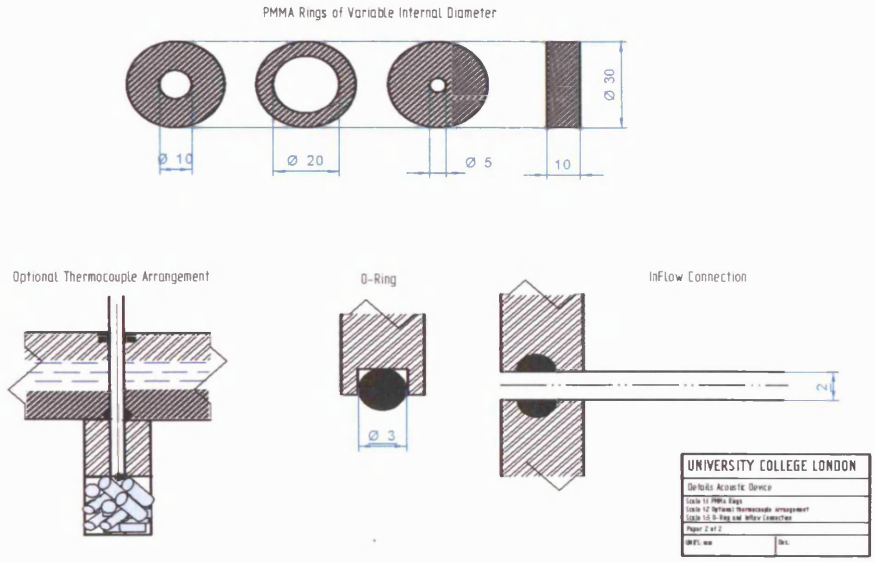

Fig. 5.2 Details of the experimental apparatus

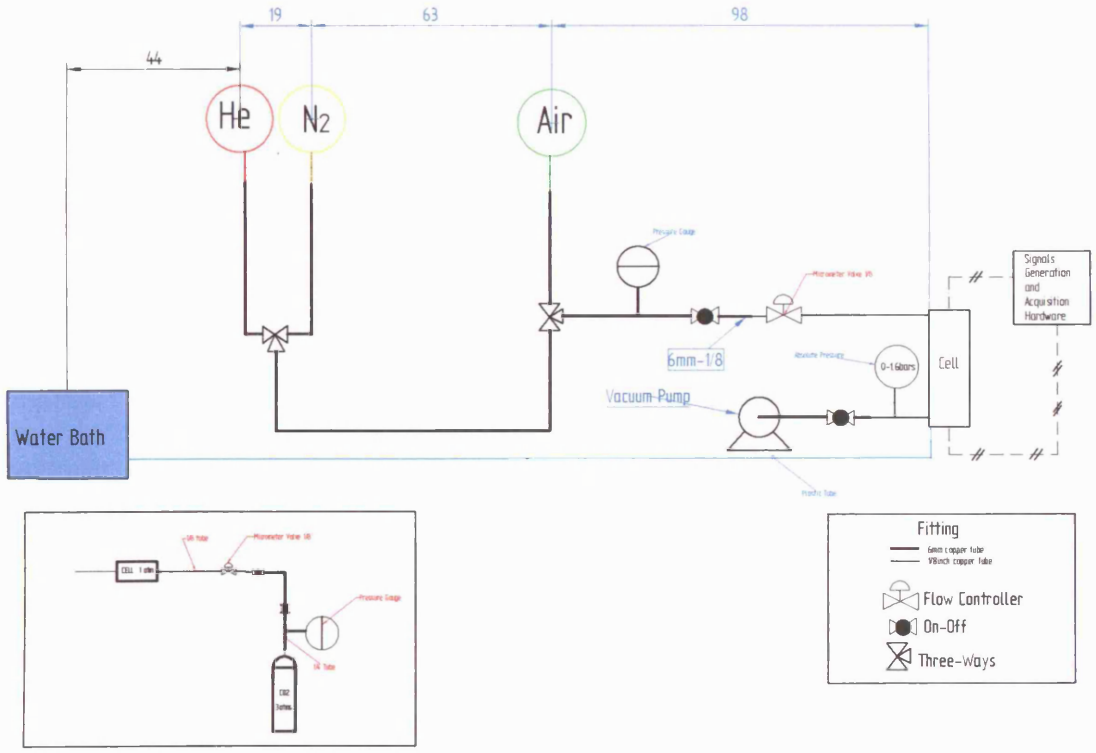

Fig. 5.3 Layout of the experimental setup

The microphone and loud-speaker are connected to a computer. The pressure is monitored using a pressure gauge. During the experiments the pressure of the system is maintained slightly above atmospheric (1.1 bar) in order to avoid any contamination from the external air. For the same reason, the system is maintained under a small flow of gas (typically 20 cc/min) in order to maintain the positive pressure difference. The flow is controlled using a micrometric valve and monitored using a soap-bubble flow meter.

5.3 Data generation and acquisition

The sound signals were generated and recorded digitally using the software SND_PC toolbox Version 1.2 (See Appendix D) for Matlab 5.0 or higher, written by Torsten Marquard. The toolbox allows the generation of sound signals of a determined frequency. The volume was fixed using the sound control interface available in the Windows operating system.

The frequencies were fixed between 50 and 2000 Hz at intervals of 50 Hz. At each frequency the sound wave was activated for more than 40000 cycles in order to achieve cyclic steady state. The last 10 cycles were used to obtain an average of the amplitude of the signal at any given frequency. Figures 5.4 to 5.8 show examples of the data generated for two gases at two different frequencies.

The Windows operating system does not activate the loudspeaker in a reproducible way, and as a result it is not possible to know exactly the starting time of the experiments. This uncertainty makes it impossible to determine with reliable accuracy phase shifts in the case of a pulse measurement, because of the time dependence of the signal. Two

microphones are usually applied in order to overcome this limitation. The configuration of the present apparatus allows recording the output normalized sound amplitudes in the case of standing wave measurements and makes comparative analysis of the systems signals possible. The position of the peaks and the high and width under the peaks depends on the PS and AC of the sound wave (Landau and Lifšits, 1976).

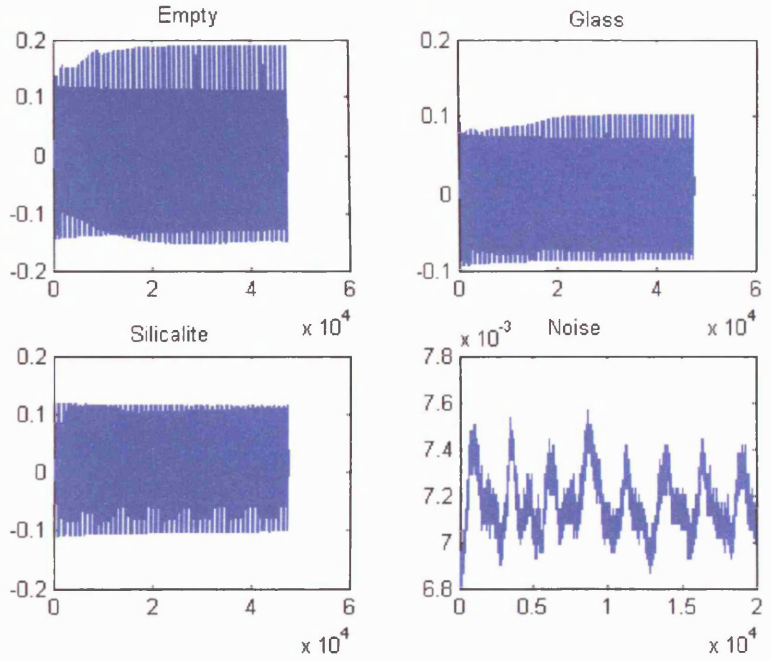

Fig. 5.4 Signals as function of the sample number for Air 100Hz

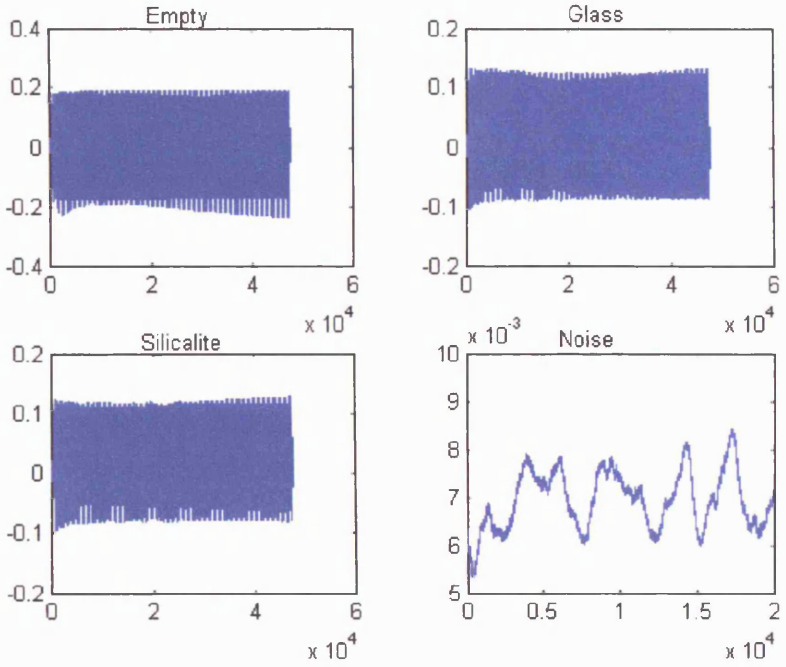

Fig. 5.5 Signals as function of the sample number for CO_2 100Hz

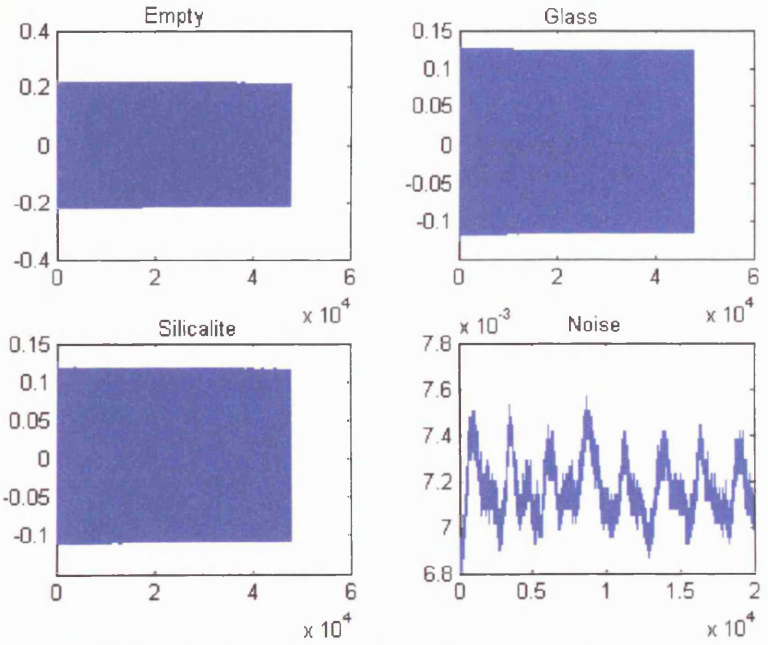

Fig. 5.6 Signals as a function of the sample number for Air 1000 Hz

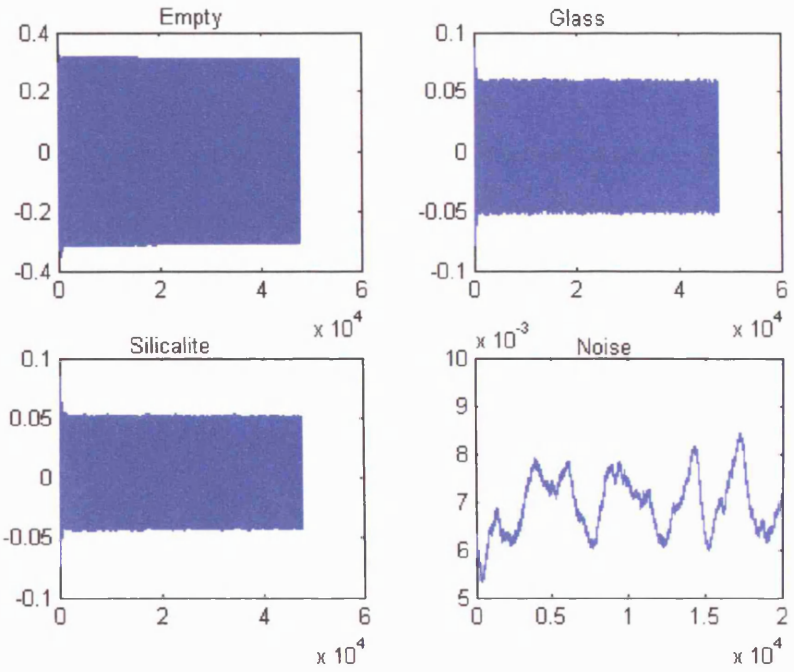

Fig. 5.7 Signals as a function of the sample number for CO_2 1000Hz

5.4 Analysis of Preliminary Experimental Data

In the frequency range 50Hz-2000 Hz, acoustic signals for air, helium, nitrogen and CO_2 are investigated in relation their interaction with packed beds of glass beads and silicalite pellets (HISIV 3000). The packed beds have a void fraction of approximately $\varepsilon \approx 0.4$. The main aim of the analysis is the identification and evaluation of "adsorption effects" on the propagation of the sound wave.[1] The following figures show the amplitudes as a function of the frequency for the empty system:

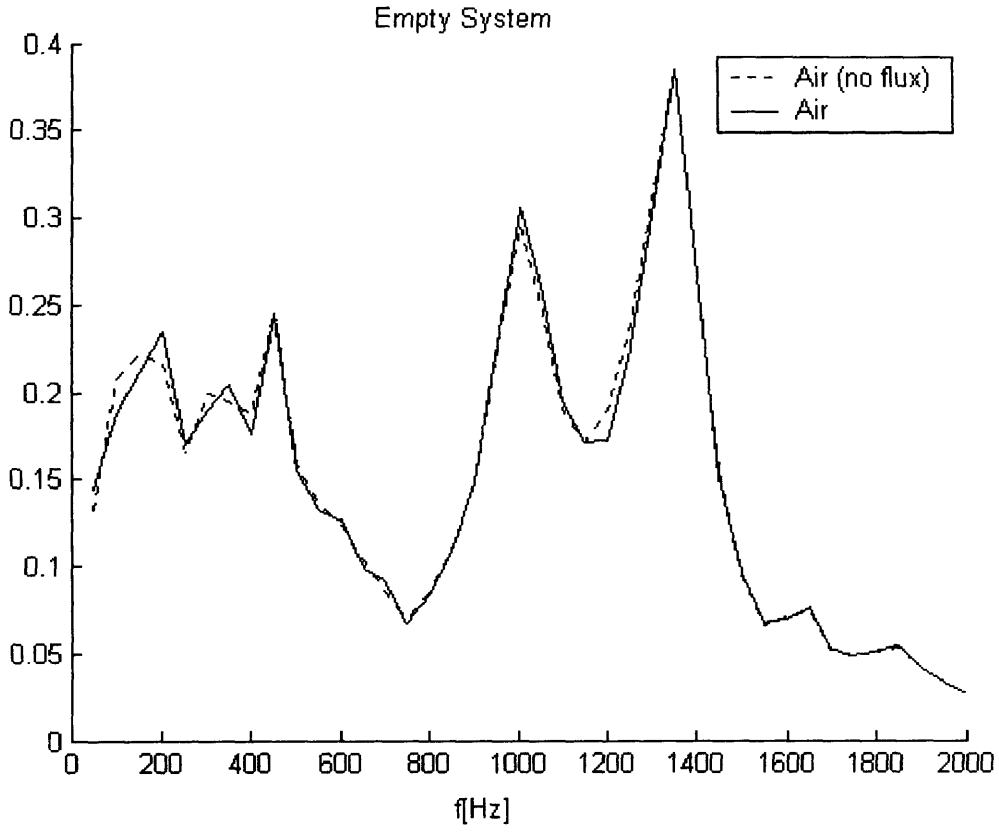

Fig.5.8a Amplitudes as a function of the frequency for the empty system.

[1] Linearity of the signals respect the amplitude has been ascertained for air.

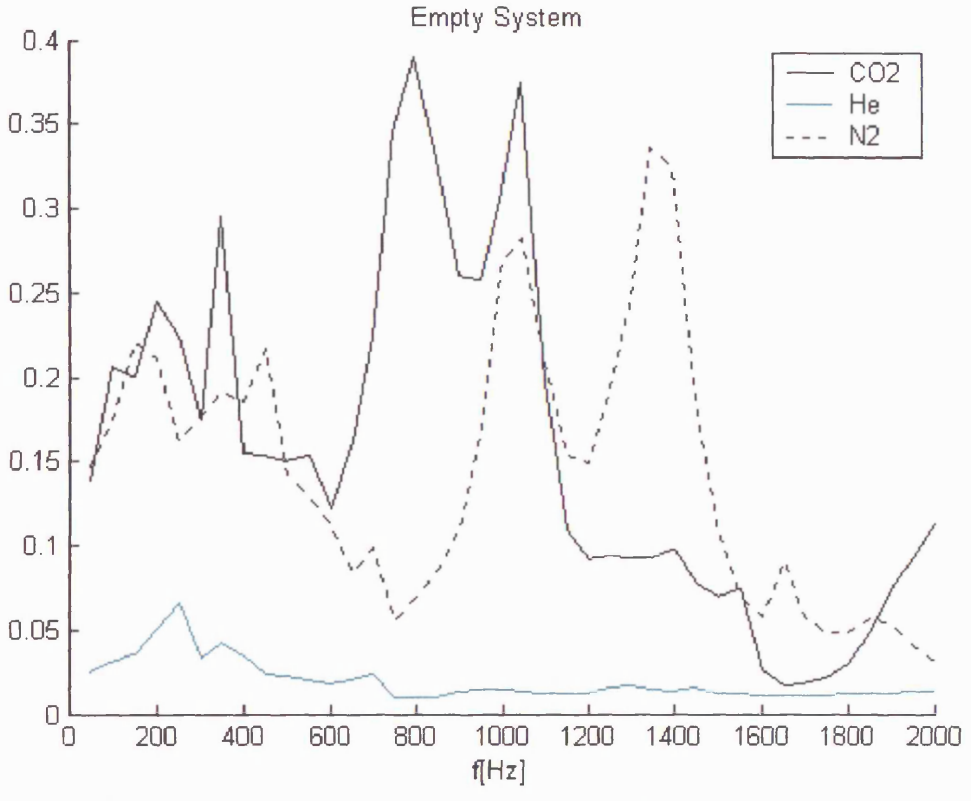

Fig.5.8b Amplitudes as a function of the frequency for the empty system.

Figure 5.8a shows that in the case of air the low velocities used in the system do not have a significant effect on the amplitude of the sound wave.

Based on these results, it is clear that resonant frequencies are present in the empty system and a simplified analysis[2] of the experimental data collected with the acoustic prototype experimental apparatus is reported in the following section.

[2] Frequency Analysis based on linearity and on pseudo-stationary dynamics of the system.

The trend of the amplitudes for the different gases (CO_2 > air > N_2 > He) is mainly due to the different densities of the gases. Table 5.1 shows the characteristic ideal impedance ($R = \rho c$).

Table 5.1 Ideal Sound Properties

Gas	C[m/s]	λ(at100Hz,1000Hz,2000Hz)[cm]	R [kg/(m^{2}s)]
Air	343	343, 34.3, 17.15	415.03
CO2	258	258, 25.8, 12.9	468.27
He	1008	1008, 108, 54	165.312
N2	349	349, 34.9, 17.45	401.35

In the Low frequency region (i.e. 0-500Hz for Air, N_2 and CO_2) the system behaves as a spatially discrete system.

5.4.1 An acoustic model of the apparatus

This analysis aims to clarify the peaks obtained in the experimental measurements. As in "organ pipes", a resonances mechanism (i.e. standing waves) is proposed to explain the peaks.

Figure 5.9 shows a simplified acoustic scheme of the apparatus. It is possible to identify three acoustic regions characterized by the specific acoustic impedances: Z2, Z3, and Z4. Z1 is the input or driven impedance of the loudspeaker and Z5 is the load impedance of the microphone.

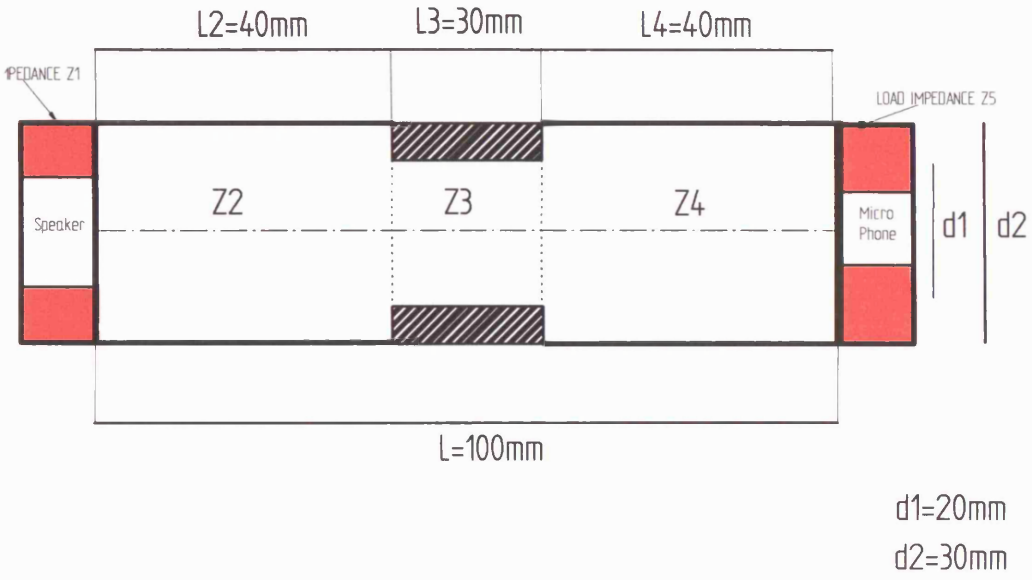

Fig.5.9 An acoustic scheme of the apparatus

To obtain an estimate of the order of magnitude of the resonant effects, we neglect in the first instance the effect of the constriction. The model reduces to the one for a driven tube (Z1 = input impedance at x = 0, Z2 = Z3 = Z4 = Z and Z5 = load impedance at x = L = 10 cm).

Assuming ideal propagation and planar waves ($\lambda > d_2$, see Table 5.1) the acoustic pressure is given by:

$$p = p_s\left(Ae^{\Gamma\xi} + Be^{-\Gamma\xi}\right)e^{i\omega t} \qquad (1)$$

At $\xi = \xi_L$, the continuities of force and particle speed require that the mechanical impedance of the wave equals the mechanical impedance of the microphone, Z5.

$$Z5 = W_0 S \frac{Ae^{\Gamma\xi_L} + Be^{-\Gamma\xi_L}}{Ae^{\Gamma\xi_L} - B^{-\Gamma\xi_L}} \tag{3}$$

The loudspeaker mechanical impedance Z1[3] at $\xi=0$ is correspondingly given by

$$Z1 = W_0 S \frac{A+B}{A-B} \tag{4}$$

Combining these equations to eliminate A and B, we obtain

$$\frac{Z1}{W_0 S} = \frac{\frac{Z5}{W_0 S} - \tanh(\Gamma\xi_L)}{1 - \frac{Z5}{W_0 S}\tanh(\Gamma\xi_L)} \tag{5}$$

Rewriting the load impedance in terms of resistance (r) and reactance (x_r) components:

$$\frac{Z5}{W_0 S} = r + jx_r \tag{6}$$

The frequency of resonance and antiresonance are determined by the vanishing of the input reactance[4]:

$$\frac{x_r \tanh^2(\Gamma\xi_L) - i\left(r^2 + x_r^{\,2} - 1\right)\tanh(\Gamma\xi) + x_r}{\left(r^2 + x_r^{\,2}\right)\tanh(\Gamma\xi_L) - 2jx_r \tan(\Gamma\xi_L) + 1} = 0 \tag{7}$$

The determination of the resonance and antiresonance frequency reduces to the determination of r and x for the microphone.

As a first approximation (i.e.$d_m/d_2 \approx 1/3$), we assume $Z5 = \infty$ and the solution reduces to the one for the closed end tube:

---

[3] Here we assume a light and "flexible" loudspeaker

[4] Fundamentals of Acoustics, Kinsler et al (1980)

$$\frac{Z1}{W_0 S} = -\coth(\Gamma \xi_L) \tag{8}$$

In the case of an ideal sound wave the reactance is zero when $\coth(\Gamma \xi_L) = 0$

$$\xi_L = (2n-1)\pi/2 \quad n = 1,2,3,..... \tag{9}$$

$$f_n = \frac{2n-1}{4}\frac{a_0}{L} \tag{10}$$

The resonance frequencies are the odd harmonics of the fundamental (n=1).

The driven closed pipe has a pressure antinode at $\xi = \xi_L$ and a pressure node at $\xi = 0$. Notice that this requires that the driver presents vanishing mechanical impedance to the tube. The following table (table1) shows fundamental and 1st resonant frequency for 4 gases.

Table 5.2 – Fundamental and 1st resonant frequencies (n=2).

Gas	Fundamental (n = 1) (Hz)	Experimental first main peak	First Resonant (n = 2) (Hz)
Air	857	1000	2572
CO_2	645	800	1935
He	2520	-	7560
N_2	872	1020	2618

The trend qualitatively coincides with that obtained in the experimental tests: CO_2 lowest resonant frequency, Air and N_2 almost the same, Helium has a small peak at the beginning that has to be clarified but doesn't show main peaks in the range (0-2000Hz).

The presence of more peaks for the empty system compared to the driven tube is due to higher modes of resonances and reflected waves associated with the constriction between 2, 3 and 4 as showed in Fig. 5.10.

5.5 Silicalite-Glass signals: A Qualitative Analysis

The following figures show the amplitude signals for the system filled with glass and with silicalite.

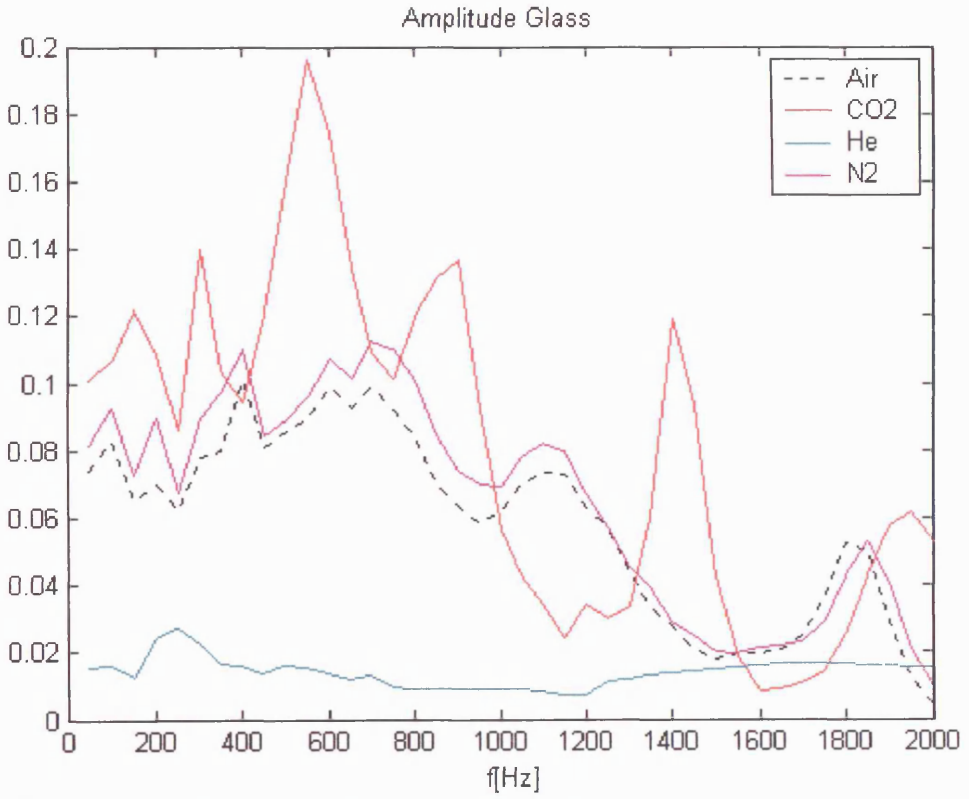

Fig.5.10 Amplitudes as a function of the frequency for the glass system.

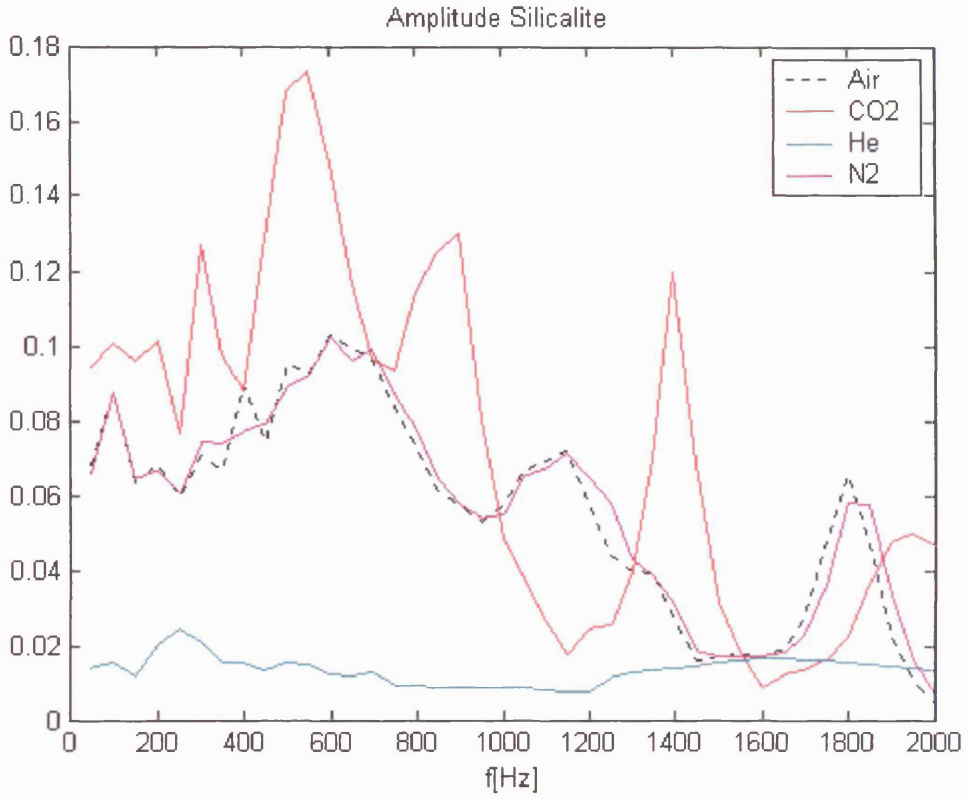

Fig.5.11 Amplitudes as a function of the frequency for the silicalite system.

Table 5.3 – Main Peaks Frequencies (bold main peak)

Gas	**Empty**	**Glass**	**Silicalite**
Air	1000Hz, **1400Hz**	100Hz,**600Hz**, 1050Hz, 1750Hz	100Hz, **600Hz,** 1100Hz, 1800Hz
Air in flux	1000Hz,**1400Hz**	**600Hz**, 1050Hz, 1750Hz	**600Hz**, 1100Hz, 1800Hz
Helium	**200Hz**	**250Hz**, 1700Hz	**250Hz**, 1600Hz
Nitrogen	1000Hz, **1400Hz**	400Hz, **700Hz**, 1100Hz, 1850Hz	**600Hz**, 1100z, 1800Hz
CO_2	**800Hz**, 1050Hz	**580Hz**,900Hz,1400Hz, 2000Hz	**550Hz**, 900Hz, 1400Hz, 1950Hz

As in the empty case for each gas the system shows different peaks. The position of the peaks for the system filled with glass and silicalite are very close. This observation

implies that the positions of the peaks are related mainly to geometrical factors, that we verified being in the order of the resonant frequencies; however comparing the mean peaks (See Table) for CO_2 (550-580 Hz) and Nitrogen (700Hz) in the glass and silicalite systems it is possible to note a reduction of amplitude in the main resonance frequencies between the two systems for both the gases (see 5.6); These experimental results are in agreement with the model as the reduction in the phase velocity implies a lower frequency peak position (Eq.10) and an increase of attenuation (Eq. 20) implies a reduction on the peak high. This last effect is maximum at the frequency corresponding to the micropore diffusion characteristic time.

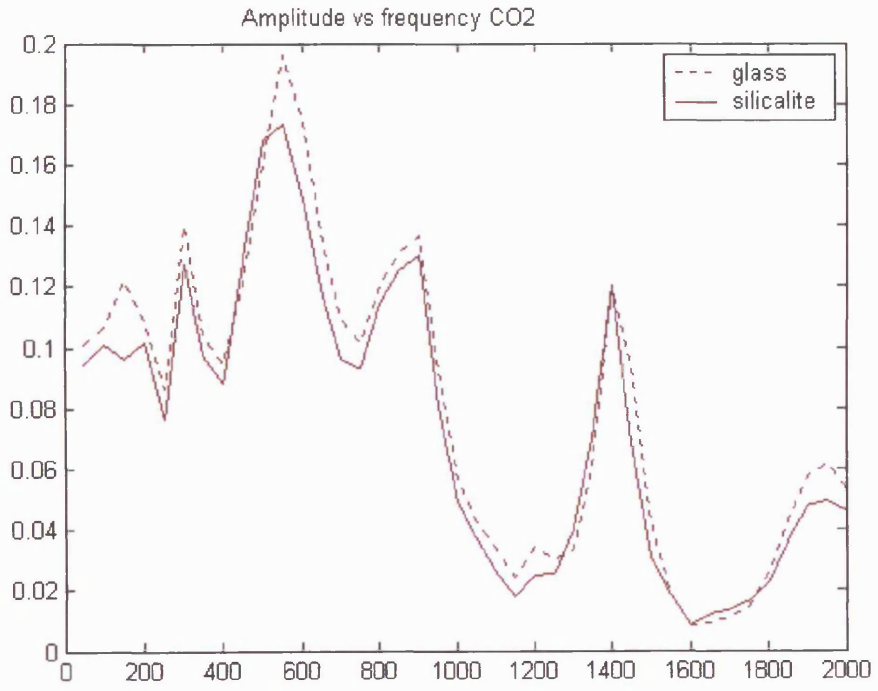

Fig. 5.12 Amplitudes as function of the frequency for CO_2

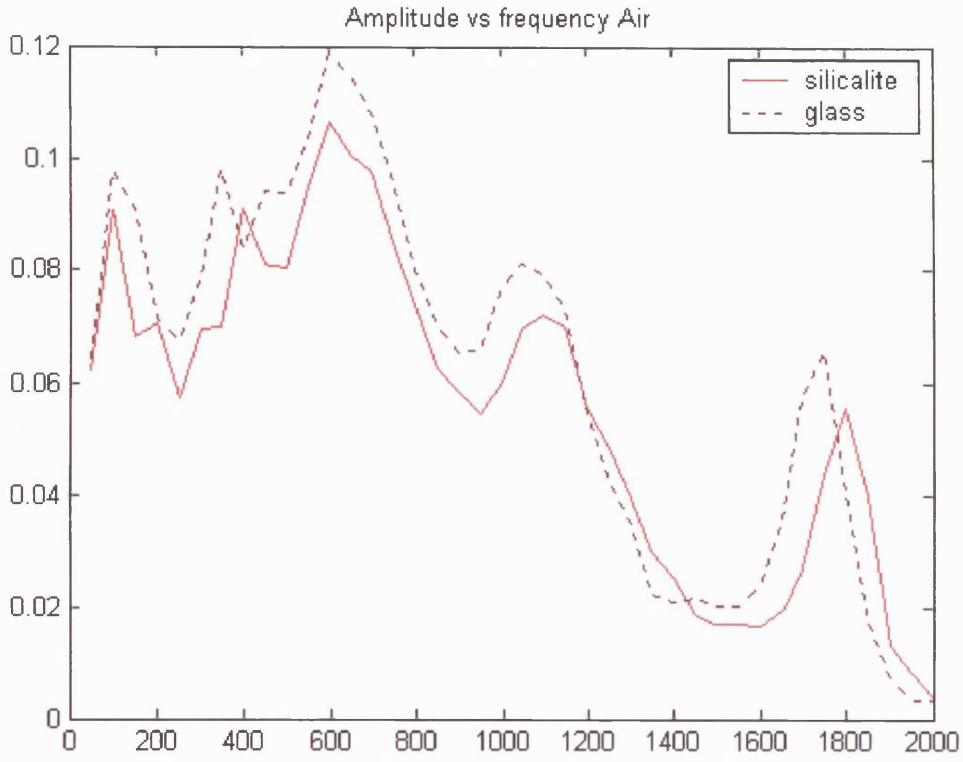

Fig. 5.13 Amplitudes as function of the frequency for air

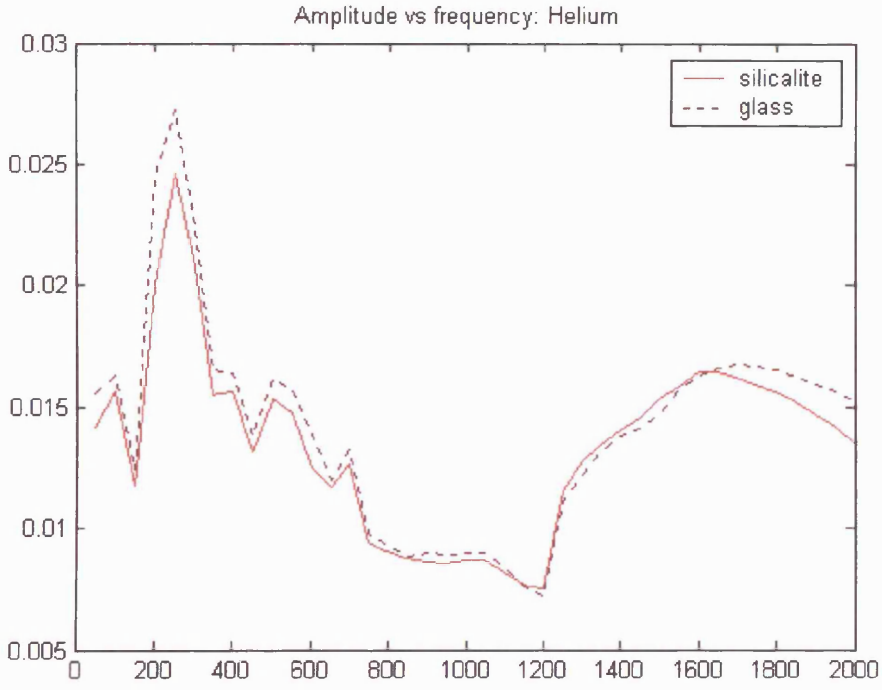

Fig. 5.14 Amplitudes as function of the frequency for Helium

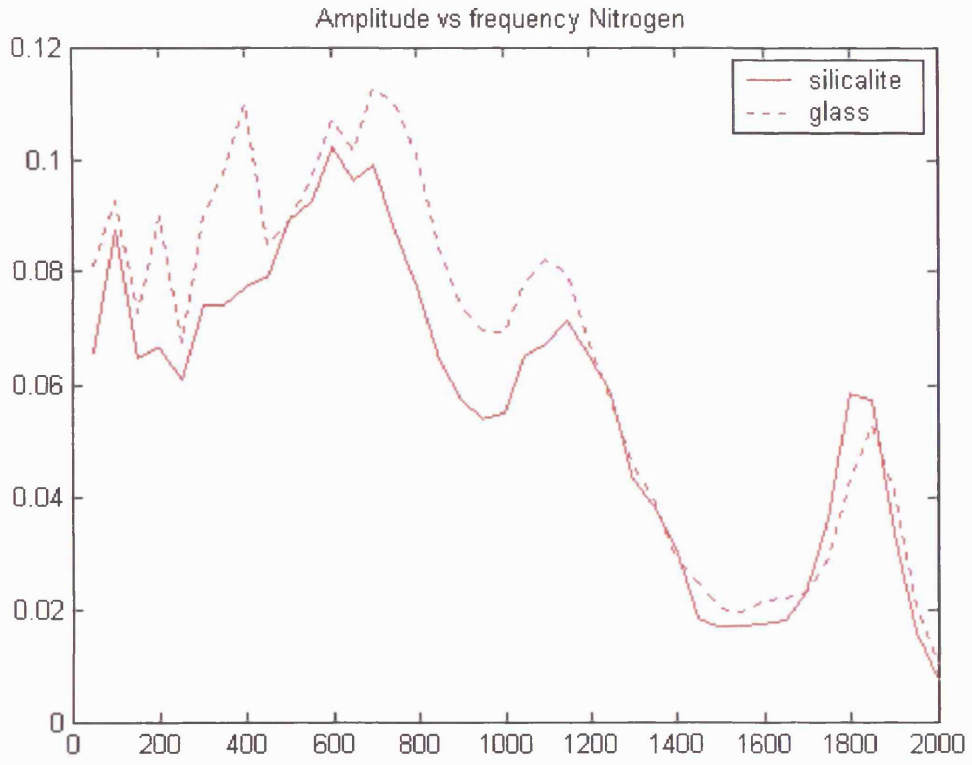

Fig. 5.15 Amplitudes as function of the frequency for N_2

To have a comparison between the glass and silicalite systems, we considered the normalized amplitudes and selected a range of Number of Samples [31500-31600], from the values and the positions of maximum and minimum Amplitude and Phase Shift have been evaluated for the 3 cases: empty, silicalite, glass. The signals are then normalized with respect to the empty case.

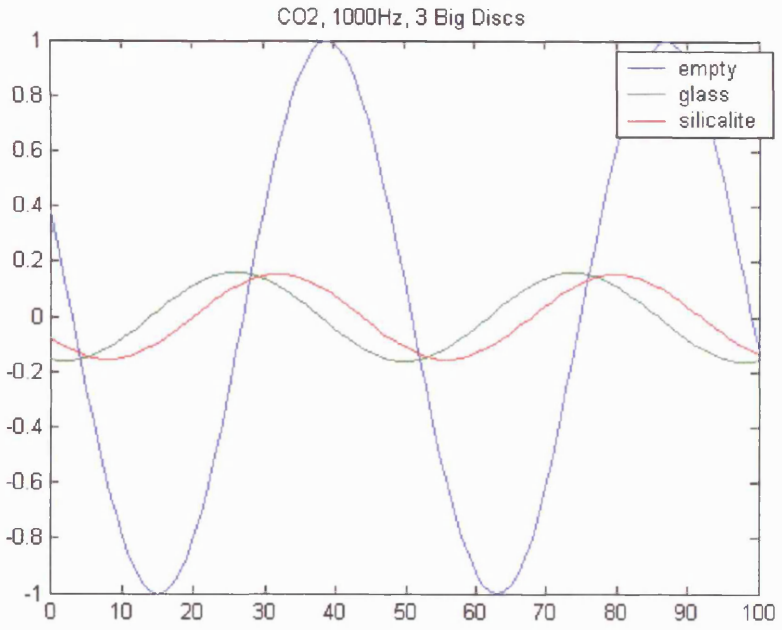

Fig. 5.16 Normalised Amplitudes as function of the number of samples for CO_2

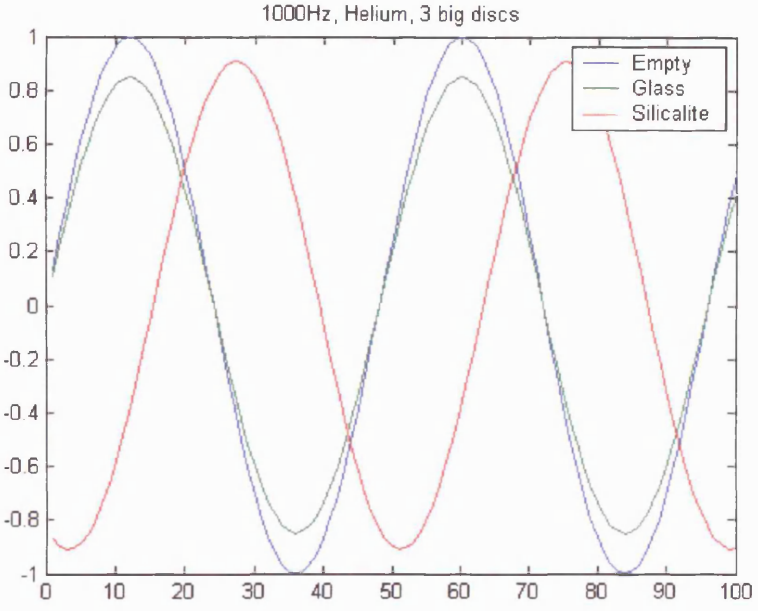

Fig 5.17 Normalised Amplitudes as function of the number of sample for Helium

In Fig. 5.16 and 5.17 experimental data showing approximately two sound cycles have been reported. It is possible to verify that the amplitude in the case of CO_2-silicalite

system is slightly lower than in the case of the CO_2-glass system; assuming the same classical effects this suggests that the micropore diffusion affects the sound propagation.

5.6 Attenuation Coefficient from resonance in a tube

If absorptive processes within the fluid and at the walls of the pipe are considered, the solution for the pipe driven at $\xi = 0$ is found by substituting the complex propagation constant

$$\Gamma = AC + iPS \tag{11}$$

into the solutions obtained in the previous sections.

As an example, for a rigid termination at $\xi = \xi_L$ the pressure is

$$p(x,t) = p_0 \frac{\cosh[\Gamma(\xi_L - \xi)]}{\cosh(\Gamma \xi_L)} e^{j\omega t} \tag{12}$$

and the input impedance is (Eq. 8)

$$\frac{Z1}{W_0 S} = \frac{i\coth(\Gamma \xi_L)}{\Gamma} = \frac{i\coth(AC\xi_L + iPS\xi_L)}{AC + iPS} \tag{13}$$

With the help of the expansions of sines and cosines of complex argument, the above expression becomes

$$\frac{Z1}{W_0 S} = \frac{iAC - PS}{AC^2 + PS^2} \frac{\left[\tanh(AC\xi_L) - i\tan(PS\xi_L) + i\tan(PS\xi_L)\tanh^2(AC\xi_L) + \tanh(AC\xi_L)\tan^2(PS\xi_L)\right]}{\tanh^2(AC\xi_L) + \tan(PS\xi_L)} \tag{14}$$

if we assume that the pipe is of reasonable length so that $(AC\xi_L) << 1$, then the input impedance assumes a simpler form

$$\frac{Z1}{W_0 S} = \frac{1}{PS} \frac{i\tan(PS\xi_L) - \tan^2(PS\xi_L)\tanh(AC\xi_L)}{\tanh^2[AC\xi_L] + \tan^2(PS\xi_L)} \tag{15}$$

A Prototype Experimental Apparatus and Preliminary Experimental Results

The major effects of absorption are to introduce a small resistance which is maximized when $k_n L = n\pi$ and to alter the behaviour of the reactance in this same region so that it no longer becomes infinite in magnitude but rather remains bounded and changes from positive to negative very rapidly.

It can be shown that the frequencies of resonance and antiresonace are close to the natural frequencies of the undamped open, rigid and rigid, rigid pipes, respectively.

Let us assume that the termination at $\xi = \xi_L$ is rigid. Then at $\xi = \xi_L$ the amplitude p_L of the reflected wave will equal that of the incident wave (pressure antinode). The resulting pressure amplitude p at any position along the pipe may be shown from

$$p = p_0 \frac{\cosh[\Gamma(\xi - \xi_L)]}{\cosh(\Gamma \xi_L)} \tag{16}$$

The nodes occur at

$$PS(\xi - \xi_L) = (2n-1)\pi/2 \quad n = 1,2,3,.... \tag{17}$$

and have relative amplitudes

$$p_{\min} / p_L = 2\sinh[\mathrm{Re}(\Gamma)(\xi_L - \xi)] \approx 2\,\mathrm{Re}(\Gamma)(\xi_L - \xi) \tag{18}$$

The antinodes occur

$$PS(\xi - \xi_L) = n\pi \quad n = 1,2,3,.... \tag{19}$$

and have relative amplitudes

$$p_{\max} / p_L = 2\cosh[\mathrm{Re}(\Gamma)(\xi_L - \xi)] \approx 2 + [\mathrm{Re}(\Gamma)(\xi_L - \xi)]^2 \tag{20}$$

At resonance the input pressure is approximately a node.

5.7 Conclusions and Future Work

The experimental apparatus has been constructed and the preliminary experimental investigation has highlighted the need to interpret the results in terms of a resonance model. The amplitudes in the case of the system filled with silicalite are for CO_2 and air lower than for the system filled with glass. This is a preliminary indication that adsorption does have an effect, which in the current configuration is not quantifiable to a sufficient accuracy.

According the ASTM E1050-98 (Standard Test Method for Impedance and Absorption of Acoustical Materials Using a Tube, Two Microphones, and a Digital Frequency Analysis System, the apparatus configuration is the same of the TC384) a new configuration for the experimental apparatus is proposed. These tests are applied to measure sound absorption coefficients of absorptive materials at normal incidence. Because the apparatus are mostly designed for air and atmospheric conditions, some additional care to isolation must be considered in order to make experiment at low pressure.

These techniques are refinement of the Kundt Tube. By measuring the pressure of the standing waves in two locations it is possible to determine the reflection coefficient that is related to the propagation constant (Zwikker and Kosten, 1949) in the material:

$$R = \frac{Z - W_0}{Z - W_0}. \tag{21}$$

where Z is the material surface impedance and W_0, the gas wave impedance

$$Z = W \coth(\Gamma \xi_d). \tag{22}$$

where W according the model is given by:

$$W = \frac{W_0}{\left[1 - \frac{\tanh\left(i^{1/2}s\right)}{i^{1/2}s}\right] i\Gamma} \tag{23}$$

$$\Gamma = \mathrm{i}\sqrt{\frac{\gamma}{\mathrm{n}}}\sqrt{\frac{1}{\left(1 - \frac{\tanh\left(\mathrm{i}^{1/2}\mathrm{s}\right)}{\mathrm{i}^{1/2}\mathrm{s}}\right)}} \tag{24}$$

This model corresponds to a slit geometry and the possibility of an experimental analysis reproducing this geometry could be considered in order to have a simplified, ductile and direct interpretation of the experimental results.

The acoustic pressure between the two layers is given by:

$$p(\xi,t) = p_0\left(Ae^{\Gamma\xi} + Be^{-\Gamma\xi}\right)e^{j\omega t} \tag{25}$$

the average acoustic velocity:

$$u(\xi,t) = a_0\frac{i\Gamma}{\gamma}\left[1 - \frac{\tanh\left(\sqrt{is}\right)}{\sqrt{is}}\right]\left(Ae^{\Gamma\xi} - Be^{-\Gamma\xi}\right)e^{j\omega t} \approx a_0\frac{i\Gamma}{\gamma}\left(Ae^{\Gamma\xi} - Be^{-\Gamma\xi}\right)e^{j\omega t} \tag{26}$$

The impedance of the infinite medium:

$$W = \frac{W_0}{i\Gamma} = \frac{W_0(PS - iAC)}{AC^2 + PS^2}$$

showing also that the Propagation constant represent the ratio of gas characteristic impedance and the impedance in the medium.

These are the equations to analyse the system in the case of a pulse measurement, or in the case of a load impedance that exactly matches the impedance of the medium (no reflection).

The impedance of the standing wave medium:

$$W_{st} = W\frac{\left(Ae^{\Gamma\xi} + Be^{-\Gamma\xi}\right)}{\left(Ae^{\Gamma\xi} - Be^{-\Gamma\xi}\right)} \tag{27}$$

at $\xi = 0$

$$Z_{in} = W\frac{(A+B)}{(A-B)} \tag{28}$$

at $\xi = \xi_L$

$$Z_{out} = W\frac{\left(Ae^{\Gamma\xi_L} + Be^{-\Gamma\xi_L}\right)}{\left(Ae^{\Gamma\xi_L} - Be^{-\Gamma\xi_L}\right)} \tag{29}$$

From (27) and (28)

$$\frac{Z_{in}}{W} = \frac{\frac{Z_{out}}{W} - \tanh\Gamma\xi_L}{1 - \frac{Z_{out}}{W}\tanh\Gamma\xi_L} \tag{30}$$

If we suppose to apply a rigid boundary as (it can be in first approximation a microphone):

$$\frac{Z_{in}}{W} = \coth\Gamma\xi_L \tag{31}$$

$$\frac{Z1}{WS} = \coth(\Gamma\xi_L) = \coth(AC\xi_L + iPS\xi_L) \tag{32}$$

Considering the standing wave pressure :

$$p = p_{.0}\frac{\cosh[\Gamma(\xi - \xi_L)]}{\cosh(\Gamma\xi_L)}$$

$$p = 2p_L\cosh[\Gamma(\xi - \xi_L)]$$

Main difficulty related to the production of layers of microporous material that the system has to satisfy the following conditions:

1) long enough for the formation of a planar wave and mechanically robust
2) relatively smooth surface so turbulence can be neglected

A Prototype Experimental Apparatus and Preliminary Experimental Results

3) To clarify the appropriate lateral dimension

The two layers provided of loudspeaker and with a rigid termination, with two lateral microphone can be inserted in a box, in order to easy control pressure and temperature. Traditional techniques are based on the measurement of surface impedance of a sample, so quantity of material and surface condition should not be problems.

The apparatus is a hollow cylinder, or tube, with a test sample holder at one end and a sound source at the other end. Microphones ports are mounted at two or more locations along the wall of the tube.

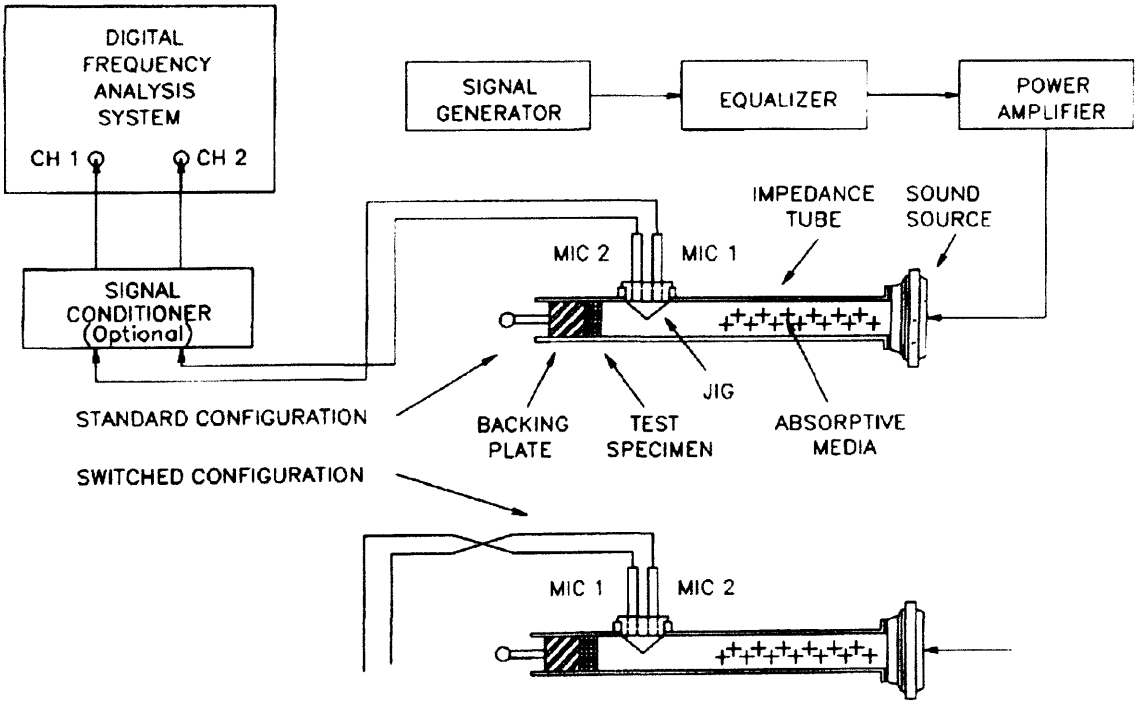

Fig. 5.18 Improved Apparatus (Taken from ASTM E1050-98)

In the test method ASTM E1050-98 plane waves are generated in the tube using a broad band signal from a noise source while in the TC384 by a discrete sinusoid from an oscillator. The ASTM E1050-86 is faster than the simpler Test Method C384.

A Prototype Experimental Apparatus and Preliminary Experimental Results

The test methods describe in details the construction and design procedure for the apparatus, and the following points are underlined:

1) Working frequency range: $f_l<f<f_u$

The lower limit depends on the spacing of the microphones: (the microphone spacing exceed one percent of the wavelength is indicated).

(for a microphone nominal diameter of 1 inch the maximum frequency is 3000 Hz).

2) Diameter of the tube to avoid higher modes of resonance, this is also related to 1): $f_u=(Kc)/d$, where K=0.586;

3) Length of the tube: the tube should be sufficiently long that planar waves are fully developed before reaching the microphones and test specimen. (a minimum of three tube diameters is indicated)

4) Backing plate (Eq. 20): A metal plate having a minimum thickness of 20 mm is recommended.

5) Location microphones: it is suggested 3 tube diameters from sound source and from the specimen.

6) Test specimen: with porous materials of low bulk density, it may be useful to define the front surface by a thin, non vibrating wire grid with wide mesh

7) In the section of the Analysis of the signals are given the relation between R to the microphones measurement

In order to extend the model to the outlined configuration it is possible to follow Attenborough capillary tube approach, (Attenborough 1993). His analysis considered the influence of pore shape in rigid porous material consisting of identical tortuous pores of arbitrary shape. The geometrical factor is generally negligible while a correction can arise due to the pores distribution (or equivalently grain size

distribution). The propagation constant of the pore (or capillary tube) to the bulk material according the following relation for the density and the compressibility:

$$\rho_b = \left(\tau^2 / \varepsilon\right)\rho_p. \tag{33}$$

$$C_b = (\gamma P_o)^{-1}\left[\gamma - (\gamma - 1)\frac{\rho_o}{\rho_b}\right] \tag{34}$$

where in Eq.(31) and (32) τ and ε represent tortuosity and porosity of the sample: and related to the propagation constant:

$$\Gamma_b = ja_0\sqrt{\frac{\rho_b}{C_b}} \tag{35}$$

Because tortuosity, porosity and eventually pore distribution can be determined independently of the acoustic measurements, the model should not require any adjustable parameters.

The quantification of adsorption parameters from the analysis of sound attenuation in the present prototype system is limited by the complex reflections and resonances in the apparatus.

References

Barrer, R.M., "Migration in Crystal lattices", Trans. Faraday Soc. 37, 590 (1941).

Barrer, R.M., "Diffusion in and trough solids", Cambridge: The University Press (1951).

Barrer, R.M., "Zeolites and Clay Minerals as Sorbent and Molecular Sieves", Academic Press, London (1978).

Bernasconi ,C.F., "Relaxation Kinetics", Academic Press, (1976).

Boniface, H. A., and Ruthven, D.M., "Chromatographic adsorption with sinusoidal input", Chem Engng Sci 40,11, 2053-2061 (1985).

Bourdin, V., Gray, P.G., Grenier, Ph. and Terrier, M.F., "An apparatus for adsorption dynamics studies using infrared measurement of the adsorbent temperature", Rev. Sci. Instrum. 69, 5, 2130-2136 (1998).

Brandani, S., Ruthven, D.M. and Kärger, J., "Concentration dependence of self-diffusivity of methanol in NaX zeolite crystals" Zeolites, 15, 494-496 (1995).

Brandani, S., and Ruthven, D.M., "Analysis of ZLC desorption curves for gaseous systems", Adsorption 2, 133-143, (1996).

Brandani, S., "Effects of nonlinear equilibrium on zero length column experiments", Chem.Engng Sci., 53, 2791-2798, (1998).

Brandani, S., Xu, Z. and Ruthven, D.M., "Transport diffusion and self-diffusion of benzene in NaX and CaX zeolites crystals studied by ZLC and tracer ZLC methods", Microporous Materials, 7, 323-331, (1996).

Brandani, S., Ruthven, D.M. and Kärger, J., "Diffusion in a unidimensional zeolites pore system: Propane in $AlPO_4$-5", Microporous Materials, 8, 193-200 (1997).

Carslaw, H.S. and Jaeger,J.C., "Conduction of heat in solids", Oxford University Press (1959).

Cohen de Lara, E.C., Kahan, R. and Mezei, F., "Determination of the Intracrystalline Diffusion Coefficient of Methane in A Zeolites by Means of Neutron Spin-echo Experiments", J.Chem.Soc.Faraday Trans.I, 79 1911-17 (1983).

Conner, W.C., Turner, Jr., Capron, M.L. and Laurence R. L. "The Design and Construction of a Frequency Response Apparatus to Investigate Diffusion in Zeolites" Rev. Sci. Inst . . 72-12, 4424-4433 (2001).

Crandall, I.B., "Vibrating Systems and Sound", pp. 229-241, Macmillan and Co., Limited, London, 1927.

Crank, J. The Mathematics of Diffusion, 2nd. Edition, Clarendon Press, (1993).

Darken, L.S., Trans. AIME 175, 184 (1948)

Eic, M. and Ruthven, D.M., "A New Experimental-Technique for Measurement of Intracrystalline Diffusivity", Zeolites 8, 40-45 (1988).

Einstein, A., "Investigations on the Theory of the Brownian Movement" R. Fürth, ed., A. D. Cowper, transl. New York: Dover Publications, 1956. *The papers on Brownian motion, translated and annotated (1905).

Eyring, H., J. Chem. Phys., 3, 107 (1935).

Evnochides, S.K., and Henley, E.J., J.Polym.Sci., 8, 1970, (1987).

Favre, D.E., Schaefer, D.J., Auerbach, S.M. and Chmelka, B.F., "Direct Measurement of Intercage Hopping in Strongly Adsorbing Guest-Zeolite Systems", Phys. Rev. Lett., 81, 5852-5855 (1998).

Golden, T.C. and Sircar, S. "Gas Adsorption on Silicalite", J. Colloid Inferface Sci., 162, 182-188, (1994)

Haag, W.O., Lago, R.M. and Weisz, P.B., "Transport and Reactivitry of Hydrocarbon Molecules in a Shape-Selective Zeolite", Faraday disc., 72, 317-330 (1981).

Haase , R. and Siry ,M., Z. Phys. Chem. Frankfurt 57, 56 (1968).

Haynes, H.W.Jr. and Sarna P.N., "A Model for the Application of Gas Chromatography to measurements of Diffusion in Bidispersed Structured Catalysts", AIChE J., 19, 1043 (1973).

Hayrust, D.T. and A. Paravar, "Direct Measurement of Diffusivity for Butane across a Single Large Silicalite Crystal", in Proc.Sixth Internat. Zeolite Conf., D. Olson and A. Bisio (Eds.), pp. 217-224, Butterworth, 1984, Guildford, (1983) (as cited in Kärger, (2003)).

Herzfeld, K. F., "Absorption and dispersion of ultrasonic waves ", Karl F. Herzfeld and Theodore A. Litovitz, New York : Academic Press , 1959.

Hirschfelder, J.O., Curtiss, C.F., and Byron, R.B. , "Molecular Theory of Gases and Liquids", pp. 728-736, John Wiley and Sons, New York, 1954.

Hufton, J.R., Brandani, S. and Ruthven, D.M., "Measurement of Intracrystalline Diffusion by Zero Length Column Tracer Exchange" Proc. 10th Internat. Zeolite Conf.,

Gramisch, 1323-1330. J. Weitkamp, H.G. Karge, H. Pfeifer and W. Holderich eds. Elsevier, Amsterdam. (1994)(As cited in Ruthven and Brandani (1997)).

Jobic, H., Kärger, J., and Bée, M. ,"Simultaneous Mesurement of Self- and Transport Diffusivities in Zeolites", Phys. Rev. Lett., 82, 4260-4263 (1999).

Jordi, R.G. and Do, D.D. "Analysis of the frequency response method applied to non-isothermal sorption studies", Chem Engng Sci, 49 , 7, 957-979 (1994).

Karge, H.G. and Niessen, W., "A New Method for the Study of Diffusion and Counter Diffusion in Zeolites", Cat. Today, 8,451-465 (1991).

Karge, H.G. and Klose, K., Ber. Bunsenges. 78 1263 (1974).

Kärger J., "Diffusionuntersuchung von Wasser an 13X- sowie an 4A- und 5A-Zeolithen mit Hilfe der Methode der gepulsten Feldgradienten", Z. phys. Chem., 248, 27-41 (1971).

Kärger, J., and Ruthven, D.M. "Diffusion in Zeolites and Other Microporous Solids", John Wiley & Sons, New York, (1992).

Kärger, J., "Measurement of Diffusion in Zeolites-A Never Ending Challenge?", Adsorption 9,29-35 (2003).

Kärger, J. and Caro, J. "Interpretation and Correlation of Zeolitic Diffusivities Obtained from Nuclear Magnetic Resonance and Sorption Experiments", J.Chem.Soc. Faraday I, 73 1363-1376 (1977).

Kinsler, L.E., Frey, A.R., Coppens, A.B., and Sanders, V.A. "Fundamentals of Acoustics", John Wiley & Sons, New York, (1980).

Kirchhoff G., "Ueber den Einfluss der Wärmeleitung in einem Gase auf die Schallbewegung", *Poggendorfer Annalen 134, 177-193* (1868).

Krishna (1990).

Landau, L., and Lifšits, E.M. "Meccanica", Editori Riuniti, Edizioni Mir, Mosca, (1976).

Markham, J.J., Lindsay, R.B., and Beyer R.T., "Absorption of sound in fluids", Review of Modern Physics, 23, 4, 353-412 (1951)

Naphtali, L.M., and Polinski, L.M., "A novel technique for characterization of adsorption rates on heregoneous surfaces", J. Phys. Chem. *67*, 369-375 (1963).

Nijhuis, T.A., Van De Broeke, L.J.P., Van De Graaf, J.P., Kapteijn, F., Makkee, M. and Moulijn, J.A., "Bridging the Gap between Macroscopic and NMR Diffusivities", Chem. Eng. Sci., 52, 3401-3404 (1997).

Oprescu, D., Rees, L.V.C. and Shen, D., "Diffusion of sorbates in zeolites by the frequency response method: Particle shape and anisotropic effects", J. Chem. Soc. Faraday Trans. 88, 2955-2958 (1992).

Park, I.S., Petrovska, M., and Do, D.D., "Frequency response of an adsorber with modulation of the inlet molar flow-rate 1. A semi-batch adsorber", Chem Engng Sci *53,4,* 819-832 (1998).

Pasheck and Krishna (2001)

Pfeifer, H., Przyborowski, F., Schirmer,W. und Stach,H., Z.phys. Chem, (236, 345-361 (1967). (as cited in Kärger (1971)).

Prigogine, I., "Introduzione alla Termodinamica dei processi irreversibili", Leonardo, Roma (1971).

Raspet, R., Hiickey, C.J., and Sabatier, J.M., "The effect of evaporation-condensation on sound propagation in cylindrical tubes using the low reduced frequency approximation", *J. Acoust. Soc. Am. 105*, 65-73 (1999).

Raspet, R., Hickey, C.J., and Slaton, W.V., "The effect of the physical properties of the tube wall on the attenuation of sound in evaporating and condensing gas-vapor mixtures", *J. Acoust. Soc. Am. 108*, 2120-2124 (2000).

Rees, L.V.C, and Shen, D., "Characterization of microporous sorbents by frequency-response methods", Gas Sep. Purif. Vol7 ,No2, 83-89 (1993).

Rees, L. V. C., "Exciting new advances in diffusion of sorbates in zeolites and microporous materials ", Zeolites and related microporous materials: State of the art studies in surface science and catalysis 84: 1133-1150 (1994).

Ruthven, D.M., "Principles of Adsorption and Adsorption Processes", Wiley, New York (1984).

Ruthven, D.M. and Brandani, S., "Measurement of Diffusion in microporous solids by macroscopic methods", Physical Adsorption: Experiment, Theory and Applications, 261-296, Kluwer Academic Publishers, Netherland (1997).

Ruthven, D.M., "Diffusion of Xe and CO_2 in 5A zeolite crystals", Zeolites, 13, 594 (1993)

Ruthven, D.M. and Eic, M., Am. Chem. Soc. Symp. Series 368, 362 (1988) (as cited in Ruthven and Brandani (1997)).

Ruthven, D.M., "Fundamentals of diffusion in porous and microporous solids", Physical Adsorption: Experiment, Theory and Applications, 241-259, Kluwer Academic Publishers, Netherland (1997).

Ruthven ,D.M., Communication (2003) given by Professor D.M. Ruthven in the NATO ASI at "La Colle sur Loup" –France, June 15-28 2003 on "Fluid Transport in Nanoporous Materials" .

Ruthven, D.M. and Loughlin, K.F., "Diffusion in molecular Sieves" Preprint 16c, 68th national meeting of Am. Inst. Chem. Engrs., Houston (1971) (as cited in Haynes et al. (1973)).

Schemmert, U., Kärger, J. and Weitkamp, J. "Interference Microscopy as a technique for Directly measuring Intracrystalline Transport Diffusion in Zeolites", Microp. Mesop. Mat., 32, 101-110 (1999).

Schumacher, R.R., Anderson, B.G., Noordhoek, N.J., De Gauw, F.J.M.M., De Jong, A.M., de Voigt, M.J.A. and Van Santen, R.A., "Tracer-Exchange Experiments with Positron Emission Profiling: Diffusion in Zeolites", Microp. Mesop. Mat., 35-36, 315-326 (2000).

Shah, D.B. and Ruthven, D.M., "Measurement of zeolitic diffusivities and equilibrium isotherms by chromatography" AIChe Jl 23, 804-809 (1977).

Shen, D. and Ress, L.V.C., "Adsorption and diffusion of n-butane and 2-butyne in silicalite-I", Zeolites 11 684-689 (1991).

Shen, D.M. and Rees, L.V.C., "Frequency response technique measurements of p-xylene diffusion in silicalite-1 and –2.", J.Chem.Soc. Faraday Trans. 89, 1063-1065 (1993).

Shen, D., and Rees, L.V.C., "Study of Fast Diffusion in Zeolites using a Higher Harmonic Frequency Response Method", J.Chem. Soc. Faraday Trans. 90(19), 3011-3015 (1994).

Stephanopoulos, G., Chemical Process Control, Prentice-Hall International, London, (1984).

Sun, L.M., and Meunier, F.,"A detailed model for nonisothermal sorption in porous adsorbents",Chem.Engng Sci., *42*, 1585-1593, (1987).

Sun, L.M., Meunier, F. and Kärger, J., "On the heat effect in measurements of sorption kinetics by the frequency response method". Chem Engng Sci, Vol.48, No.4,715-722 (1993).

Sun, L.M. and Meunier, F., "Measurement of intracrystalline diffusion by the frequency response method: Analysis and interpretation of bimodal response curves", Chem Engng Sci, Vol.48, 22, 3783-3793 (1993).

Sun, L.M., Meunier, F., Grenier Ph. and Ruthven, D.M., " Frequency response fon nonisothermal adsorption in biporous pellets". Chem Engng Sci, Vol.49, No.3,373-381 (1994).

Sward, B.K. and leVan, M.D.,"New Frequency Response Method for Measuring Adsorption Rates via pressure Modulation: Application to Oxygen and Nitrogen in a Carbon Molecular Sieve", Ind. Eng. Chem. Res ,42, 4213-4222 (2003a).

Sward, B.K. and leVan, M.D., "Frequency Response Method for Measuring Mass Transfer Rates in Adsorbents via Pressure Perturbation", Adsorption, 9, 37-54 (2003b).

Tijdeman, H., "On the propagation of sound waves in cylindrical tubes", *J. Sound Vib. 39*, 1-33 (1975).

Tiselius, A., Z. Phys. Chem. A 169, 425 (1934) (as cited in Kärger and Ruthven (1992)).

Tiselius, A., " Sorption und Diffusion von Ammoniak in Analcim", Z. Phys. Chem. A 174, 401 (1935).

Truesdell, (1962)

Van-Den-Begin, N.G. and Rees, L.V.C., "Diffusion of hydrocarbons in silicalite using a Frequency-Response method", Zeolites: facts, Figures, Future, 1989 Elsevier Science Publishers B.V., Amsterdam

Yasuda, Y., "Frequency Response method for Study of the Kinetic behaviour of a Gas-Surface System.1.Theoretical Treatment", J. Phys. Chem., Vol.80, No.17, 1867-1869 (1976).

Yasuda, Y. and Sugasawa, G., "A Frequency Response technique to Study Zeolitic Diffusion of Gases", J. Phys. Chem ., 86, 1913-1917 (1982).

Yasuda, Y., Suzuki, Y., and Fukada, H. ,"Detection of Surface Resistance in a Gas/Porous-Adsorbent System by Frequency Response Method", Bull. Chem. Soc. Jpn.,*64*, 954-961 (1991).

Yasuda,Y., "Frequency Response Method for Investigation of gas/Surface Dynamic Phenomena" , Heter. Chem. Rev. *1*,103-124 (1994).

Zwikker, C. and Kosten,C., "Sound Absorbing Material", Elsevier, Amsterdam, (1949).

Appendix A

In and out characteristic functions for micropore diffusion

$$\bar{V} = V_e\left(1 - ve^{i\omega t}\right) \qquad \text{Volume modulation} \qquad (2)$$

$$\bar{p} = p_e\left(1 + pe^{i(\omega t+\phi)}\right) \qquad \text{Pressure} \qquad (3)$$

$$\bar{q} = q_e\left(1 + \gamma e^{i(\omega t+\phi-\chi)}\right) \qquad \text{concentration in the pores} \qquad (A1)$$

$$\bar{B} = B_e\left(1 + Ae^{i(\omega t+\phi+\psi)}\right) \qquad \text{amount of adorbate in the sample} \qquad (A2)$$

$$\frac{d}{dt}\left(\frac{\bar{p}\bar{V}}{RT_0}\right) + \frac{d\bar{B}}{dt} = 0 \qquad \text{mass balance} \qquad (4)$$

It should be noted that this equation is valid only if the pressure is homogeneous throughout the gas space; this the very fundamental assumption in this method.[i]

$$\frac{1}{RT_0}\left(\bar{p}\frac{d\bar{V}}{dt} + \bar{V}\frac{d\bar{p}}{dt}\right) + \frac{d\bar{B}}{dt} = 0 \qquad (A3)$$

$$\frac{P_eV_e}{RT_0}\left(pve^{i(\omega t+\varphi)} + v - pe^{i\varphi} + pve^{i(\omega t+\varphi)}\right) = Ae^{i(\varphi+\psi)} \qquad (A4)$$

Cancelling the pv terms (disappear the time dependence)

$$\frac{P_eV_e}{RT_0A}\left(ve^{-i\varphi} - p\right) = Ae^{i\psi} \qquad (A5)$$

Equalling real and imaginary parts

$$\frac{P_eV_e}{RT_0A}\left(v\cos\varphi - p\right) = \cos\psi \qquad (A6)$$

$$-\frac{P_eV_e}{RT_0A}\sin\varphi = \sin\psi \qquad (A7)$$

A and ψ are obtained from the solution of Eq. (A8) (Crank, 1959)

$$\frac{\partial\bar{q}}{\partial t} = D(q_e)\left(\frac{\partial^2\bar{q}}{\partial x^2}\right) \qquad (A8)$$

with boundary conditions that the concentration is proportional to a sinusoidally varying vapor pressure at the boundaries

$$\bar{q} = K\bar{p} \tag{A9}$$

K can be related to the gradient of a sorption isotherm at $P = P_e$, i.e.

$$K = \left(\frac{RT_0}{V_e}\right)\left(\frac{dB_e}{dP_e}\right) \tag{A10}$$

$$A = (Kp)\left(\frac{RT_0}{V_e P_e}\right)\left[\sqrt{2}\left(\sin^2\eta + \sinh^2\eta\right)^{\frac{1}{2}} / [\eta(\cos\eta + \cosh\eta)]\right] \tag{A11}$$

$$\psi = \tan^{-1}\left(\frac{\sin\eta - \sinh\eta}{\sin\eta + \sinh\eta}\right) \tag{A12}$$

Using $\cos\psi = \dfrac{1}{\sqrt{1 + tg^2\psi}}$ and $\sin\psi = \dfrac{1}{\sqrt{1 + \dfrac{1}{tg^2\psi}}}$

Introducing A.11 and A.12 in (A6) and (A7) eqs (9) and (10) are obtained.

Appendix B

Sound Propagation between two slabs of non-adsorbent solid.

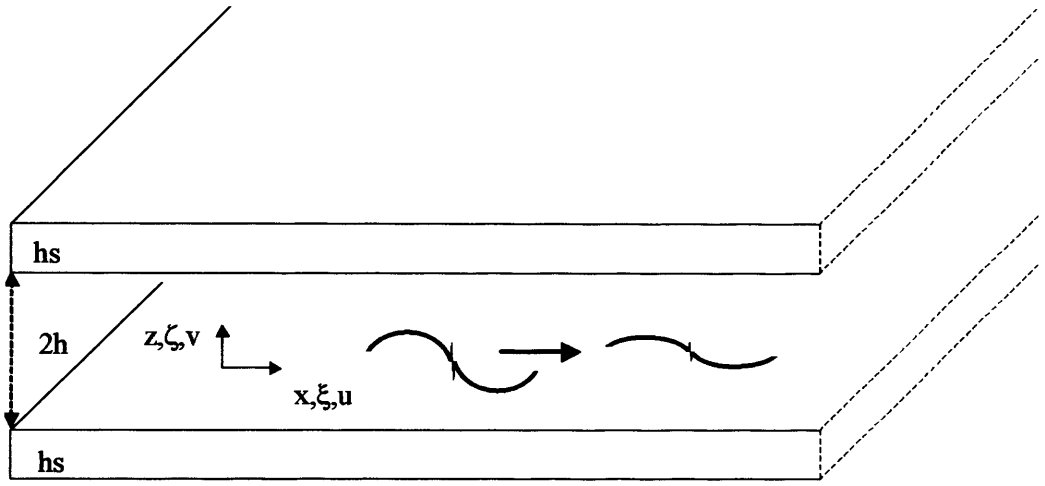

Fig.A.1 LRFA in rectangular geometry.

Eqs (5-10) in Chapter 3 describe the motion of a fluid between two slabs of infinite width. From these equations it is possible to obtain the solution to the LRFA in the absence of adsorption.

If the following assumptions are introduced:

(a) homogeneous medium, which means that the wave length and the distance between the two slabs must be large in comparison with the mean free path; for air of normal atmospheric temperature and pressure, this condition breaks down for $f > 10^8$ Hz and $h < 10^{-5}$ cm;

(b) no steady flow;

(c) small amplitude, sinusoidal perturbations (no circulation and no turbulence);

(d) slab long enough, so that end effects are negligible.

Upon assuming

$$\bar{u} = a_o u(x,z) e^{i\omega t}$$

$$\bar{v} = a_o v(x,z) e^{i\omega t}$$

$$\bar{p} = p_s\left(1 + p(x,z)e^{i\omega t}\right) = \frac{\rho_s a_o^2}{\gamma}\left(1 + p(x,z)e^{i\omega t}\right)$$

$$\bar{\rho} = \rho_s\left(1+\rho(x,z)e^{i\omega t}\right)$$

$$\bar{T} = T_s\left(1+T(x,z)e^{i\omega t}\right)$$

with u,v,p,ρ and T being small sinusoidal perturbations, and by introduction of the dimensionless co-ordinates

$$\xi = \frac{\omega x}{a_o}, \qquad \zeta = \frac{z}{h}$$

the Eqs (5)-(9) can be rewritten as

$$iu = -\frac{1}{\gamma}\frac{\partial p}{\partial \xi} + \frac{1}{s^2}\left\{\left[k^2\frac{\partial^2 u}{\partial \xi^2} + \frac{\partial^2 u}{\partial \zeta^2}\right] + \frac{1}{3}k\frac{\partial}{\partial \xi}\left[k\frac{\partial u}{\partial \xi} + \frac{\partial v}{\partial \zeta}\right]\right\} \tag{B1}$$

$$ivk = -\frac{1}{\gamma}\frac{\partial p}{\partial \zeta} + \frac{k}{s^2}\left\{\left[k^2\frac{\partial^2 v}{\partial \xi^2} + \frac{\partial^2 v}{\partial \zeta^2}\right] + \frac{1}{3}\frac{\partial}{\partial \zeta}\left[k\frac{\partial u}{\partial \xi} + \frac{\partial v}{\partial \zeta}\right]\right\} \tag{B2}$$

$$ik\rho = -\left[k\frac{\partial u}{\partial \xi} + \frac{\partial v}{\partial \zeta}\right] \tag{B3}$$

$$p = \rho + T \tag{B4}$$

$$iT = \frac{1}{\sigma^2 s^2}\left[\frac{\partial^2 T}{\partial \zeta^2} + k^2\frac{\partial^2 T}{\partial \xi^2}\right] + i\frac{\gamma-1}{\gamma}p \tag{B5}$$

where $s = h\sqrt{\frac{\rho_s \omega}{\mu}}$, the shear wave number,

$\sigma = \sqrt{\frac{\mu C_p}{\lambda}}$, the square root of the Prandtl number,

$k = \frac{\omega h}{a_o}$, the reduced frequency, being proportional to the ratio of half distance slabs to wave length,

$\gamma = \frac{C_p}{C_v}$, specific heats ratio.

As for a given gas σ and γ often can be considered as constants, the two main parameters are the shear wave number and the reduced frequency.

When the slabs distance is small in comparison with the wave length and the vertical velocity component, v, is small with respect to the horizontal velocity, u (i.e., $\frac{\omega h}{a_o} << 1$ and $\frac{v}{u} << 1$), the basic Eqs (A1)-(A5) can be reduced to

$$iu = -\frac{1}{\gamma}\frac{\partial P}{\partial \xi} + \frac{1}{s^2}\frac{\partial^2 u}{\partial \zeta^2} \tag{B6}$$

$$0 = -\frac{1}{\gamma}\frac{\partial P}{\partial \zeta} \tag{B7}$$

$$ik\rho = -\left[k\frac{\partial u}{\partial \xi} + \frac{\partial v}{\partial \zeta}\right] \tag{B8}$$

$$p = \rho + T \tag{B9}$$

$$iT = \frac{1}{\sigma^2 s^2}\frac{\partial^2 T}{\partial \zeta^2} + i\frac{\gamma - 1}{\gamma}p \tag{B10}$$

To obtain the solution for the two slabs geometry, eqs (B6)-(B10) have to satisfy the following boundary conditions and assumptions:

(a) at the rigid slabs wall the horizontal and vertical velocity must be zero: i.e.,

at $\zeta = 1,-1 \quad v = 0 \quad and \quad u = 0$

(b) the vertical velocity must be zero at the centre due to the symmetry of the problem: i.e.,

at $\zeta = 0, \quad v = 0$

(c) the heat conductivity of the slab wall is large in comparison with the heat conductivity of the fluid: i.e.,

at $\zeta = 1,-1 \quad T = 0$
(isothermal walls)

B.1 Derivation of the LRFA solution

From Eq. (B7) : P=P(ξ)

Assuming $u = f(\xi)h(y)$ with $y = i^{3/2}\zeta s$

The Eq. (B6) becomes:

$$\frac{\partial^2 h(y)}{\partial y^2} + h(y) = \frac{i}{\gamma f(\xi)} \frac{\partial p}{\partial \xi} \tag{B11}$$

Solution is given by:

$$h(y) = Ae^{iy} + Be^{-iy} + \frac{i}{\gamma} \frac{\partial p}{\partial \xi} \frac{1}{f(\xi)} \tag{B12}$$

A and B can be determined from the boundary conditions:

$$\begin{cases} u(\xi,1) = 0 \\ u(\xi,-1) = 0 \end{cases} \longrightarrow \begin{cases} h\left(i^{3/2} s\right) = 0 \\ h\left(-i^{3/2} s\right) = 0 \end{cases}$$

$$A = B = -\frac{1}{\gamma} \frac{\partial p}{\partial \xi} \frac{1}{f(\xi) 2\cosh\left(i^{5/2} s\right)} \tag{B13}$$

$$u = \frac{i}{\gamma} \frac{\partial p}{\partial \xi} \left[1 - \frac{\cosh\left(i^{1/2} \zeta s\right)}{\cosh\left(i^{1/2} s\right)} \right] \tag{B14}$$

Following the previous procedure we can determine the temperature:

Assuming $T = g(\xi) j(w)$

Eq. (B10) becomes:

$$\frac{\partial^2 j(w)}{\partial w^2} + j(w) = \frac{\gamma - 1}{\gamma} \frac{1}{g(\xi)} p \tag{B15}$$

the solution is given by:

$$j(w) = Ce^{iw} + De^{-iw} + \left(\frac{\gamma - 1}{\gamma} \right) \frac{1}{g(\xi)} p \tag{B16}$$

C and D can be determined from the boundary conditions:

$$\begin{cases} T(\xi,1) = 0 \\ T(\xi,-1) = 0 \end{cases} \longrightarrow \begin{cases} j\left(i^{3/2} \sigma s\right) = 0 \\ j\left(-i^{3/2} \sigma s\right) = 0 \end{cases}$$

$$C = D = -\frac{\gamma - 1}{\gamma} p \frac{1}{g(\xi) 2\cosh\left(i^{5/2} \sigma s\right)} \tag{B17}$$

$$T = \frac{\gamma - 1}{\gamma} p \left[1 - \frac{\cosh\left(i^{1/2}\zeta\sigma s\right)}{\cosh\left(i^{1/2}\sigma s\right)} \right] \tag{B18}$$

Substituting Eq. (B18) in Eq. (B9):

$$\rho = p - T = p\left[1 - \frac{\gamma - 1}{\gamma}\left[1 - \frac{\cosh\left(i^{1/2}\zeta\sigma s\right)}{\cosh\left(i^{1/2}\sigma s\right)} \right] \right] \tag{B19}$$

using Eqs (A15) and (A19), the continuity equation can be rewritten as

$$\frac{\partial v}{\partial \zeta} = k\left[i\rho + \frac{\partial u}{\partial \xi} \right] = ik\left\{ p\left[1 - \frac{\gamma - 1}{\gamma}\left(1 - \frac{\cosh\left(i^{1/2}\zeta\sigma s\right)}{\cosh\left(i^{1/2}\sigma s\right)} \right) \right] + \frac{1}{\gamma}\frac{\partial^2 p}{\partial \xi^2}\left[1 - \frac{\cosh\left(\left(i^{1/2}\zeta\right)s\right)}{\cosh\left(i^{1/2}s\right)} \right] \right\} \tag{B20}$$

By integration:

$$v = ik\left\{ p\left[\zeta - \frac{\gamma - 1}{\gamma}\left(\zeta - \frac{\sinh\left(i^{1/2}\zeta\sigma s\right)}{i^{1/2}\sigma s\cosh\left(i^{1/2}\sigma s\right)} \right) \right] + \frac{1}{\gamma}\frac{\partial^2 p}{\partial \xi^2}\left[\zeta - \frac{\sinh\left(i^{1/2}\zeta s\right)}{i^{1/2}s\cosh\left(i^{1/2}s\right)} \right] + F(\xi) \right\} \tag{B21}$$

From the boundary condition $\zeta = 1 \quad v = 0$

$$-F(\xi) = p\left\{ 1 - \frac{\gamma - 1}{\gamma}\left[1 - \frac{\tanh\left(i^{1/2}\sigma s\right)}{i^{1/2}\sigma s} \right] \right\} + \frac{1}{\gamma}\frac{\partial^2 p}{\partial \xi^2}\left[1 - \frac{\tanh\left(i^{1/2}s\right)}{i^{1/2}s} \right] \tag{B22}$$

From the symmetry condition $\zeta \to 0\ v = 0$, it follows $F(\xi) = 0$

$$p\left\{ 1 - \frac{\gamma - 1}{\gamma}\left[1 - \frac{\tanh\left(i^{1/2}\sigma s\right)}{i^{1/2}\sigma s} \right] \right\} + \frac{1}{\gamma}\frac{\partial^2 p}{\partial \xi^2}\left[1 - \frac{\tanh\left(i^{1/2}s\right)}{i^{1/2}s} \right] = 0 \tag{B23}$$

The solution of this second order homogeneous linear equation is given by:

$$p = Ae^{\Gamma\xi} + Be^{-\Gamma\xi} \tag{B24}$$

where

$$\Gamma = i\sqrt{\frac{\gamma}{n}}\sqrt{\frac{1}{\left(1 - \frac{\tanh\left(i^{1/2}s\right)}{i^{1/2}s} \right)}} \tag{B25A}$$

$$n = \left[1 - \frac{\gamma - 1}{\gamma}\left(1 - \frac{\tanh\left(i^{1/2}\sigma s\right)}{i^{1/2}\sigma s} \right) \right]^{-1} \tag{B25B}$$

The real part of Γ corresponds to the attenuation coefficient (AC), the imaginary part to the phase shift (PS). The constants A and B can be determined by specifying additional boundary conditions at both ends of the slabs.

The solution for the other acoustic variables becomes

$$u = \frac{i\Gamma}{\gamma}\left[1 - \frac{\cosh\left(i^{1/2}\zeta s\right)}{\cosh\left(i^{1/2}s\right)}\right]\left[Ae^{\Gamma\xi} - Be^{-\Gamma\xi}\right] \tag{B26}$$

$$v = ik\left\{\left[Ae^{\Gamma\xi} + Be^{-\Gamma\xi}\right]\left[\zeta - \frac{\gamma-1}{\gamma}\left(\zeta - \frac{\sinh\left(i^{1/2}\zeta\sigma s\right)}{i^{1/2}\sigma s\cosh\left(i^{1/2}\sigma s\right)}\right)\right] + \right.$$
$$\left.\frac{\Gamma^2}{\gamma}\left[Ae^{\Gamma\xi} + Be^{-\Gamma\xi}\right]\left[\zeta - \frac{\sinh\left(i^{1/2}\zeta s\right)}{i^{1/2}s\cosh\left(i^{1/2}s\right)}\right]\right\} \tag{B27}$$

$$\rho = \left[1 - \frac{\gamma-1}{\gamma}\left[1 - \frac{\cosh\left(i^{1/2}\zeta\sigma s\right)}{\cosh\left(i^{1/2}\sigma s\right)}\right]\right]\left[Ae^{\Gamma\xi} + Be^{-\Gamma\xi}\right] \tag{B28}$$

$$T = \frac{\gamma-1}{\gamma}\left[1 - \frac{\cosh\left(i^{1/2}\zeta\sigma s\right)}{\cosh\left(i^{1/2}\sigma s\right)}\right]\left[Ae^{\Gamma\xi} + Be^{-\Gamma\xi}\right] \tag{B29}$$

From the solution for the vertical velocity, v, it can be verified that the condition $v/u << 1$ is fulfilled if k<<1 and k/s<<1.

As a solution identical to Eq. (B25) can be obtained if the equation of state, Eq.(4), and the energy Eq. (9) together are replaced by the polytropic relation $\frac{\bar{p}}{\bar{\rho}^n} = const.$

B.2 Derivation General Solution

$$\frac{\partial q}{\partial \tau} = \frac{1}{k_d'}\frac{\partial^2 q}{\partial \zeta^2} \tag{B30}$$

$$\frac{\partial T_{hm}}{\partial \tau} = \frac{1}{k_\lambda'}\frac{\partial^2 T_{hm}}{\partial \zeta^2} \tag{B31}$$

We start solving the diffusive and the conductive problem in the microporous solid[1].

Assuming $q(\xi,\zeta,\tau)=\mu_a(\zeta,\tau)\cdot\phi(\xi)$ and $T_{hm}(\xi,\zeta,\tau)=\nu_a(\zeta,\tau)\cdot\psi(\xi)$

We refer to the lower microporous layer (note 6).

Eqs (A30) and (A31) become respectively

$$\frac{\partial\mu_a}{\partial\tau}=\frac{1}{k_d'}\frac{\partial^2\mu_a}{\partial\zeta^2} \tag{B32}$$

$$\frac{\partial\nu_a}{\partial\tau}=\frac{1}{k_\lambda'}\frac{\partial^2\nu_a}{\partial\zeta^2} \tag{B33}$$

In the Laplace domain Eqs (B32) and (B33) become

$$\vartheta\tilde{\mu}_a-\mu_a(0)=\frac{1}{k_d'}\frac{\partial^2\tilde{\mu}_a}{\partial\zeta^2} \tag{B34}$$

$$\vartheta\tilde{\nu}_a-\nu_a(0)=\frac{1}{k_\lambda'}\frac{\partial^2\tilde{\nu}_a}{\partial\zeta^2} \tag{B35}$$

Introducing the initial conditions: $\mu_a(0)=0$

$$\nu_a(0)=0$$

$$\vartheta\tilde{\mu}_a=\frac{1}{k_d'}\frac{\partial^2\tilde{\mu}_a}{\partial\zeta^2} \tag{B36}$$

$$\vartheta\tilde{\nu}_a=\frac{1}{k_\lambda'}\frac{\partial^2\tilde{\nu}_a}{\partial\zeta} \tag{B37}$$

$$\tilde{\mu}_a=Ae^{\sqrt{k_d'\vartheta}}+Be^{-\sqrt{k_d'\vartheta}} \tag{B38}$$

$$\tilde{\nu}_a=Ce^{\sqrt{k_\lambda'\vartheta}}+De^{-\sqrt{k_\lambda'\vartheta}} \tag{B39}$$

Applying the boundary conditions (c) and (e) in Eq. (B38) and the boundary conditions (d) and (e) in Eq. (B39)

$$\tilde{\mu}_a=\left(\frac{e^{\sqrt{k_d'\vartheta}\left[2\left(\frac{h+h_s}{h}\right)+\zeta\right]}+e^{-\sqrt{k_d'\vartheta}\zeta}}{e^{\sqrt{k_d'\vartheta}\left(\frac{h+2h_s}{h}\right)}+e^{\sqrt{k_d'\vartheta}}}\right)\left(K_p\tilde{p}+K_T\tilde{T}\right)\frac{1}{\varphi(\xi)} \tag{B40}$$

---

[1] Because of the symmetry respect to the ξ axis , the concentration and the temperature in the upper and lower microporous layers are even functions respect ζ ($T_{hmu}(\zeta)=T_{hml}(-\zeta)=T_{hm}$ and $q_{hmu}(\zeta)=q_{hml}(-\zeta)=q_{hm}$).Consequently the derivatives respect ζ are odd functions . $\left(\frac{\partial T_{hmu}}{\partial\zeta}(\zeta)=-\frac{\partial T_{hml}}{\partial\zeta}(-\zeta)\right)$

$$\tilde{v} = \left(\frac{e^{\sqrt{k_\lambda' \vartheta}\left[2\left(\frac{h+h_s}{h}\right)+\zeta\right]} + e^{-\sqrt{k_\lambda' \vartheta}\zeta}}{e^{\sqrt{k_\lambda' \vartheta}\left(\frac{h+2h_s}{h}\right)} + e^{\sqrt{k_\lambda' \vartheta}}} \right) \frac{\tilde{T}}{\psi(\xi)} \tag{B41}$$

From Eqs (B40) and (B41) it follows respectively:

$$\tilde{q} = \left(\frac{e^{\sqrt{k_d' \vartheta}\left[2\left(\frac{h+h_s}{h}\right)+\zeta\right]} + e^{-\sqrt{k_d' \vartheta}\zeta}}{e^{\sqrt{k_d' \vartheta}\left(\frac{h+2h_s}{h}\right)} + e^{\sqrt{k_d' \vartheta}}} \right) \left(K_p \tilde{p} + K_T \tilde{T}\right) \tag{B42}$$

$$\tilde{T}_{hm} = \left(\frac{e^{\sqrt{k_\lambda' \vartheta}\left[2\left(\frac{h+h_s}{h}\right)+\zeta\right]} + e^{-\sqrt{k_\lambda' \vartheta}\zeta}}{e^{\sqrt{k_\lambda' \vartheta}\left(\frac{h+2h_s}{h}\right)} + e^{\sqrt{k_\lambda' \vartheta}}} \right) \tilde{T} \tag{B43}$$

where $\tilde{p} = L_T\left\{p \cdot e^{i\omega t}\right\}$ and $\tilde{T} = L_T\left\{T \cdot e^{i\omega t}\right\}$.

To simplify the notation, we rewrite Eqs (B42) and (B43) as:

$$\tilde{q} = Q(\vartheta)\left(K_p \tilde{p} + K_T \tilde{T}\right) \tag{B44}$$

$$\tilde{T}_{hm} = \Theta(\vartheta)\tilde{T} \tag{B45}$$

where $Q(\vartheta) = \left(\frac{e^{\sqrt{k_d' \vartheta}\left[2\left(\frac{h+h_s}{h}\right)+\zeta\right]} + e^{-\sqrt{k_d' \vartheta}\zeta}}{e^{\sqrt{k_d' \vartheta}\left(\frac{h+2h_s}{h}\right)} + e^{\sqrt{k_d' \vartheta}}} \right)$ and $\Theta(\vartheta) = \left(\frac{e^{\sqrt{k_\lambda' \vartheta}\left[2\left(\frac{h+h_s}{h}\right)+\zeta\right]} + e^{-\sqrt{k_\lambda' \vartheta}\zeta}}{e^{\sqrt{k_\lambda' \vartheta}\left(\frac{h+2h_s}{h}\right)} + e^{\sqrt{k_\lambda' \vartheta}}} \right)$

Because of the linearity of the Laplace operator, and making use of the inversion theorem of the Laplace trasform for a transfer function subjected to a periodic input, we have respectively from Eqs (B40) and (B41):

$$q = \left(K_p p + K_T T\right)\left|Q(i)\right| e^{i(\omega t + \arg(Q(i)))} \tag{B46}$$

$$T_{hm} = T\left|\Theta(i)\right| e^{i(\omega t + \arg(\Theta(i)))} \tag{B47}$$

Because for the boundary conditions (b) and (d) we need only the gradient of q and T_{hm} calculated at the interface gas-microporous solid:

$$\left.\frac{\partial \tilde{q}}{\partial \zeta}\right|_{\zeta=-1} = \left(K_p \tilde{p} + K_T \tilde{T}\right) dG_q(\vartheta) \tag{B48}$$

$$\left.\frac{\partial \tilde{T}_{hm}}{\partial \zeta}\right|_{\zeta=-1} = \tilde{T} \cdot dG_T(\vartheta) \tag{B49}$$

Because of the linearity of the Laplace operator, and making use of the inversion theorem of the Laplace transform for a transfer function subjected to a periodic input, we have respectively from Eqs (B46) and (B47):

$$\left.\frac{\partial q}{\partial \zeta}\right|_{\zeta=-1} = \left(K_p p + K_T T\right)\cdot\left|dG_q(i)\right|\cdot e^{i\left(\omega t+\arg\left(dG_q(i)\right)\right)} \tag{B50}$$

$$\left.\frac{\partial T_{hm}}{\partial \zeta}\right|_{\zeta=-1} = T\left|dG_T(i)\right|\cdot e^{i(\omega t+\arg(dG_T(i)))} \tag{B51}$$

$$\zeta = 1 \quad \frac{-\Delta H D q_s}{h}\frac{\partial q}{\partial \zeta} - \frac{\lambda_{hm} T_{hms}}{h}\frac{\partial T_{hm}}{\partial \zeta} = -\frac{\lambda T_s}{h}\frac{\partial T}{\partial \zeta}e^{i\omega t} \tag{B52}$$

$$\zeta = -1, \quad \frac{-\Delta H D q_s}{h}\frac{\partial q}{\partial \zeta} - \frac{\lambda_{hm} T_{hms}}{h}\frac{\partial T_{hm}}{\partial \zeta} = -\frac{\lambda T_s}{h}\frac{\partial T}{\partial \zeta}e^{i\omega t} \tag{B53}$$

Introducing the Eqs (B52) and (B53), Eqs (B50) and (B51) become respectively:

$$\begin{aligned}&\zeta = 1\\ &\frac{\Delta H\cdot D\cdot q_s}{h}\left[\left|dG_q(i)\right|\cdot e^{i\arg\left(dG_q(i)\right)}\left(K_p p + K_T T\right)\right]+\\ &\frac{\lambda_{hm} T_{hm}}{h} T\left|dG_T(i)\right|\cdot e^{i\arg\left(dG_T(i)\right)} = -\frac{\lambda T_s}{h}\frac{\partial T}{\partial \zeta}\\ &\zeta = -1\end{aligned} \tag{B54}$$

$$\begin{aligned}&-\frac{\Delta H\cdot D\cdot q_s}{h}\left[\left|dG_q(i)\right|\cdot e^{i\arg\left(dG_q(i)\right)}\left(K_p p + K_T T\right)\right]+\\ &-\frac{\lambda_{hm} T_{hm}}{h} T\left|dG_T(i)\right|\cdot e^{i\arg\left(dG_T(i)\right)} = -\frac{\lambda T_s}{h}\frac{\partial T}{\partial \zeta}\end{aligned} \tag{B55}$$

Introducing the new variables in Eq. (B53), we obtain:

$$-\frac{\Delta H\cdot D\cdot q_s}{h}\left[\left|dG_q(i)\right|\cdot e^{i\arg\left(dG_q(i)\right)}\left(K_p p+K_T\left\{g(\xi)\left(Ce^{-i^{5/2}\varpi s}+De^{i^{5/2}\varpi s}\right)+\frac{\gamma-1}{\gamma}p\right\}\right)\right]+$$

$$-\frac{\lambda_{hm}T_{hm}}{h}\left\{g(\xi)\left(Ce^{-i^{5/2}\varpi s}+De^{i^{5/2}\varpi s}\right)+\frac{\gamma-1}{\gamma}p\right\}\left|dG_T(i)\right|\cdot e^{i\arg\left(dG_T(i)\right)}= \tag{B56}$$

$$i^{1/2}\varpi s\cdot g(\xi)\frac{\lambda T_s}{h}\left(Ce^{-i^{5/2}\varpi s}-De^{i^{5/2}\varpi s}\right)$$

Because of the symmetry C=D, then solving for C:

$$C=\left[\frac{\frac{\Delta H\cdot D\cdot q_s}{h}\left[K_p+K_T\frac{\gamma-1}{\gamma}\right]\left|dG_q(i)\right|e^{i\arg\left(dG_q(i)\right)}+\frac{\lambda_{hm}T_{hms}}{h}\frac{\gamma-1}{\gamma}\left|dG_T(i)\right|e^{i\arg\left(dG_T(i)\right)}}{\frac{\Delta H\cdot D\cdot q_s}{h}\left[K_T\frac{\gamma-1}{\gamma}\right]\left|dG_q(i)\right|e^{i\arg\left(dG_q(i)\right)}-\frac{\lambda_{hm}T_{hms}}{h}\left|dG_T(i)\right|e^{i\arg\left(dG_T(i)\right)}+\frac{\lambda T_s}{h}i^{1/2}\varpi s\tanh\left(i^{5/2}\varpi s\right)}\right]$$

$$\cdot\frac{p}{g(\xi)}\frac{1}{\left[e^{i^{5/2}\varpi s}+e^{-i^{5/2}\varpi s}\right]}$$

$$T(\zeta,\xi)=p\left[-\Xi\frac{\cosh\left(i^{1/2}\varpi s\zeta\right)}{\cosh\left(i^{1/2}\varpi s\right)}+\frac{\gamma-1}{\gamma}\right] \tag{B57}$$

The expression for Ξ is reported in Appendix C.

Substituting Eq. (B65) in Eq. (B19):

$$\rho=p-T=p\left[1-\left[-\Xi\frac{\cosh\left(i^{1/2}\varpi s\zeta\right)}{\cosh\left(i^{1/2}\varpi s\right)}+\frac{\gamma-1}{\gamma}\right]\right] \tag{B58}$$

using Eqs (B57) and (B66) the continuity equation (B8) can be rewritten as

$$\frac{\partial v}{\partial\zeta}=-k\left[i\rho+\frac{\partial u}{\partial\xi}\right]=-ik\left\{p\left[1-\left[-\Xi\frac{\cosh\left(i^{1/2}\varpi s\zeta\right)}{\cosh\left(i^{1/2}\varpi s\right)}+\frac{\gamma-1}{\gamma}\right]\right]\right.$$

$$\left.+\frac{1}{\gamma}\frac{\partial^2 p}{\partial\xi^2}\left[1-\frac{\cosh\left(\left(i^{1/2}\zeta\right)s\right)}{\cosh\left(i^{1/2}s\right)}\right]\right\} \tag{B59}$$

By integration:

$$v=-ik\left\{p\left[\zeta-\left[-\Xi\frac{\sinh\left(i^{1/2}\varpi s\zeta\right)}{i^{1/2}\varpi s\cosh\left(i^{1/2}\varpi s\right)}+\frac{\gamma-1}{\gamma}\zeta\right]\right]\right.$$

$$\left.+\frac{1}{\gamma}\frac{\partial^2 p}{\partial\xi^2}\left[\zeta-\frac{\sinh\left(i^{1/2}\zeta s\right)}{i^{1/2}s\cosh\left(i^{1/2}s\right)}\right]+F(\xi)\right\} \tag{B60}$$

From the boundary conditions a)

$$\zeta = 1,\ v = -\frac{Dq_s}{h\rho_s a_0 e^{i\omega t}}\frac{\partial q}{\partial \zeta} = -ik\left\{p\left[1-\left[-\Xi\frac{\tanh\left(i^{1/2}\sigma s\right)}{i^{1/2}\sigma s}+\frac{\gamma-1}{\gamma}\right]\right]\right.$$
$$\left.+\frac{1}{\gamma}\frac{\partial^2 p}{\partial \xi^2}\left[1-\frac{\tanh\left(i^{1/2}\zeta s\right)}{i^{1/2}s}\right]+F(\xi)\right\} \qquad \text{(B61)}$$

$$\zeta = -1,\ v = -\frac{Dq_s}{h\rho_s a_0 e^{i\omega t}}\frac{\partial q}{\partial \zeta} = ik\left\{p\left[1-\left[-\Xi\frac{\tanh\left(i^{1/2}\sigma s\right)}{i^{1/2}\sigma s}+\frac{\gamma-1}{\gamma}\right]\right]\right.$$
$$\left.+\frac{1}{\gamma}\frac{\partial^2 p}{\partial \xi^2}\left[1-\frac{\tanh\left(i^{1/2}\zeta s\right)}{i^{1/2}s}\right]-F(\xi)\right\} \qquad \text{(B62)}$$

Noting that $\left.\frac{\partial q_l}{\partial \zeta}\right|_{\zeta=-1} = -\left.\frac{\partial q_u}{\partial \zeta}\right|_{\zeta=1}$ it follows:

$$F(\xi) = 0 \qquad \text{B63)}$$

Introducing Eqs (B61) and (B63) in Eq. (B60):

$$\frac{1}{\gamma}\frac{\partial^2 p}{\partial \xi^2}\left[1-\frac{\tanh\left(i^{1/2}s\right)}{i^{1/2}s}\right]+p\left\{\frac{D\cdot q_s}{\rho_s \gamma h a_0 \cdot ik}\left(K_p p+K_T\left[-\Xi+\frac{\gamma-1}{\gamma}\right]\right)\cdot\left|dG_q(i)\right|\cdot e^{\left(i\arg\left(dG_q(i)\right)\right)}+\right.$$
$$\left.\left[1-\left[-\Xi\frac{\tanh\left(i^{1/2}\sigma s\right)}{i^{1/2}\sigma s}+\frac{\gamma-1}{\gamma}\right]\right]\right\}=0 \qquad \text{(B64)}$$

Appendix C

Description of the SND-PC TOOLBOX

Copyright:

The SND_PC toolbox is written by Torsten Marquardt (torsten.marquardt@gmx.net)
and is subject to the GNU GENERAL PUBLIC LICENCE (see COPYING_GPL.TXT).